Durability of Concrete under Combined Attack. Frost Salt Scaling
in Carbonated Concrete and Chloride Ingress in Mechanically Loaded Concrete

Hugo Eguez Alava

Promotoren: prof. dr. ir. N. De Belie, prof. dr. ir. G. De Schutter
Proefschrift ingediend tot het behalen van de graad van
Doctor in de ingenieurswetenschappen: bouwkunde

UNIVERSITEIT
GENT

Vakgroep Bouwkundige Constructies
Voorzitter: prof. dr. ir. L. Taerwe
Faculteit Ingenieurswetenschappen en Architectuur
Academiejaar 2016 - 2017

ISBN 978-94-6355-031-4
NUR 955
Wettelijk depot: D/2017/10.500/66

Supervisors

prof. dr. ir. Nele De Belie
prof. dr. ir. Geert De Schutter

Research institute

Magnel Laboratory for Concrete Research
Department of Structural Engineering
Faculty of Engineering and Architecture
Ghent University, Belgium

Examination committee

prof. dr. ir. Luc Taerwe (chairman)
Ghent University
Faculty of Engineering and Architecture
Department of Structural Engineering

prof. dr. ir. Tom De Mulder (secretary)
Ghent University
Faculty of Engineering and Architecture
Department of Civil Engineering

prof. Alexandra Bertron
Institut National des Sciences Appliquées (INSA) Toulouse,
France

prof. Christoph Gehlen
Technische Universität München
Germany

prof. dr. ir. Robby Caspeele
Ghent University
Faculty of Engineering and Architecture
Department of Structural Engineering

dr. ir.-arch. Philip Van Den Heede
Ghent University
Faculty of Engineering and Architecture
Department of Structural Engineering

Research funding

I would like to thank The National Secretary for Science and Technology of Ecuador (SENESCYT) and Ghent University for the financial support.

Copyright © Hugo Eguez Alava 2017

All rights reserved. No part of this publication may be reproduced, stored in a retrieval system or transmitted in any form or by any means, electronic, mechanical, photocopying, recording or otherwise, without prior written permission of the author and his supervisors.

Acknowledgements

I would like to thank the members of the jury for reviewing this work: prof. Nele De Belie, prof. Geert De Schutter, prof. Alexandra Bertron, prof. Tom De Mulder, prof. Christoph Gehlen, prof. Robby Caspeele, dr. Philip Van Den Heede. I am very grateful for your suggestions and comments which were inspiring for improving this work.

I also want to thank all the staff from The Magnel Laboratory, professors, secretaries, technicians and Ph.D. students that offered me guidance, support, friendship and made these 4 years of research a wonderful time.

Special thanks to my promotors Nele, Geert and to our department chairman prof. Luc Taerwe, thank you for your advice, support and patience as well. As part of many activities you organized, I enjoyed the team building activities during the Magnel seminars and the summer walks with the research group.

My thanks to the technical staff from the lab., Nicolas, Stefan, Sandra, Dieter, Peter (Lampaert), Nathan, Jan, Marc, Tom, Peter (Van den bussche), Tom (Planckaert), Tommy and Bart who gave me the support and their time to finish this research.

Dear colleagues, Elke, Kim, Philip, Jianyun, Ruben, Mathias, Didier, Eleni, Arn, João, Sandra, Desire, Julia, Yusuf, Romy, Corina, Cornelia, Aneeta, Florent, Farid, Adelaide, Yang Lv, Lijie, Kunpeng, Yihua, Yury, Natalia, Evin, Wen Hao, Xiang, Yu, we had so much fun. Thanks.

Farid, thank you for your hospitality, remember “mi Casa es tu casa”.

To our secretaries, Christel, Marijke, Viviane, I appreciate very much your support and friendship.

Finally, to my family, Cecilia, Ma. Isabel, Gaby and Hugo thanks for your patience and support for all these years.

TABLE OF CONTENTS

ABBREVIATIONS AND SYMBOLS

Abbreviations

ACI – American Concrete Institute

ANOVA - Analysis Of Variance tests

ASTM - American Society for Testing and Materials

b - Binder

BFS - Blast-Furnace Slag

BSE - Backscattered Electron

C - Calcite

CR - Cracked

DTA - Differential Thermal Analysis

EDX - Energy Dispersive X-ray spectroscopy

EN – European Standard

erf( ) Error function

FA - Fly Ash

GGBFS - Ground Granulated Blast-Furnace Slag

HSR - High Sulphate Resistant

ISO - International Organization for Standardization

LA - Low Alkali

LOI - Loss On Ignition

NBN – The Bureau for Standardization (Belgium)

OPC - Ordinary Portland Cement

ppm - parts per million

Ref. - Reference

RH - Relative Humidity

s/b - Slag-to-Binder ratio

S50 - mixture with 50 % OPC and 50 % BFS as binder

S70 - mixture with 30 % OPC and 70 % BFS as binder

SCC - Self-Compacting Concrete

SCMs - Supplementary Cementitious Materials

SEM - Scanning Electron Microscope

SF - Silica Fume

S-N-K - Student-Newman-Keuls

SP - Superplasticizer

TC - Technical Committee

TG - Thermogravimetry

TGA - Thermogravimetric Analysis

w/b - Water-to-Binder-ratio

w/c- Water-to-Cement ratio

WL - Weight Loss

XRD - X-Ray Diffraction

Cement chemistry

A - Aluminium oxide (Al_2O_3)

AFm –Monosulphate hydrates

AFt - Trisulphate hydrates (Ettringite)

C - Calcium oxide (CaO)

$\overline{C}$ Carbon di-oxide, CO_2

C_2S - Dicalcium silicate (Belite)

C_3A - Tricalcium aluminate (Aluminate)

C_3S - Tricalcium silicate (Alite)

C_4AF - Tetracalcium aluminoferrite (Ferrite)

CC Calcium - carbonate ($CaCO_3$)

CH - Calcium hydroxide ($Ca(OH)_2$), Portlandite

CSH - Calcium silicate hydrates

F - Iron oxide (Fe_2O_3)

MSH - Magnesium silicate hydrates

S - Silicium oxide (SiO_2)

$\overline{S}$ Sulfur tri-oxide, SO_3

Greek symbols

ρ dry - Dry density (kg/m³)

φ – Permeable/Open porosity (%)

Φ - Total porosity (%)

ω m - Evaporable water content relative to the mass of dry concrete (%)

Roman symbols (lowercase)

a_c = the amount of carbonatable matter per volume $(\frac{\mathrm{kg}}{\mathrm{m}^3})$

c_s = the CO_2 concentration at concrete surface $(\frac{\mathrm{kg}}{\mathrm{m}^3})$

d - Concrete cover (mm)

D_c = diffusion coefficient of CO_2 $(\mathrm{m}^2/\mathrm{s})$

l - Length (m)

n - Number of samples / number of measurements

t - Test duration/Immersion time (s or years)

$t = \mathrm{time}\ (\mathrm{s})$

t_0 - Reference time (years)

t_{SL} - Design service life (years)

w - Crack width (mm)

w c - Weight of cementing materials for 1 m³ concrete (kg)

w w - Weight of mixing water for 1 m³ concrete (kg),

x - Distance from the surface until the middle of the considered layer (m)

x_c = carbonation depth (m)

y = Carbonation depth (mm)

Δx - Depth of the skin layer/convection zone (mm)

Roman symbols (uppercase)

A - Cross-section (m²), Carbonation coefficient "(mm/(day)$^{0.5}$"

C - Chloride content (g/l, mol/l or wt.%)

C(x,t) – Total chloride concentration at depth *x* and time *t* (wt. %)

C_i - Initial chloride concentration (wt. % of concrete)

C_s - Chloride surface concentration (wt. % of concrete)

$C_{S\Delta x}$ - Chloride content at depth *Δx* (wt.% of concrete)

D - Diffusion coefficient (m²/s)

D_a - Apparent chloride diffusion coeffcient (mm²/years)

$D_{app,0}$ - Apparent chloride diffusion coefficient at t_0 (mm²/years)

D_{nssd} - Non-steady-state diffusion coefficient (m^2/s)

DIC – Digital Image Correlation

L - Thickness of the specimen (m or mm)

M- Molarity (mole/liter)

Ø - Diameter (mm)

R - Gas constant (8.314 J/(mol·K))

T - Temperature (K)

Summary

Five basic things that civilization depends on are clothing, water, food, shelter, and transportation. Of which the last two depend in turn, on construction materials.

Since its invention nearly 200 years ago, Ordinary Portland Cement (OPC) and more specifically concrete is one of the most widely used modern building materials per-capita in the world. Concrete is the

preferred material because of its low cost and excellent mechanical performance. World production of cement in 2016 was of 4.3 x 10^9 tons [www.statista.com] and is projected to rise to 5.8 x 10^9 tons by 2050 [Scrivener K., 2012]. A way to cope with the demand is the incorporation of supplementary cementitious materials (SCMs) to partially replace OPC. Blast Furnace Slag (BFS) along with Fly Ash (FA) are among the preferred SCMs which are frequently utilized to replace Portland cement.

In modern construction, a material, in addition to its mechanical performance, must offer resistance over time. This property is defined as durability. Concrete structures must resist the environmental conditions, maintaining the design properties over the defined service life time.

One of the advantages that OPC provides to the reinforced concrete is its high alkalinity. It is generated by the alkali components in the cement (Na_2O and K_2O, which will give rise to NaOH and KOH in the concrete pore solution) and Portlandite ($Ca(OH)_2$ or CH) which is the product of cement's hydration. This high alkalinity could rise the pH to values higher than 13.0 which provide the reinforcement with a passivated stable oxide film that avoid its corrosion. However, atmospheric CO_2 can diffuse into the concrete pores and start carbonation. This reaction can diminish the paste pH to values lower than 9. When this occurs, the reinforcement loses its passive film and corrosion starts. The damage caused by carbonation of cementitious materials has been well studied as an independent mechanism. However, it is well known from field observation that damaged

structures show evidence of more than one environmental load acting at the same time in concrete. And that the combination of mechanical loads with deleterious environmental actions creates a synergetic effect.

Although carbonation and freeze-thaw attack have been studied independently, there are new studies that suggest that both attacks should not be considered separately. Additionally, most structures that resist these loads also are in contact with deicing salts.

Many mechanisms have been proposed to explain the frost scaling damage to carbonated concrete in the presence of deicing salts. Most of the proposed theories offer a mechanical explanation due to the increased volume of ice when water freezes in the pores of carbonated concrete. This would be the most obvious explanation, but for two small details. First, the point of formation of ice in the presence of salts and in the microstructure of the concrete is significantly depressed. Second, there is evidence of frost scaling at low temperatures but above the freezing point of water.

In this research four concrete types using OPC, high sulfate resistant (HSR) Portland cement and a BFS based binder with two different OPC replacement ratios (slag/binder: 0.5 and 0.7), were previously carbonated before subjecting samples to frost scaling tests made by ponding in 3% sodium chloride solution.

The carbonation test confirmed the well-known studies that Portland cements have higher resistance to carbonation than BFS binders. XRD analyses made on the extracted paste of carbonated samples determined that the most abundant carbonate was the meta-stable phase Vaterite. It was also determined, that the amount of CSH carbonation increased with BFS replacement. Therefore, a sensitivity towards carbonation was established in the following increasing order: HSR, OPC, S50 and S70. The results of the carbonated samples in the frost scaling test showed the same order for increasing severity of the attack.

Several observations were made on the formed scales after the 56th cycle. With the aid of a petrographic microscope, a cluster of bi-refringent oxychloride minerals was observed growing underneath the produced cementitious flakes. It was concluded that this salt growth is disruptive. It was somewhat disorienting to find oxychloride when the concentration of the attacking chloride solution was only 0.5 M, when literature cites conditions for its formation with requirements of up to 10 times that concentration.

Studies on chloride profiling were made in the samples exposed to that solution. A peak in the chloride diffusion curve was observed with its maximum value located at 3-4 mm inside the surface. It seems that high chloride concentration is available on CSH sites of cement paste. At the location of the chloride peak, more physical concentration of this ion on CSH does occur. A chemical mechanism was proposed to explain oxychloride formation. A thermodynamic model was analyzed, where reactions are occurring at low temperatures, carbonates dissolve to provide calcium ions and the pH has its role in the equilibrium. It was also concluded that the use of high amounts of SCMs, low pH and carbonation, provide better conditions for oxychloride formation.

A second part of the research was focused on the combined attack of concrete by chlorides and mechanical loading. The same binders utilized for the previous study were also analyzed in this case. Concrete samples were subjected to a 3% chloride solution attack. Simultaneously, one set of prisms were subjected to compressive stresses. While the other studied samples were subjected to splitting tensile stresses and chloride solution.

Chloride profiles were measured in the exposed samples over time. In the compression test, a progressive decrease in the chloride levels was noticed when the load was gradually increased. The causes of this decrease are not clear, but are probably related to electrochemical alteration of the cement membrane due to mechanical damage. It seems that the chloride adsorption capacity of hardened cement paste is affected. It was also noticed that a skin layer was formed over time.

This layer grows with load level. The diffusion coefficient in this layer is also large compared with the one obtained further inside the concrete where the material is not yet damaged.

In the splitting tensile test, also the formation of a skin or damaged layer was noticed. A low chloride content in the near surface zone was also observed. The shape of the chloride profiles was very similar to the ones observed after chloride attack in carbonated concrete, or in zones were the concrete is subjected to cycles of drying and wetting or in cracked concrete. A main crack was observed in the concretes with BFS. This was associated with the splitting loading plane. A smaller set of micro-cracks was observed to develop perpendicularly to the main crack. These micro-cracks show an intergranular pattern around aggregate grains. This feature has similarities with the “stress-corrosion cracking” observed in other materials subjected to permanent stresses in the presence of a corrosive environment.

Samenvatting

Vier belangrijke basisbehoeften van de mens zijn kleding, voeding, beschutting en transportmogelijkheden. De laatste twee hiervan zijn op hun beurt afhankelijk van de beschikbaarheid van constructiematerialen.

Sinds de uitvinding bijna 200 jaar geleden, is Portlandcement en meer specifiek beton, het meest gebruikte moderne bouwmateriaal per capita in de wereld. Beton is vaak het meest verkieselijke materiaal omwille van de lage kostprijs en de excellente mechanische prestaties. De wereldproductie van cement in 2010 bedroeg 3,6 x 10^9 ton en een stijging tot 5,8 x 10^9 ton is voorzien tegen 2050 (Scrivener, 2012). Een manier om tegemoet te komen aan deze stijgende vraag is het gebruik van supplementaire cementerende materialen ("supplementary cementitious materials" of SCMs); dit zijn toevoegsels die gedeeltelijk het Portlandcement in beton kunnen vervangen. Hoogovenslak en vliegas zijn voorbeelden van SCMs die frequent gebruikt worden in cement en beton.

In moderne constructies moet een materiaal naast het vertonen van de nodige mechanische eigenschappen, ook voldoende weerstand tegen omgevingsomstandigheden bieden. Betonconstructies moeten hun ontwerpeigenschappen behouden gedurende de ganse voorziene gebruiksduur.

Een van de voordelen van het gebruik van Portlandcement in gewapend beton, is het creëren van een hoge alkaliniteit. Deze wordt gegenereerd door de alkalicomponenten in het cement (Na_2O en K_2O, die leiden tot NaOH en KOH in de poriënoplossing) en portlandiet ($Ca(OH)_2$ of CH) dat een product is van de cementhydratatie. Deze hoge alkaliniteit kan de pH doen stijgen tot waarden boven 13,0 zodat de wapening voorzien wordt van een passiveringslaag, een stabiele oxidefilm die corrosie tegengaat. Echter, atmosferische CO_2 kan diffunderen in de betonporiën en carbonatatie initiëren. Door deze reactie kan de pH in de cementpasta dalen tot waarden beneden 9. Wanneer dit gebeurt, verliest de wapening zijn passiveringslaag en

corrosie kan starten. De schade veroorzaakt door carbonatatie van cementgebonden materialen is ruim onderzocht als onafhankelijk mechanisme. Het is echter duidelijk uit praktijkonderzoek dat beschadigde constructies tekenen vertonen van aantasting door meerdere gelijktijdig optredende mechanismen. De combinatie van mechanische belasting met schadelijke omgevingsinvloeden leidt tot synergistische effecten.

Alhoewel carbonatatie en vorst-dooischade reeds veelvuldig onafhankelijk onderzocht werden, zijn er nieuwe studies die aangeven dat beide acties samen bekeken moeten worden. Bovendien komen de meeste constructies die onderhevig zijn aan deze omstandigheden ook in contact met dooizouten.

Vele mechanismen zijn reeds voorgesteld om de vorstschade aan beton in de aanwezigheid van dooizouten te verklaren. Meestal wordt beroep gedaan op een mechanische verklaring, gerelateerd aan het toenemende volume wanneer water in de poriën van (gecarbonateerd) beton bevriest tot ijs. Dit zou de meest voor de hand liggende verklaring zijn, ware het niet dat hierbij twee details over het hoofd gezien worden. Vooreerst is het vriespunt waarbij water overgaat tot ijs in de aanwezigheid van zouten en binnenin de fijne microstructuur van beton significant verlaagd. Ten tweede is er ook bewijs voor afschilfering bij lage temperaturen die zich nochtans boven het vriespunt van water bevinden.

In dit onderzoek werden vier betonsoorten aangemaakt, gebruik makend van gewoon Portlandcement (PC), een Portlandcement met hoge sulfaatresistentie (HSR) en een bindmiddel waarin hoogovenslak gebruikt werd om Portlandcement te vervangen in twee verschillende percentages (slak/bindmiddel-verhouding van 0.5 (S50) en 0.7 (S70)). Het vooraf gecarbonateerd beton werd dan blootgesteld aan vorstproeven in contact met een 3% natriumchloride oplossing.

De carbonatatieproef bevestigde eerdere studies die aantonen dat beton met Portlandcement een hogere weerstand vertoont tegen carbonatatie dan beton met hoogovenslak. X-stralenanalyses op cementpasta geëxtraheerd uit gecarbonateerd beton, toonden aan

dat het meest voorkomende carbonaat het metastabiele vateriet was. Ook werd bevestigd dat de mate van carbonatatie van de calciumsilicaathydraten (CSH) verhoogde met toenemende vervanging van Portlandcement door hoogovenslak. De gevoeligheid ten opzichte van carbonatatie nam daarom toe in de volgorde: HSR, PC, S50, S70. De resultaten van afschilfering in de vorstproeven op gecarbonateerde monsters namen toe met dezelfde volgorde.

Verschillende bijkomende observaties werden gedaan op het afgeschilferde materiaal na de 56^{e} vorst-dooicyclus. Met behulp van een petrografische microscoop werd een cluster van dubbelbrekende oxychloridemineralen geobserveerd, die groeiden onder de geproduceerde cementgebonden schilfers. Er werd geconcludeerd dat deze groei van zouten de samenhang verstoort. Het was op zich onverwacht om oxychloride te vinden in deze omstandigheden, waarbij de concentratie van de oplossing slechts 0.5 M bedroeg, terwijl literatuur wel 10 keer hogere concentraties aanhaalt als voorwaarde voor hun vorming.

Op dezelfde proefstukken werden ook chlorideprofielen bepaald. Er werd een piek in chlorideconcentratie vastgesteld die zich 3-4 mm onder het oppervlak bevond. Op deze locatie werden dus de concentratievoorwaarden voor oxychloridevorming bereikt. Er werd een chemisch mechanisme voorgesteld om de oxychloridevorming te verklaren. Er werd ook een thermodynamisch model geanalyseerd, waarbij reacties optreden bij lage temperaturen, en carbonaten oplossen om calciumionen aan te leveren, waarbij de pH een belangrijke rol speelt in het evenwicht. Er werd geconcludeerd dat het gebruik van hoge hoeveelheden SCMs, een lage pH en carbonatatie, betere condities geven voor oxychloridevorming.

In een tweede deel van dit werk werd gefocust op de gecombineerde aantasting van beton door chloriden en mechanische belasting. Dezelfde bindmiddelen als in voorgaand onderdeel werden gebruikt. Betonmonsters werden blootgesteld aan een 3% chlorideoplossing en tegelijk aan drukspanningen. Bijkomende proefstukken werden onderworpen aan splijttrekspanningen en de chlorideoplossing.

Chlorideprofielen werden bepaald voor de blootgestelde proefstukken in functie van de tijd. In de drukproef werd een voortschrijdende vermindering van de chlorideniveaus vastgesteld wanneer de belasting gradueel opliep. De reden hiervoor was niet duidelijk, maar is wellicht gerelateerd aan de elektrochemische wijziging van het cementmembraan door mechanische schade. Het lijkt alsof de chloride-adsorptiecapaciteit van de verharde cementpasta beïnvloed werd. Er werd ook vastgesteld dat een oppervlakkige zone met gewijzigde eigenschappen ontstaat in functie van de tijd. Deze zone groeit bij toenemend belastingsniveau. De diffusiecoëfficiënt in deze laag is groot in vergelijking met deze dieper in het beton waar het materiaal nog niet beschadigd is.

Bij de proeven met splijtbelasting werd ook de vorming van een oppervlakkige laag vastgesteld. Hierin was tevens de chlorideconcentratie lager. De vorm van de chlorideprofielen was zeer gelijkaardig aan deze in gecarbonateerd beton, of in zones waar beton is blootgesteld aan nat/droog cycli, of in gescheurd beton. In beton met hoogovenslak werd een scheur vastgesteld die samenviel met het belastingsvlak van de splijtbelasting. Fijnere microscheuren ontwikkelden zich loodrecht op de voorgaande scheur. Deze microscheuren vormden een patroon rond de granulaten, een fenomeen dat gelijkenissen vertoont met de intergranulaire scheuren in geval van spanningscorrosie, bij andere materialen die onderworpen zijn aan permanente spanningen in een corrosief milieu.

I INTRODUCTION

CHAPTER 1 GENERAL INTRODUCTION

1.1 Literature review.

1.1.1. Chloride's role in the dissolution or precipitation of salts in materials and their damage

Chlorine is the second lightest of the halogens in the periodic table of the elements. With symbol Cl and atomic number 17, it appears in this table between fluorine and bromine and its properties are generally in-between them. Chlorine is a yellow-green gas at room temperature. It is a strong oxidizing agent and extremely reactive element. It has a highest electron affinity and the third-highest electronegativity, behind only oxygen and fluorine.

Due to its great reactivity, all chlorine in the Earth's crust is in the form of ionic chloride compounds, which includes common salt (NaCl). It is twenty-first most abundant chemical element in Earth's crust. However, the highest reserves of this element are in sea water.

Because of its chemical activity, chloride is involved in forming new compounds. It has special affinity for enhancing the dissolution of minerals and stabilizing compounds in aqueous solution. It is capable to dissolve even a noble metal as gold. Aqua Regia (Royal water) dissolves gold, is a solution that combines 1 part of concentrated nitric acid and 3 parts of hydrochloric acid [1]. In the combination, each acid accomplishes a separate mission. Nitric acid has the role of oxidizing gold to its Auric state (III). On the other hand, chloride provide the ions to form a stable complex molecule of chloroaurate anions [$AuCl_4^-$] which are stable in aqueous solution. Under this conditions, gold dissolution is possible.

But not only pure metals can interact with chloride, natural stones and common building materials can also be affected by this ion in the presence of water.

Salt weathering with a honeycomb pattern has been observed shaping several natural stone landscapes Figure 1-1.

Rodriguez-Navarro "et al." [2] reproduced in the lab incipient honeycomb weathering in a homogeneous limestone that was exposed to wind exposure and salt crystallization.

Figure 1-1: Tafoni weathering produced by salt, Skye Scotland [2].

Their experiments showed that varied wind flow over a stone surface is important in the development of this erosion pattern. Wind promotes evaporative salt growth between grains on a stone surface, and develops small, randomly distributed cavities. A reduction in air pressure within the cavities results in increased wind speed and rapid evaporation. The high rate of evaporation and cooling of the saline solution in the cavity leads to more rapid and greater granular disintegration than in the surrounding areas. It seems that this local supersaturation and subsequent buildup of salt crystallization pressure ultimately result in the formation of honeycomb features. Salt crystallization is thought to be a common surface phenomenon affecting a variety of rocks in a wide range of situations. It develops on building stones and it shapes ocean cliffs, rocks in hot deserts, and Arctic landscapes.

Chapman R. (1980) [3]. Also, reported salt weathering by sodium chloride in calcareous sandstones. The field characteristics of the weathered rocks among others are: thin exfoliation scales that covered soft spongy surfaces, salt crystals in pores and veins on the rock surface. He found that the presence of calcite in the affected zone of the stone, varied inversely with the presence of Halite (NaCl). The lack of calcium mineral, suggested that $CaCO_3$ has been removed by the salt presence. He found that rock disintegration is as rapid on faces sheltered from direct sun light as on faces directly exposed to it. He

also found disintegration in caves where temperature ranges are minimal. He could not explain the damaging mechanism, however, due to the systematic presence of salt in the most weathered zones he suggested sodium chloride as the principal agent causing rock deterioration.

Figure 1-2 [4] show a diagram that relate the properties, factors and processes for salt crystallization in natural stone. It is important to differentiate the properties that contribute to a benign or a damaging salt behaviour. Typical damaging behaviours or processes for salts can include surface scaling, deep cracking, expansion, granular disintegration, surface powdering and microcracking. The degree of damage is often attributable to specific properties. For instance, in the case of sodium sulphate crystallization, the degree of supersaturation and the location of crystallization appear to be the keys to understanding the degree of damage (Rodriguez-Navarro & Doehne 1999). There are some significant properties and kinetic aspects, such as the evaporation rate, that largely controls how much damage results from this mechanism. The same can be said for the salt scaling damage in concrete under temperature cycles. The thermodynamic and kinetic conditions seem to play a key role in provoking damage.

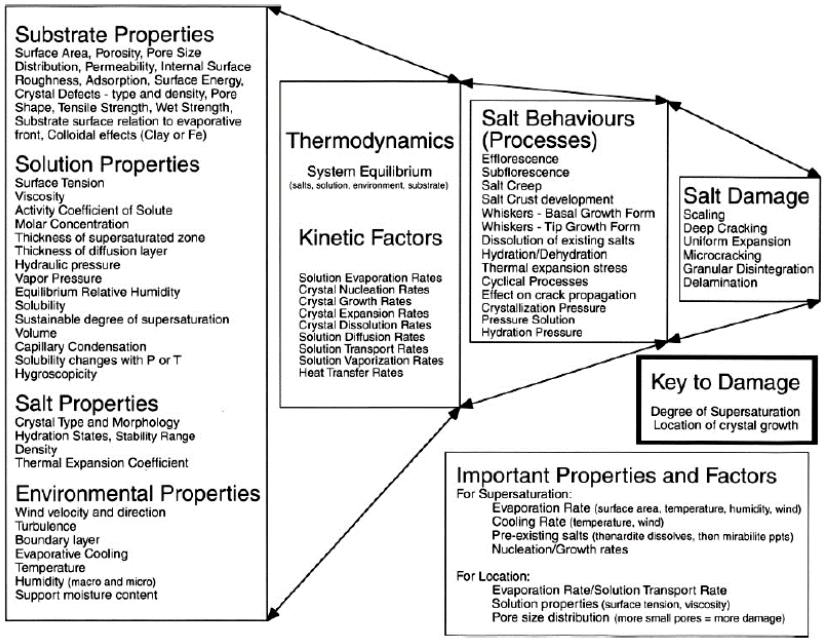

Figure 1-2: Diagram of properties, factors and processes for salt crystallization damage [4].

Another deterioration mechanism where chloride commonly participates is the corrosion of the reinforced steel in concrete. Corrosion is an electrochemical reaction where transference of electrons occurs in aqueous solution. Figure 1-3 shows the Pourbaix diagram showing the stability of metallic iron in aqueous solution as a function of hydrogen standard potential and pH.

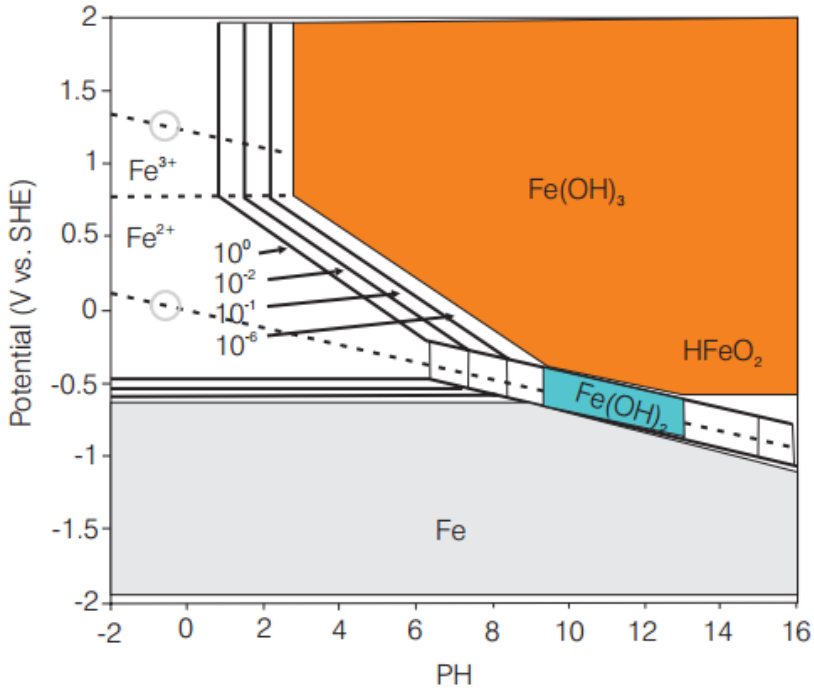

Figure 1-3: Pourbaix diagram for iron showing regions of stability, dissolution and passivation. Metallic iron is stable (grey region); active corrosion occurs (white areas) and the metal is passivated (blue and orange areas) [5].

The high alkalinity found in OPC concrete pastes (greater than 12.0) [6], provides the protective coating on the steel (a passive film) according to Pourbaix diagram shown in Figure 1-3. However, this passive film is not stable in presence of chlorides ions or when pH drops to values below 9 as seen in Figure 1-3. The ingress of acidic CO_2 through the concrete cover that protects the reinforcement also neutralize this protective alkalinity and reduces the pH. Thus, the reinforcement is devoid of the passive film and corrosion takes place at high rates of several mm/year. Corrosion is an electrochemical

reaction comprised by 2 half-cell reactions as shown in equations 1-1 and 1-2 [5].

$$Fe \rightarrow Fe^{2+} + 2e^{-} \quad \text{1-1}$$

$$^{1}/_{2}\, O_2 + H_2O + 2e^{-} \rightarrow OH^{-} \quad \text{1-2}$$

During high pH conditions Fe^{2+} combines with OH^{-} ions to create a passive oxide film that protects reinforcement from further corrosion. The passive corrosion is presented in the scheme of Figure 1-4 (a) [5].

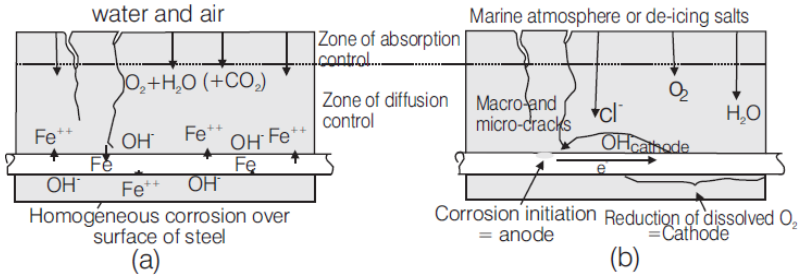

Figure 1-4: Corrosion with passive film formation (a). Active corrosion of steel, that has been induced by chloride ions (b) [5].

The process of how chlorides increase the breakage of the oxide passive film from the surface of the reinforcement is not well understood [7]. One hypothesis is that the chlorides ions combine with ferrous ions in the passive film and forms ferrous chloride. Subsequently, it is further oxidized in presence of oxygen and water (Martin-Perez 1999, Sandberg, 1998) [8], equation 1-3.

$$4\, Fe\, Cl_2 + O_2 + 6\, H_2O \rightarrow \text{FeOOH} + 8\ \text{HCl} \quad \text{1-3}$$

Chloride reaches the reinforcement in localized zones where anodic oxidation sites are formed while the remaining parts act as cathodic passive zones, Figure 1-4 (b). The reaction consumes ferrous ions and produces hydrogen ions (acidification), forcing further oxidation of the metal.

1.1.2.Frost salt scaling in carbonated OPC and BFS concrete

Due to its low cost and because of environmental benefits, BFS has been an attractive SCMs for using in concrete. Thus, this material has been used for several applications such as low heat concrete for massive structures. Besides, due to its characteristics of low heat generation, it is also preferred due to its known characteristics against aggressive environments such as acidic environments, chloride and sulfate attack.

However, carbonation of BFS concrete is known as the most detrimental processes for Frost salt scaling of concrete.

Due to the larger amount of CH found in hydrated OPC pastes, CH carbonation seems to be the preferred reaction in these binders. Calcite shows to be the main product of Portland cement paste carbonation. The larger volume produced by calcite compensates any shrinkage from CSH carbonation [Sisomphon “et al.” (2010)]. On the contrary, binders which partially replaced OPC by a supplementary cementitious material (SCM’s) have been found to develop higher porosities after carbonation [De Ceukelaire and Van Nieuwenburg (1993)].

The simple frost damage has received more attention due to its simplicity and less complicated causes of attack. Thus, the works of Powers, Litvan, Pigeon, Marchand, Setzer [9–12], and numerous others researchers have described the problem significantly well. However, for Frost salt scaling there are questions that cannot be answered by a single theory.

Recently Valenza II and Scherer [13] offered a mechanism to clarify the scaling. They name it “the Glue-Spall theory” in which the saline ice stuck to the underlying concrete, at temperatures under its freezing point, experiences higher shrinkage than concrete due to its thermal expansion coefficient which is about 5 times higher. The stresses to which ice is submitted produces cracks; these cracks are further propagated to the concrete which exfoliates producing flakes.

This mechanism works well for very low temperatures below the normal water freezing point. However, it does not explain scaling damage that has been observed to occur at low temperatures but

some degrees above 0 ^{o}C [14]. The deleterious mechanism of chloride attack on cementitious materials at low temperatures from a chemical point of view has also been suggested. Stark J. and Luidwig H.-M. [15], observed the dissolution of metastable calcium carbonate in presence of sodium chloride in carbonated BFS concretes subjected to freezing. They found a scaling rate 2 times larger in 55% BFS carbonated concrete which showed lower capillary porosity than the equivalent OPC carbonated concrete.

The synergetic effect that chloride attack could develop in combination with carbonated materials is not very well understood.

1.1.3.Chloride ingress in mechanically loaded concrete

One distinguishing feature presented by hardened concrete is its porosity. The nature of openings in cement paste depend on different conditions. For instance, the type of cement and binder along with their physical and chemical characteristics shape the porous nature of this material. Furthermore, other conditions such as water/binder ratio, hydration time, curing temperature, and aggregate/paste ratio also outline the nature of this more or less changeable assembly. Micro-structure can be modified in time due to external factors of chemical and physical nature. Some of them can be considered aggressive and affect the durability of concrete. In contrast others help to improve the pore system. Concretes at field sites commonly have their voids partly occupied by solutions. Water containing salt can enter the concrete pores by capillary absorption. This process is also called convection. The penetration magnitude of convection will be governed by other material features for example the size of the pores, existence of cracks and initial saturation degree. Once harmful salts have gone into the pore system they can travel further inside through diffusion, the degree of salt ingress is captured in the so-called diffusion coefficient. It depends not only on voids volume and size and amount of saturation, but also on the physicochemical nature of the cement or binder gel and its interaction with the aggressive ions in solution. Movement of ions into concrete is also influenced by cycles of wetting and drying, pressure and temperature. These factors contribute to the complexity of ionic transportation into the concrete.

The volume of pores in concrete is always changing, sometimes due to an on-going paste hydration and another time it is modified by its deterioration. It also can be considerably modified by an applied load to the concrete. Consequently, it is probable that the movement of deleterious ions into concrete by convection and diffusion may be altered by the type and magnitude of the load applied to it. For instance, the velocity of chloride ingress could increase by a factor of 2 under the influence of an applied tensile stress [16,17]

Chloride movement produced by convection and diffusion is depressed when a slight compressive load is applied to concrete [18,19]. Contrarily an opposite effect is observed when the applied load exceeds a certain threshold level. In saturated concrete this value is understood to occur at stresses levels lower than the critical which is usually determined in non-saturated state. Usually, when 30 or 50 % of the concrete's full compressive capability is surpassed, some micro cracks are created. These fresh pathways give an increase to the chloride intrusion. Under direct tensile load the rate of chloride infiltration surges gradually as the load is increased. While in splitting tensile loading, a threshold level must be surpassed to increase the chloride transport into concrete.

The proposition of this research is not only to analyse the chloride ingress into loaded concrete from a physical point of view. Conversely, the high chemical interaction that chloride ions have with cementitious binders it is well known. To compare these influences, concretes made of ordinary Portland cement (OPC), high sulfate-resistant cement (HSR) and OPC with 2 replacement levels of blast furnace slag (BFS) were exposed to a 3% sodium chloride solution while maintaining concrete specimens under permanent compressive and splitting tensile loads.

1.2 Research significance

After Joseph Aspdin had patented cement in 1824, concrete has become the preferred building material due to its excellent mechanical properties and low cost. For this reason, this material is the most consumed by mankind after water. The global construction needs are on the rise. For the year 2050, a world cement production of around 5.8 x 10^9 tons is expected as shown in Figure 1-1 [20].

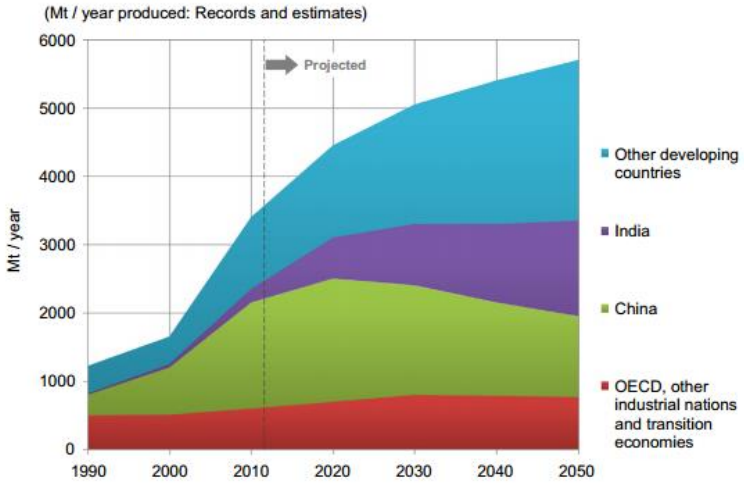

Figure 1-1: World cement production since 1990 and its projection up-to the year 2050 [20].

However, this high demand brings along some challenges the cement industry must deal with. Among others, exhaustion of fossil fuels, shortage of raw materials, increasing environmental concerns connected to climate change and a damaged world economy.

Supplementary cementitious material (SCM) has been defined by RILEM committee TC-SCM, as "inorganic material that, when used in conjunction with Portland cement, contributes to the properties of the hardened concrete through chemical reaction e.g. hydraulic or pozzolanic activity". These materials, finely ground and intermixed with OPC in the presence of water plus an appropriate curing, can improve the fresh and hardened properties of concrete. Among such materials are: fly ash (FA), ground granulated blast furnace slag (BFS), silica fume (SF), calcined clay and natural pozzolans. Another characteristic of this material is its considerable lower footprint

regarding CO_2 emission compared to that of OPC which is around 1 ton of this gas per 1 ton of OPC produced.

Therefore, the use of these materials as partial substitution for Portland clinker can help to somewhat relieve the great future demand of cement. The use of SCMs as a replacement for cement clinker is on the rise. In 2003, the world average use of clinker in cement (in percentage by weight) was 85, in 2010 around 77 and this amount is projected to further decrease in (2050) to 71 (Schneider "et al." (2011), International Energy Agency "Cement Road Map"). Increasing the utilization of SCMs in concrete brings another challenge to the construction industry. The trends towards the use of new materials bring laterally the necessity of working with concrete that may vary from its familiar properties. In this context, durability issues may come along with SCMs usage. That is why durability research on concrete elaborated with SCMs will be crucial for the coming developments.

Traditionally, durability design of concrete has been made considering a dominant deteriorating process present at the site where the expected structure is going to be situated. However, it has been recognized that the resulting deterioration that concrete structures face is far beyond the effects of a single process working independently. The resulting process depends on several other processes, which may act in parallel or successively. Consequently, there is a need to consider the combined action of mechanical and environmental loads to make a more accurate approach to real conditions.

1.3. Objective

The research topic is focused on the study of two combined actions affecting concrete durability. The first study considers the influence of carbonation on subsequent frost action with deicing salt. The second investigation deals with the chloride penetration into concrete when this material is under permanent compressive or splitting tensile loads.

Figure 1-2 [21], presents a summary of the types of concrete deterioration. There are two broad categories of deterioration: (i)

degradation of concrete; (ii) corrosion of steel reinforcement. The same graph classifies the causes of (i) and (ii).

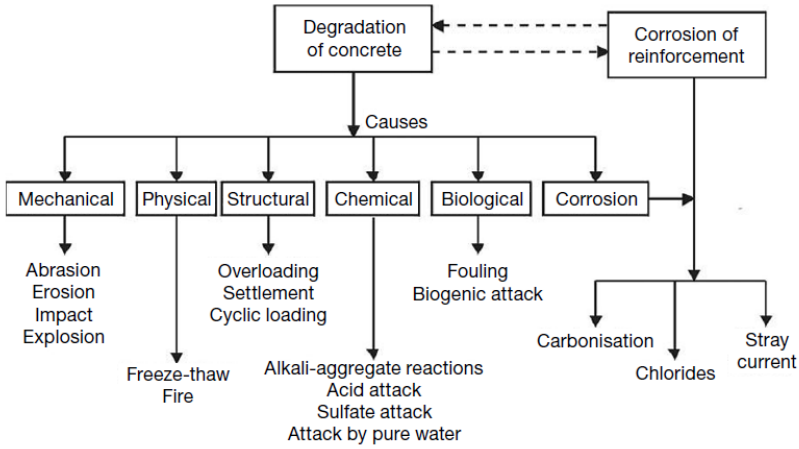

Figure 1-2: Deterioration in concrete and its causes (Carbonisation = Carbonation)[21]

This classification is a good approach to identify which cause corresponds to a type of deterioration process. Nevertheless, the picture seems to be more complex in the case of several causes interacting in the same process. Here, the action of the freeze-thaw process has been classified as executed by a physical cause which is responsible of concrete degradation. The classification of causes follows a narrow border, whereas more than one cause can take part or in the same process. That could mean for instance, that a chemical and a physical cause could be interrelated and form part of the same deterioration process.

There is evidence that severe damage to concrete in the presence of deicing salt has been seen to occur at low temperatures but above the water freezing point [14]. Consequently, the physical action of ice should not be considered as a deteriorating cause for this situation.

This research tries to identify the link between the carbonated products of concrete, deicing salt and low temperatures that could explain this deterioration process.

The study also analyses the role of BFS in the performance of the studied concretes.

For the second part of the research, a series of tests have been performed to assess the influence of an applied load on the rate of penetration of chlorides into concrete.

For the compression tests, OPC concrete prisms were subjected to a combination of permanent compression of 0, 50 and 60 % stress levels while being exposed to a 3% sodium chloride solution.

Additional concrete mixtures were made with OPC, HSR (high sulfate resistant cement), and 2 replacement levels of OPC by BFS of 50 and 70 %, and were tested in splitting tensile condition plus chloride attack.

The Magnel laboratory of Ghent University was part of the five laboratories that were involved in a Round-Robin test organized by the RILEM committee TC 246-TDC on "Durability of Reinforced Concrete Structures under Combined Mechanical Loads and Environmental Actions", where equivalent materials were used to replicate the combined conditions of chloride penetration and mechanical load and compare the results. The results were presented in the publication "Test methods to determine durability of concrete under combined environmental actions and mechanical load: final report of RILEM TC 246-TDC", in Materials and Structures (2017) 50:123. Ghent University had the responsibility of analyzing the experimental data obtained by all laboratories and writing in chapter 3 the section 3.1 corresponding to the compression results. Considering the importance of the results and its connection with present research, the previously cited work is presented as an introduction to Part IV on combined actions in chapter 5 of this thesis.

1.4. Outline of this thesis

The outline of this thesis is presented in Figure 1-3.

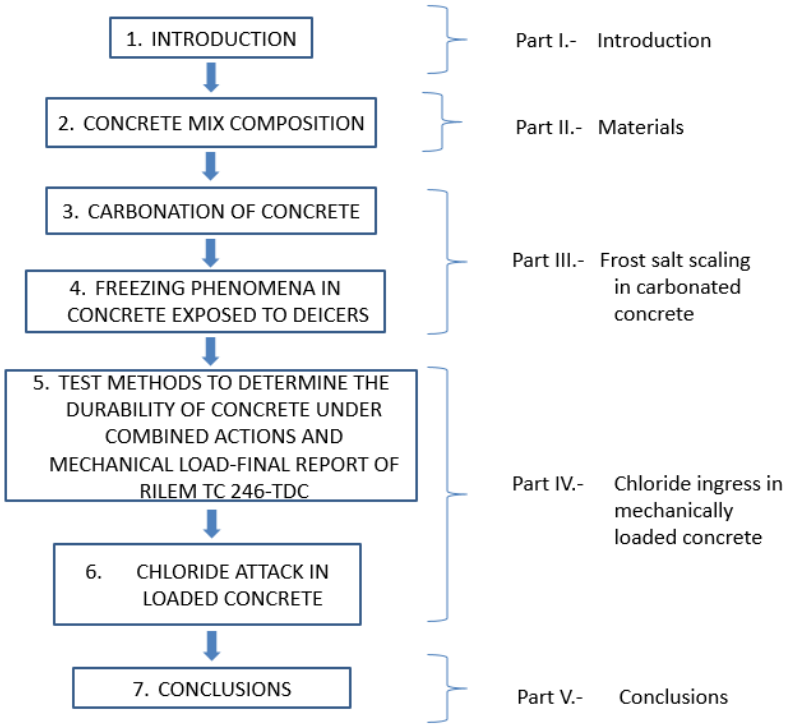

Figure 1-3: Thesis outline.

The research is divided into 5 parts. Part I gives an introduction about the research significance and the objective of the study (Chapter 1).

Part II, shows the material characterization and the concrete mixtures utilized in the tests (Chapter 2).

Part III, deals with the frost scaling phenomena in carbonated concrete. This part is divided into chapter 3 that comprises the carbonation tests on 4 types of concretes and their characterization. Subsequently, chapter 4 deals with the freezing phenomena occurring in previously carbonated concrete and in the presence of a deicing salt.

Part IV, comprises the study of the chloride ingress of mechanically loaded concrete. It is divided into chapter 5 which comprises the recommendation related to this combined attack from the result of a Round-Robin test performed by 5 laboratories. Chapter 6, presents the results and analysis of the chloride ingress into concrete subjected to compressive and splitting tensile loads.

Part V, includes chapter 7 which presents the conclusions and recommendations of the current research.

References

[1] https://www.britannica.com/science/aqua-regia

[2] Rodríguez-Navarro C. ""et al.", Origins of honeycomb weathering: The role of salts and wind, 1999, Geological Society of America Bulletin, 111 (8):1250–1255.

[3] Chapman R., Salt weathering by sodium chloride in the Saudi Arabian desert. 1980, American journal of science, vol. 280: 116-129

[4] Doehne E., Salt weathering: A selective review, in "Natural Stone, Weathering Phenomena, Conservation Strategies and Case Studies". Siegesmund S. ""et al." " ed., 2002, The Geological Society, London.

[5] Hansson C., Poursaee A., Jaffer S., Corrosion of reinforced bars in concrete, The Masterbuilder, December 2012: 106-124 www.masterbuilder.co.in

[6] Vollpracht A. ""et al." ", The pore solution of blended cements: a review. Materials and structures. 2016; 49 (9): 3341-3367.

[7] Rosenberg A., Hansson C. and Andrade C., Mechanisms of Corrosion of Steel in Concrete; 1989, The Materials Science of Concrete, J. Skalny, Editor, The American Ceramic Society, pages 285-313.

[8] Martin-Perez B., SERVICE LIFE MODELLING OF R.C. HIGHWAY STRUCTURES EXPOSED TO CHLORIDES, 1999, PhD thesis, University of Toronto.

[9] Setzer M.J., Micro-ice-lens formation in porous solid, 2001, Journal of Colloid and Interface Science 243: 193–201.

[10] Powers T.C., The mechanisms of frost action in concrete, Stanton Walker, Lecture Series on the Material Science, 1965.

[11] Litvan G.G., Frost action in cement paste, 1973., Materials and Structures, 34, July–August

[12] Pigeon M, R. Pleau, Durability of concrete in cold climates, 1995.

Modern Concrete Technology, E&FN Spon,

[13] Valenza II J, Scherer G. Mechanism for Salt Scaling. 2006, J. Am.Ceram. Soc.; 89(4): 1161-1179.

[14] Collepardi M. “et al.”, Durability of concrete structures exposed to $CaCl_2$ based deicing salts, 1994, in: V.M. Malhotra (Ed.)

[15] Stark J. and Ludwig H.-M., Freeze-deicing salt resistance of concretes containing cement rich in slag, in: Frost resistance of concrete, 1997, Setzer M. and Auberg R. ed., E & FN Spon publish., London.

[16] F. H. Wittmann, T. Zhao, F. Jiang, and X. Wan (2012) Influence of combined actions on durability and service life of reinforced concrete structures exposed to aggressive environment, Restoration of Buildings and Monuments 18: 105-112

[17] X. Wan, F. H. Wittmann, and T. Zhao (2011) Influence of mechanical load on service life of reinforced concrete structures under dominant influence of carbonation, Restoration of Buildings and Monuments 17: 103-110

[18] Jiang F., Wittmann F.H., Zhao T., Influence of Sustained Compressive Load on Penetration of Chloride Ions into Neat and Water repellent Concrete, Proceeding of the first internal conference on performance-based and life-cycle structural engineering, Editors: J.G. Teng, J.G. Dai., S.S. Law, Y.Xia, and S.Y. Zhu, Hong Kong. 2012;992-997

[19] Yao Y. “et al.”. Test methods to determine durability of concrete under combined environmental actions and mechanical load: final report of RILEM TC 246-TDC, Materials and Structures. 2017; 50:123

[20] Imbabi M., Trends and developments in green cement and concrete technology. 2012, International Journal of Sustainable Built Environment (1): 194–216

[21] Bertolini L. “et al.”, Corrosion of Steel in Concrete. 2004, WILEY-VCH Verlag GmbH & Co. KGeA, Weinheim.Concrete ACI SP-145, 3rd CANMET/ACI International Conference, Nice, France, 107-115.

II MATERIALS

CHAPTER 2. CONCRETE MIX COMPOSITION

2.1. Materials

2.1.1. Cementitious materials.

One portion of the experimental concrete samples were elaborated utilizing an ordinary Portland cement (OPC) CEM I 52N which complies with NBN EN 197-1 (2011), and American standard ASTM C150-12 as type III (a high early strength type). A second set of concrete was made with CEM I 52.5 N HSR which complies with the previously mentioned European standard as a high sulfate resistant Portland cement and with the ASTM C150-12 as a cement type V, also named as high sulfate resistant in that standard.

Two more concrete types were made using replacements of the OPC cement by a ground granulated blast furnace slag (BFS), which meets chemical and physical requirements of NBN EN 15167-1 (2007) standard.

The chemical composition of cement and slag was determined by using wavelength dispersive X-Ray spectroscopy (WD-XRF). For Portland cement, the mineralogical composition of the cementitious phases was determined using Bogue's calculations as described in ASTM C150-12 and shown in equation (2-1).

$$C_3S = 4.071*C-(7.6*S+6.718*A+1.43*F+2.852*\overline{S} +5.188*\overline{C}) \quad (2\text{-}1)$$

$$C_2S =2.867*S-0.7544*(C_3S)$$

$$C_3A =2.65*A-1.692*F$$

$$C_4AF =3.043*F$$

Where:

C_3S	Alite	C	CaO
C_2S	Belite	S	SiO_2
C_3A	Aluminate	A	Al_2O_3
C_4AF	Ferrite	F	Fe_2O_3
$\overline{S}$	SO_3	$\overline{C}$	CO_2

Table 2-1 shows a summary of the determined properties on these materials.

Table 2-1: Chemical-mineralogical composition and physical properties of cements and slag. *Bogue calculation of mineral phases.

CONTENT %	OPC	HSR	SLAG
CaO	63.37	63.90	41.24
SiO_2	18.90	21.62	36.37
Al_2O_3	5.74	3.53	9.83
Fe_2O_3	4.31	4.05	0.26
SO_3	3.34	2.40	1.62
MgO	0.89	1.82	7.41
K_2O	0.73	0.51	0.41
CO_2	0.50	0.34	0.90
Na_2O	0.47	0.15	0.28
Cl^-	-	0.026	0.020
Sulphide	-	0.05	0.79
Ins. Resid.	0.41	0.48	0.43
Loss On In.	1.51	0.95	1.30
C_3S*	57.49	57.71	-
C_2S*	10.81	18.45	-
C_4AF*	13.12	12.32	-
C_3A*	7.90	2.50	-
OTHER PROPERTIES			
Blaine (m^2/kg)	353	447	394
Density (kg/m^3)	3122	3137	2830

2.1.2. Aggregates.

Two natural gravels size fractions (2-8 mm) and (8-16 mm) and a natural sand of a size range (0-4 mm), were used to compose the granular skeleton of the concrete mixtures. The size distribution of aggregates is shown in Figure (2-1).

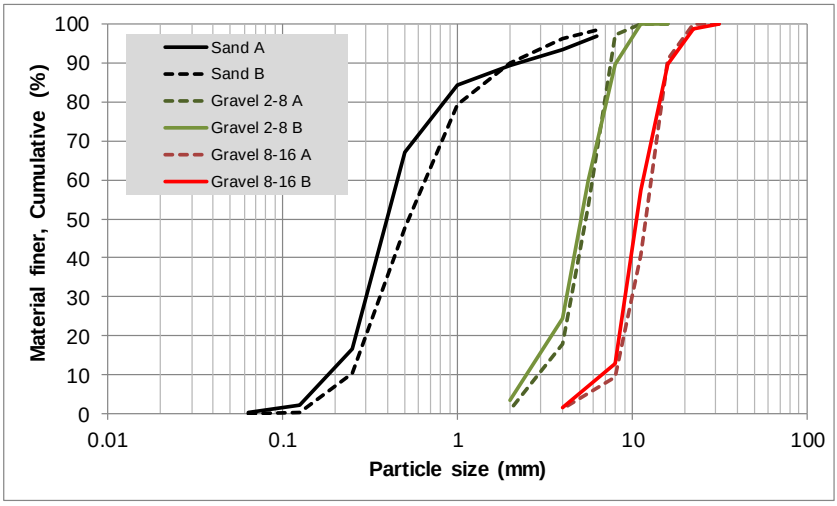

Figure 2-1: Particle size distribution of aggregates. Composed of a fine natural siliceous river sand and two quartz gravel with size fractions 2-8 mm and 8-16 mm.

The main characteristics of aggregates is their siliceous nature. Sand is composed mainly of silica which confers to this material its low absorption of 0.8%. The gravel 2-8 and the 8-16 fractions have also relatively low absorption of 1.8 and 1.1% respectively. They are composed of round clastic particles where quartz is the most abundant mineral, but also limestone is found (carbonate shells), and some igneous and metamorphic rocks which provide some silicate minerals such as feldspar, pyroxenes and mica. To have a broad view of the mineral assemblages, a weighted mixture of the aggregates representing their percentage in concrete was crushed using a press, a mill, and mortar and pestle to obtain a powdered size sample (Figure 2-2). Afterwards, an XRD test was performed to the carefully ground sample.

Figure 2-2: Preparation of aggregate composition for mineral analysis with XRD.

The XRD data were collected on a Thermo Scientific ARL X'tra diffractometer equipped with a Peltier cooled detector. Samples were measured in 2θ (CuKa radiation) scan type in a range of 5^{o} - 70^{o} initial and final angle, respectively, using an 0.02^{o} 2θ step size and 1 s/step counting time.

Subsequently, quantitative analysis was done by means of the Rietveld method for whole-powder pattern fitting to differentiate minerals assemblage; special attention was giving to the carbonate phases. Topas Academic V4.1 software was used for Rietveld refinement [1,2]. The quantified mineral assemblage is presented in Table 2-2. and Figure 2-3. In Figure 2-3, the highest intensity peaks for quartz can be observed, which occur mainly at 2Θ angles 26.62°, 20.82°, 36.52°, and 50.10°. The same intensity points can be seen for calcite, whose highest peaks are shown at a 2Θ angle of 29.42°, 39.43°, 43.19°, 47.14°-47.53°. Finally, high intensity peaks are also noticed for the zinc oxide internal standard at 31.75°, 34.42°, 36.23°, 56.54°, 62.82°, 67.88°. [3].

Table 2-2: Main mineral composition of aggregates. Determined by XRD quantification.

Aggregate composition			
Phase Name	Wt% Rietveld		Corrected
Zincite	11.40	10.00	-
Calcite	13.58	11.90	13.23
Quartz low	75.02	65.78	73.09
Other: Silicates		12.31	13.68

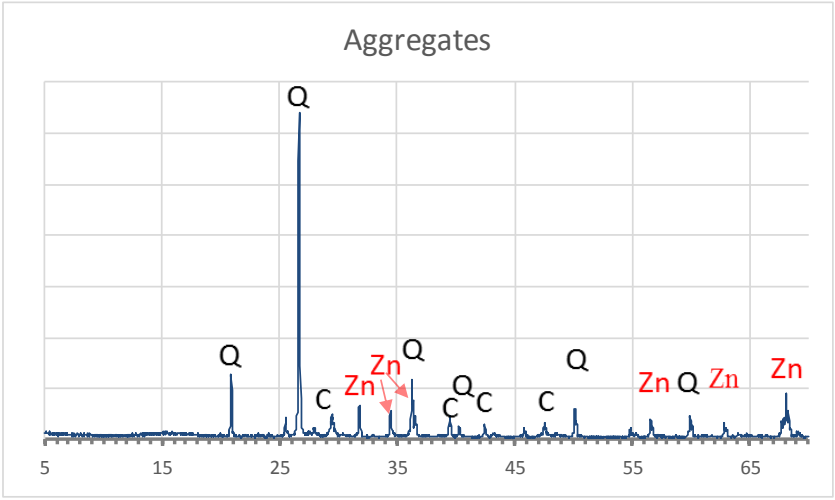

Figure 2-3: XRD pattern for aggregates combinations. Sand-grav.2/8-grav.8/16 (41.5-32.9-25.5, composition % by weight). Angles 2Θ degrees CuKα. Q: quartz, C: calcite, Zn: Zincite (internal standard)

2.1.3. High range water reducer.

A Polycarboxylic ether superplasticizer was utilized. This admixture complies with ASTM C 494 standard as type F, which can reduce the water content between 12 and 30 %. However, its function in this research was mainly to maintain flowability of concrete to a S4 type of slump (160-210 mm) according to EN 206-1 (2000), as shown in Figure 2-4. This was achieved with an amount of admixture between 0.2 – 0.4 % by weight of binder.

Figure 2-4: Fresh concrete slump test. Concrete slump class S4 (160-210 mm).

2.2. Mix design

Five concrete mixtures without specified properties regarding durability conditions were prepared for this investigation, as presented in table 2-3. The research purpose was to compare materials behaviour without analysing specification compliance.

Concrete fresh properties were evaluated according with the following standards: Slump test-ASTM C-143-00, Density (Unit weight, gravimetric method)-ASTM C 138-01, Air content (Pressure method)-ASTM C 231-01. The type of mixer utilized was a horizontal pan-type mixer with vertical shaft, with 50 dm^3 nominal capacity.

Room conditions for batching were; 21 $\pm 2^{\circ}$ C, relative humidity 70$\pm$5%.

The following mixing order for the materials and used times were as follow:

- 1 minute of dry mixing of aggregates and binder.

- 2 minutes wet mixing with all the water content minus 50 ml of the batch water to be used for rinsing the admixture container.
- 1 minute for checking bottom edges from the mixer for dry unmixed mixtures. Re-mixing.
- 1 minute of additional mixing pouring the admixture to obtain final slump.

The slump test was taken 8 minutes after starting the mixing of the batch. Subsequently, air content and density was measured from the fresh concrete. Concrete test samples were cast on the test moulds and then compacted using a vibrating table between 1 and 1.5 minutes, depending on concrete flowability. After compacting the samples, they were transported in a pallet with a lifter towards the curing room and maintained at 20 $\pm$2° C and ≥95% relative humidity.

Mixtures proportions were corrected fitting them to their measured fresh density (unit weight).

Table 2-3: Concrete mixtures with w/b : 0.45 and slump class S4.

MATERIAL TYPE	**S0**	**S50**	**S70**	**HSR**	**OPC**
CEM I 52.5 N	345	173	102	0	369
CEM I 52.5 N HSR	0	0	0	347	0
BFS	0	173	238	0	0
Water	156	156	154	157	166
Sand 0/4	771	771	759	774	840
Gravel 2/8	611	611	601	614	575
Gravel 8/16	474	473	466	476	450
Admix. (% W. Binder)	0.255	0.346	0.320	0.210	0.310
Fresh Properties					
Slump (mm)	170	180	190	160	170
Air content (%)	3.4	2.4	3.9	3.0	1.7
Density kg/m^3	2356	2356	2320	2368	2400

To produce a batch of 45 dm^3, the aggregates were taken from outside stockpiles where they were not protected from the rain. They were left over-night for drying. The following day, they have a moisture content about 80 % of the saturated surface dry condition (SSS). This state in

the aggregates provokes a reduction of about 2-3 % in the amount of mixing water. This will reduce the w/b ratio about 0.01 units. Therefore, we can assure a maximum w/b ratio of 0.45 for all the mixtures.

Former research at the Magnel Laboratory already used these concrete mixtures for durability studies such as combinations of sulphate and chloride attack and others [4-6].

References

[1] Coelho AA. Topas Academic Version 4.1, 2007. Available at: http://www.topas-academic.net. 2012.

[2] Snellings R, De Schepper M, De Buysser K, Van Driessche I, De Belie N. Clinkering Reactions During Firing of Recyclable Concrete. J Am Ceram Soc. 2012; 95(5): 1741-9.

[3]. Downs, R.T., K.L. Bartelmehs, G. V. Gibbs, and M. B. Boysen, Jr. Interactive software for calculating and displaying X-ray or neutron powder diffractometer patterns of crystalline materials. American Mineralogist. 1993; 78: 1104-1107.

[4] Maes M, De Belie N. Resistance of concrete and mortar against combined attack of chloride and sodium sulphate. Cement and Concrete Composites J. 2014; 53: 59-72.

[5] Maes M, Gruyaert E, De Belie N. Resistance of concrete with blast-furnace slag against chlorides, investigated by comparing chloride profiles after migration and diffusion. Materials and Structures J. 2013; 46(1-2): 89-103

[6] Gruyaert E, Van den Heede P, Maes M, De Belie N. A comparative study of the durability of ordinary Portland cement concrete and concrete containing (high) percentages of blast-furnace slag. RILEM proceedings; PRO 77: 241-251.

III FROST SALT SCALING IN CARBONATED CONCRETE

CHAPTER 3. CARBONATION OF CONCRETE

The development of chapters 3 and 4 have considered part of the content published by: HUGO EGUEZ ALAVA, ELENI TSANGOURI, NELE DE BELIE, GEERT DE SCHUTTER, "Proposed mechanism for the formation of oxychloride crystals during sodium chloride as a deicer salt in carbonated concrete". Construction and Building Materials 109 (2016) 188-197

3.1. Background

There are several mechanisms that can deteriorate reinforced concrete and reduce its service life.

One common aggressive mechanism acting in concrete is carbonation, a process occurring when CO_2 diffuses through it and reacts with some cement hydration products such as calcium hydroxide (CH) and calcium silicate hydrates (CSH), to produce calcium carbonate in the presence of water. Equation (3-1) presents a summary of calcium hydroxide carbonation [Gruyaert et al (2011).

$$CO_2 + H_2O \rightarrow H_2CO_3 \qquad (3\text{-}1)$$
$$Ca(OH)_2 + H_2CO_3 \rightarrow CaCO_3 + H_2O$$

In the first part of equation (3-1), gaseous carbon dioxide is continuously supplied by air and during its slow diffusion into water it dissociates to the pH dependant species HCO_3^- and CO_3^{2-} as the pH increases. In the second part of the equation and at certain pH value, CO_3^{2-} ions react with Ca^{2+} ions to precipitate $CaCO_3$ [Thiery “et al.” (2017), Borges “et al.” (2010)].

Portlandite (CH) is not the only source of calcium to form carbonates. Calcium silicate hydrates (CSH), hydrated calcium aluminates and ferro-aluminates also react with CO_2 to form some types of carbonates, silica gel and hydrated oxides of aluminium and iron [Parrot (1987), Borges (2010)].

Since CSH is the main product in hydrated cement paste, its carbonation is important. The reaction products are $CaCO_3$ and silica

gel [cited by Thiery (2007)]. The carbonation of CSH is presented in equation (3-2) [Gruyaert (2011), Van den Heede (2014)].

$$(CaO)_x.(SiO_2)_y.(H_2O)_z + x.CO_2 \rightarrow CaCO_3 + (SiO_2)_y.(H_2O)_{z-w} + w.H_2O \quad (3\text{-}2)$$

The carbonation of CH reduces the porosity of cement paste due to the volume increase of this product. Calcite is between 11-12% greater in volume than original CH [Borges "et al." (2010). However, the carbonation of CH and CSH occur simultaneously [Grooves "et al." (1991), Thiery "et al." (2007)]. When calcium is removed from CSH by carbonation, a re-assemblage of the silicate chain is produced by polymerization. This re-arrangement comes along with a volume decrease that causes cracking and growth of the pore structure [Chen et al (2006), Borges "et al." (2010).

Formerly studies made by Papadakis "et al." (1989) [1], stablished a reaction model to explain a semi-empirical equation that correlated carbonation depth with the squared root of exposition time. The carbonation vulnerability of a concrete depends mostly on the facility that carbon dioxide has for diffusion and on the amount of carbonatable matter available. Visser (2010) cited equation (3-3) to estimate carbonation.

$$x_c = \sqrt{(2.D_c.C_s.t)/a_c} \quad (3\text{-}3)$$

Where:

$x_c = carbonation\ depth\ (m)$

$D_c = diffusion\ coefficient\ of\ CO_2\ (m^2/s)$

$c_s = the\ CO_2\ concentration\ at\ concrete\ surface\ (\frac{kg}{m^3})$

$a_c = the\ amount\ of\ carbonatable\ matter\ per\ volume\ (\frac{kg}{m^3})$

$t = time\ (s)$

Besides calcium and hydroxyl ions present in the pore solution of concrete, the ability of CO_2 diffusion into concrete interior is important for the carbonation reaction rate. It has been observed that the best

environmental conditions occur at a relative humidity within the 50-70% range [1-3]. In such conditions, the pore system in concrete is not fully saturated and air can easily penetrate carrying carbon dioxide to deep sites. Also, the pore system has the water content needed for the reaction. At relative humidity, lower than 50 % the reaction is diminished by the lack of water needed to dissolve Calcium hydroxide or the CO_2 needed to react. While at R.H. higher than 70% the reaction is also hindered, due to the slow diffusion of the gaseous phase in a near-saturated condition. The carbonation rate is accelerated with temperature. Consequently, higher carbonation rates are expected in relatively high temperature environments.

Also, deduced from equation (3-3), another parameter that affects carbonation is the concentration of CO_2 in the air. In the atmosphere, this value is 0.03%. But in industrial zones, tunnels and bridges this value can exceed even 0.1% [4]. The carbonated front progresses proportionately to the square root of CO_2 concentration [1] and the carbonation depth also increases with the square root of time [5-7].

In non-carbonated cement paste, the high alkalinity of the pore solution (pH ≥ 13) is responsible for the passivation and protection against corrosion of the steel reinforcement. A thin layer of oxide and hydroxide protects the metal in such conditions [Thiery “et al.” (2007)]. ACI 201.2R-08 (Guide to durable concrete) reports that the pH of carbonated pastes can be reduced to values lower than 9. Carbonation can induce corrosion of the reinforcement, as the lower pH leads to removal of the passive film that protects the reinforcement surface.

Corrosion products may grow in volume up to almost 5 times the initial metal volume as shown in Figure 1 and the expansive force derived from this volume increase easily leads to tensile stresses that exceed the low tensile strength of concrete, causing cracking. Corrosion is enhanced after chloride ions reach the concrete rebar through diffusion. This case is typically found in concrete which is in contact with chloride bearing environments.

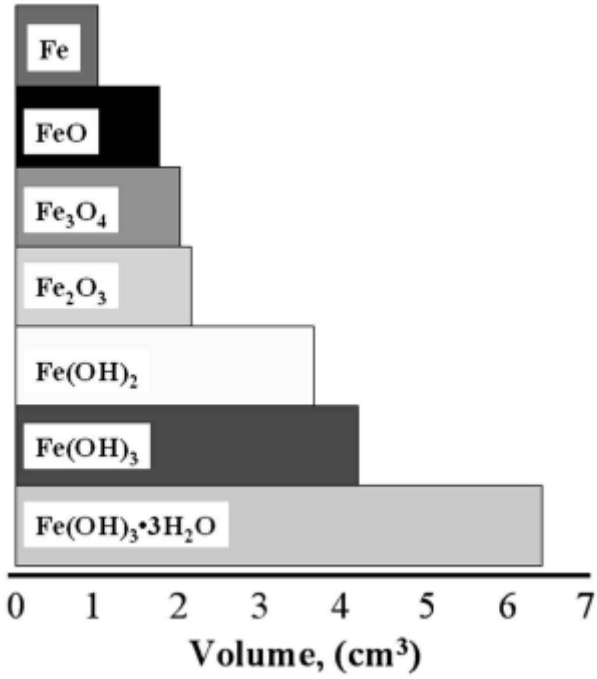

Figure 3-1: The relative products of iron and its reaction products. Source. - ACI 222R-1 "Protection of metals in concrete against corrosion".

Another type of deterioration that involves volume increase inside hardened concrete, is the effect of water and de-icing salts. Expansion and scaling is produced on concrete surface during freeze and thaw cycles.

Although the surface scaling mechanism is not yet fully understood, it is generally believed that the deleterious action of deicing salts is mainly physical in nature and that chemical reaction of salts with cement hydration products just plays a minor role in the deterioration mechanism. This assumption seems to be in contraposition with the work obtained by Verbeck and Klieger whose results indicate that despite the type of deicer, a relatively low concentration (2-5 %) produces more surface scaling damage than a higher concentration or pure water [8]. On the other hand, the frost scaling performance of

uncarbonated concrete is considered good. However, its resistance is considerably affected by carbonation and the presence of deicing salts.

There is some indication that contradicts the general belief that the major single mechanism that contributes to frost-scaling damage is purely mechanical. One indication is the experimental evidence of scaling deterioration on concrete that has been exposed to chloride deicers at temperatures just above freezing without the influence of ice formation [9,10]. Another indication is given by some recent ideas on the role of carbonation in the salt scaling damage to concrete [11]. These facts are suggestive of another deterioration mechanism besides mechanical damage that is occurring at low temperatures.

Thus, carbonation plays an important role in concrete deterioration. However, the question that stands out would be, what type of cementitious material is most affected by carbonation.

Due to the larger amount of CH found in hydrated OPC pastes, CH carbonation seems to be the most important reaction in these binders. Calcite shows to be the main product of Portland cement paste carbonation. The larger volume produced by calcite compensates any shrinkage from CSH carbonation [Sisomphon “et al.” (2010)]. On the contrary, binders which partially replaced OPC by a supplementary cementitious material (SCM’s) have been found to develop higher porosities after carbonation [De Ceukelaire and Van Nieuwenburg (1993)].

3.2. Sample preparation, curing and exposure conditions

The motivation of current investigation is twofold. Primarily, analysing the comparative susceptibility towards carbonation between concretes made with different types of binders. Secondly, studying the influence of the carbonated samples towards the frost resistance in the presence of a deicing salt environment.

Four concrete mixtures (S0, S50, S70, and HSR) shown in table (2-3), were prepared for carbonation exposures.

After mixing, concrete was cast in cylindrical molds (diam. 100 mm, h. 100 mm). Subsequently, 7 days of wet curing at 20 °C and RH > 95% was applied (Figure 3-2) followed by 21 days at 20 ± 2 °C and 60 ± 5 % RH.

The intention was to apply a relatively short interval of wet curing to the concrete, followed by a comparatively dry period condition. In this way, it was attempted to replicate a real curing situation, as is commonly found at job site.

Figure 3-2: Cylinders at curing chamber, 7 days at 20 °C and RH > 95%

3.2.1. Accelerated and natural carbonation exposures.

After curing, adhesive aluminum foil was glued to the external cylinder's surfaces, leaving only 2 faces (top and bottom faces) uncovered to permit free CO_2 exposure only to these two uncovered faces. At least 18 cylinders representing each type of concrete were exposed to a 10 % CO_2 concentration in a carbonation chamber (Figure 3-3, left), while a similar number were exposed to natural carbonation, in a climate controlled room (Figure 3-3, right). For both exposure conditions, the samples were maintained at 20 ± 2 °C and 60 ± 5 % RH until the time for testing.

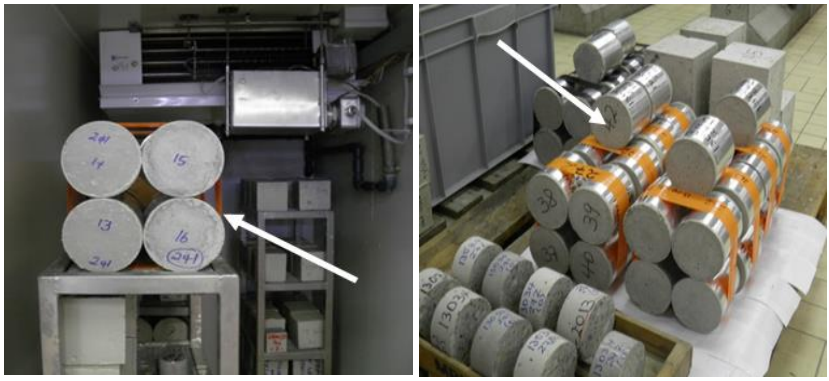

Figure 3-3: Cylinders with 2 exposed faces at 20 ± 2 °C, 60 ± 5 % RH and natural CO_2 in a climate controlled room.

For each testing age, 3 cylinders were taken out from the curing place (accelerated and normal carbonation), each sawn parallel to the exposed surfaces into 2 half cylinders (diam. 100 mm, h. 50 mm) and the aluminum foil was removed (Figure 3-4).

Figure 3-4: Cylinder cutting operation. One half of the cylinder is used to characterize carbonation depth, the other half for frost scaling studies on the remaining carbonated face.

Half of the carbonated discs were utilized to measure the carbonation depth in a freshly split surface made perpendicular to the exposed face. The carbonated front identification was done using phenolphthalein solution. The other half of the cylinders, were utilized to study the frost scaling resistance with deicing salts in carbonated and no-carbonated samples. This latter topic is discussed in the following Chapter 4.

3.2.2. Paste extraction for X-ray diffraction analysis (XRD)

After one year of CO_2 exposure, carbonated and non-carbonated concrete's hardened paste was extracted for mineral composition determination, this was done by separating by wet cutting the samples at the location of the carbonated front after phenolphthalein identification (Figure 3-5).

Figure 3-5: Carbonated slice, separated by cutting, for XRD analysis

The non-carbonated paste was extracted from cubic samples corresponding to the same concrete batch. Here a core (diam.= 70 mm, h= 150 mm) was extracted from the center of one face. Afterwards the two 40 mm edges of the core were removed to avoid carbonated paste contamination (Figure 3-6).

Figure 3-6: Uncarbonated sample taken from the middle part of a core

The paste was obtained by crushing the remaining core using a hydraulic press followed by wet grinding in plastic cylindrical containers on two moving rollers. The purpose of wet grinding was to loosen the hardened concrete paste through friction and rubbing action between aggregates and its adhering paste while keeping the crushed concrete's particles immersed in isopropanol. Afterwards fine particles were separated by wet sieving in isopropanol solution using a sieve of 63 micrometre size opening. The obtained paste (finer than 63 micrometre) was treated by vacuum drying (Figure 3-7); the collected powdered samples were kept in air free containers which had lime pellets to avoid carbonation while waiting for the XRD tests.

Figure 3-7: Extracted cement paste from concrete, for XRD analysis.

To perform the XRD-analysis, the one year cured carbonated and non-carbonated powders extracted from the concrete samples were mixed with 10% by weight ZnO used as an internal standard, the sample was prepared using a mortar and pestle to obtain a homogenized 2 g size sample. The XRD data were collected on a Thermo Scientific ARL X'tra diffractometer equipped with a Peltier cooled detector. Samples were measured in 2θ (CuKa radiation) scan type in a range of 5° - 70° initial and final angle, respectively, using an 0.02° 2θ step size and 1 s/step counting time.

Subsequently, quantitative analysis was done by means of the Rietveld method for whole-powder pattern fitting to differentiate minerals assemblage. Special attention was giving to the carbonate phases. Topas Academic V4.1 software was used for Rietveld refinement [12, 13].

3.3. Experimental results

3.3.1. Carbonated front determination

The carbonation was measured on the sample's freshly split surface, spraying a solution made of 1% phenolphthalein in 70% ethyl alcohol. The carbonated surface is colourless while the non-carbonated zone turns purple (at pH between 8-9.8 or higher) due to the presence of free metal hydroxides. The carbonated depths for accelerated 10% CO_2 and environmental exposures taken from 3 specimens per concrete type were measured. A one-way ANOVA analysis was performed to determine if the means obtained from different specimens were significantly different from each other. In all cases a level of significance of 0.05 was used. After the analysis, it was found that in most cases the mean carbonation depths per sample of each group were not significantly different from each other. Therefore, always the average and overall standard error per three samples were considered for further evaluation. The results are shown in Fig. 3-8 and 3-9. In the graph the carbonation depth "y" (mm) is plotted against the square root of the CO_2 exposure time "T" (in days), to obtain the carbonation coefficient "A" which is the slope of the straight line and y_o is the initial carbonation depth at the beginning of the carbonation exposure as presented in equation (2) according to Borges "et al." [14], ($in\ our\ case, y_0 = 0$ for t=0).

$$y = y_0 + A\sqrt{t} \qquad (3\text{-}4)$$

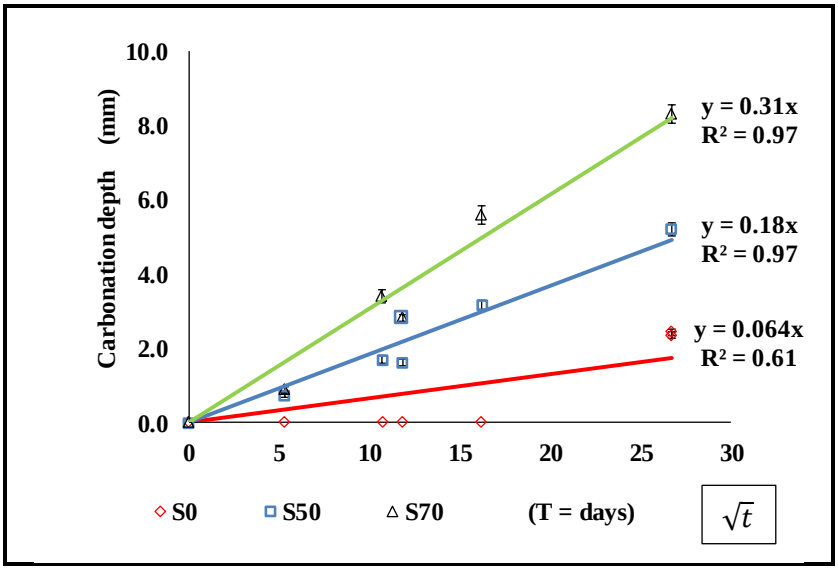

(a)

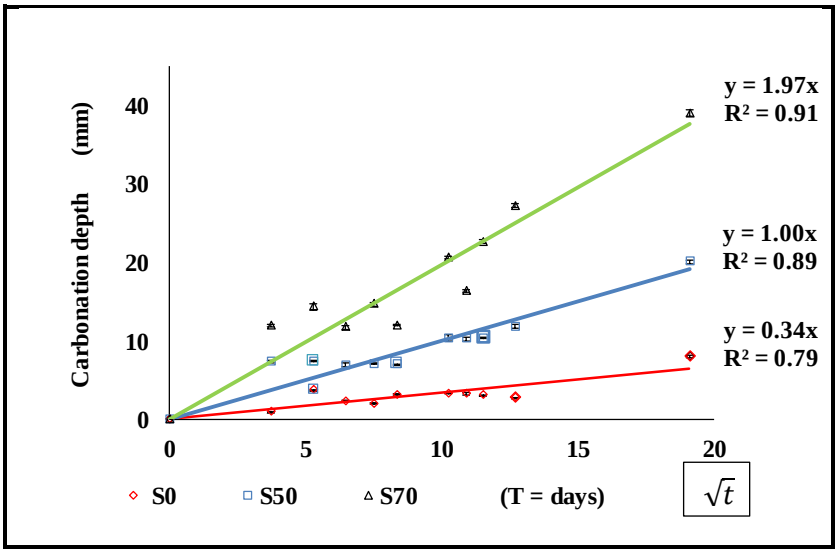

(b)

Figure 3-8: Carbonation depth of concrete exposed to natural carbonation (a) and 10% CO_2 (b) vs. the square root of time (error bars show standard error, n=29).

The results show that concrete's sensibility to carbonation increases with increasing slag replacement content, while the reference concrete (with slag/binder ratio, s/b = 0) during the test period has a low carbonation coefficient which means that its carbonation rate is very slow. The carbonation rate for concretes with 70 % slag replacement was between 5.8 and 4.8 higher than the rates found for the Portland cements submitted to accelerated and normal CO_2 conditions respectively, while the carbonation rates found for concretes with 50 % slag replacement were between 2.8 and 2.9 times higher than those found for the HSR and S0 subjected to accelerated and normal exposure.

No noticeable differences between their carbonation rates was noticed for HSR and S0.

3.3.2. Open porosity characterization

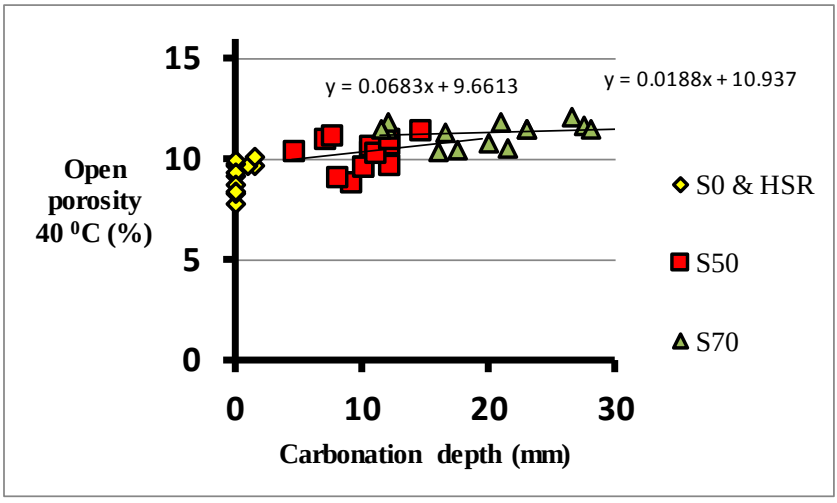

(a)

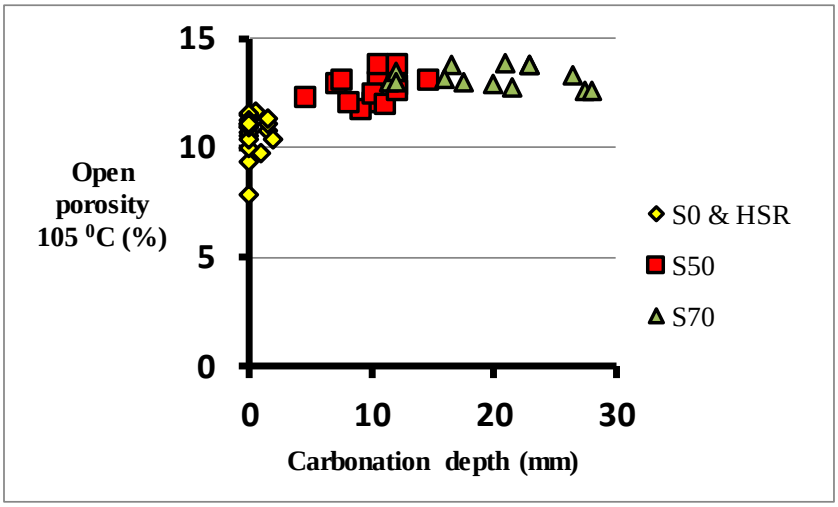

(b)

Figure 3-9: Open porosity of BFS **c**oncretes (s/b = 0., 0.5, 0.7) subjected to 10% CO_2 as function of the exposure time, determined after drying at 40 ^oC (a) or 105 ^oC (b).

Carbonated samples, half cylinders (Ø 100 mm, h 50 mm) were oven dried at 40 ^oC and 100 ^oC until constant mass (< 0.1 % @ 24h) before vacuum saturation according to NBN B05-201 paragraph 6.1 (1976), the corresponding porosity was then calculated by hydrostatic weighting (air & water), the obtained results are shown in Figure 3-9.

The open porosity at 40 ^oC gives a rough estimate of what is happening with capillarity after the samples are exposed to accelerated carbonation, thus capillary porosity tends to increase after CO_2 exposures for samples S_{50} and S_{70}, while average porosity for S_o concrete has remained almost unchanged. On the other hand, overall concrete porosity at 105 ^oC, seems to remain unaltered in all the samples.

3.3.3. X ray diffraction (XRD)

Tables 3-1 and 3-2 show the main mineral assemblage obtained after XRD analysis for carbonated (0.03 % & 10 % CO_2) and non-carbonated Portland and BFS concretes respectively, after 1 year of exposure.

Table 3-1: One year non-carbonated ($_N$) and carbonated ($_{0.03\%;\ 10\%}$) high sulfate resistance (HSR) and OPC (S0) concretes, (A) and (B) two different specimen, assemblage of main minerals after XRD Rietveld quantification.

Phase %	**HSR_N**	**$HSR_{0.03\%}$**	**$S0_{N-(A)}$**	**$S0_{N-(B)}$**	**$S0_{0.03\%}$**	**$S0_{10\%}$**
C4AF	3.0	6.7	4.2	4.7	3.4	3.5
Portlandite	21.1	-	18.6	19.8	-	-
Ettringite	-	-	7.6	4.9	-	-
Calcite	-	4.9	-	-	24.1	32.6
Vaterite	-	29.2	-	-	29.5	19.8
Other	75.9	59.1	69.7	70.6	43.1	44.1
Calcite+Vaterite	-	34.2	-	-	53.5	52.4
Calcite/Vaterite	-	17.0	-	-	82.0	164.0

Table 3-2: One year non-carbonated ($_N$) and carbonated ($_{0.03\%;\ 10\%}$) 50 and 70 % blast furnace slag replacement (S50 and S70) concretes, assemblage of main minerals after XRD Rietveld quantification.

Phase %	**$S50_N$**	**$S50_{0.03\%}$**	**$S50_{10\%}$**	**$S70_N$**	**$S70_{0.03\%}$**	**$S70_{10\%}$**
C4AF	1.4	1.8	1.1	1.0	0.7	0.9
Portlandite	8.3	-	-	4.4	-	-
Ettringite	3.9	-	-	4.8	-	-
Calcite	-	11.0	10.6	-	5.2	7.7
Vaterite	-	33.8	34.3	-	43.1	42.2
Other	86.4	53.4	54.0	89.8	51.0	49.2
Calcite+Vaterite	0.0	44.8	44.9	0.0	48.3	49.9
Calcite/Vaterite	0.0	32.5	31.0	0.0	12.0	18.3

A summary of Portlandite (CH) and carbonates contents and their correlations are shown in table 3-3.

Table 3-3: Portlandite (CH) and carbonates correlations for non-carbonated ($_N$) and carbonated (0.03 and 10 % CO_2) samples; from high sulfate resistant (HSR), ordinary Portland cement (S0), 50 and 70 % blast furnace slag (S50, S70) concretes, after XRD Rietveld analysis, 1 year exposure.

Uncarbonated (1 Yr.)	**HSR_N**	**Ave. $S0_N$ Samp. A & B**		**$S50_N$**		**$S70_N$**	
CH content %	21.1	19.2		8.3		4.4	
Carbonated (1 Yr.)	**$HSR_{0.03\%}$**	**$S0_{0.03\%}$**	**$S0_{10\%}$**	**$S50_{0.03\%}$**	**$S50_{10\%}$**	**$S70_{0.03\%}$**	**$S70_{10\%}$**
Carbonates ratio Calcite/Vaterite %	17.0	82.0	164.0	32.5	31.0	12.0	18.3
Total Carbonates (Calcite+Vaterite) %	34.2	53.5	52.4	44.8	44.9	48.3	49.9
Carb.from CH carb. (CH * 1.35) %	28.5	25.9	25.9	11.2	11.2	6.0	6.0
Carb. from C-S-H & minor phases %	5.6	27.6	26.5	33.6	33.7	42.2	43.9
Carbonation from CH % of total carbonates	83.5	48.5	49.5	25.0	25.0	12.4	12.0
Carb. from C-S-H & minor phas. % of total carb.	16.5	51.5	50.5	75.0	75.0	87.6	88.0
Carb. ratio CSH/CH	0.2	1.1	1.0	3.0	3.0	7.0	7.3

Among the main characteristic found for non-carbonated concretes is the CH content which is high for HSR and S0 concretes (21.1 and 19.2 %) respectively, while for the slag concretes it decreases as the BFS content increases (8.3 and 4.4 % for S50 and S70 respectively). The Portlandite content follows a logic trend considering the hydration time for pure cements and the BFS replacement level.

For the carbonated concretes the total amount of carbonates fluctuates between 45 and 54 % for samples S0, S50 and S70 without noticeable trend, on the other hand HSR concrete shows a smaller carbonate content of 34 %. Two kinds of carbonate mineral were identified, one is the metastable form Vaterite and the other the more crystalline form Calcite. It was found that the ratio Calcite/Vaterite was greater in carbonated S0 concretes reaching values of 0.82 and 1.64 for 0.03 and 10 % CO_2 exposures respectively, and this ratio decreases with BFS content replacement to values of 0.33 and 0.31 % for S50 and

0.12 and 0.18 % for S70 for similar CO_2 exposures; it was also found that HSR concrete had a small Calcite/Vaterite value of 0.17 %.

To build tables 3-1, 3-2 and 3-3, it is assumed that pastes extracted from concretes that were not exposed to any of the two CO_2 conditions were free of carbonate minerals. The mineral composition shown in these tables are corrected by subtracting the amount of carbonate minerals from other sources (for example, aggregates) that were already present in these samples. This background value for carbonate was calculated for every type of concrete. Thus, non-carbonated samples are set to zero considering the carbonate background content, while carbonated samples were also corrected using this value.

Carbonate minerals found in these pastes come mainly from aggregates. Another important minerals along with carbonates were quartz and also minor amounts of feldspar. The amounts of these compounds were also subtracted in order to display only the cement related minerals. It is noteworthy that extracting the paste by the wet grinding method provides a light rubbing action between the concrete particles. This method selectively promotes disaggregation of cement paste particles and prevents the incidence of significant amounts of quartz in the extracted pulp after wet screening. Consequently, the mineralogical interference of quartz in the XRD analysis is minimized.

For the balance of carbonate minerals shown in Table 3-3, the amount of carbonate that comes from CH carbonation was calculated. This was done by multiplying the content of portlandite present in the non-carbonated phases by the stoichiometric factor of 1.35. The excess of carbonate mineral that does not originate from portlandite was generated after the carbonation of other cement phases where the CSH is the main source.

If we consider the carbonation products coming mainly from silica gel decomposition and other minor cement hydrates relative to the total amount of measured carbonate (carbonation ratio C-S-H % of total as shown in table 3-3) we may establish an increasing sensibility of the CSH to carbonation in the order HSR, S0, S50, S70 with mean values of 17-50-75-88 % respectively, the complement to 100 % being the

amount related to CH carbonation. These findings show corresponding equivalences with other parameter found in the studied concretes such as carbonation depths, open porosity and deicing scaling resistances.

3.4 Discussion

The mineral assemblage shown by XRD summarizes the amount of carbonatable matter in the studied concretes. Portland cement concretes (S0 and HSR), have high amounts of CH in their pastes. Consequently, Portlandite is readily available for carbonation. The formation of voluminous carbonates coming mainly from the available CH reaction, compensates the CSH decalcification which produces shrinkage [Sisomphon "et al." (2010)]. Therefore, the porosity can be reduced and the carbonation rate is diminished compared to BFS concretes.

On the other hand, due to a lower CH content, the carbonation of the BFS concretes would affect mostly to the CSH gel. This is also in agreement with the findings of De Ceukelaire and Van Nieuwenburg (1993), with respect to the higher porosities found after carbonation in blended cement pastes.

3.5. Conclusion

Carbonation is a complex process which depends not only on the nature of materials used to prepare the concrete, but also on the amount and proportions utilized, curing conditions and the amount of CO_2 the concrete is exposed to.

The purpose of this research is to acquire information from BFS and OPC concretes towards their de-icer scaling resistance when subjected to unfavourable conditions for hydration and the best situations for carbonation, such as a short period of wet curing, followed by a long and steady period of intermediate relative humidity. In such

circumstances BFS consumes part of the produced $Ca(OH)_2$ for its hydration and competes with CO_2 in its depletion. In this scenario and when CH is not available, carbonation of CSH is started [15] giving thus a leached microstructure, the progress of hydration is reduced. Porosity and permeability are increased enabling the ingress of more CO_2 to the system continuing the damage.

The augmented BFS concrete's porosity and permeability driven by carbonation in the concrete microstructure, provides the most unfavourable condition for its deicer scaling resistance.

References

[1] Papadakis V, “et al.”, Fundamental modeling and experimental investigation of concrete carbonation, ACI Materials journal; 1991, 88 (4): 363-373.

[2] Andrade M.C., Report on the background on carbonation of concrete structures, Institute of construction science ''Eduardo Torroja", SCIC, Madrid, 1996.

[3] Andrade C, Sarria J. and Alonso C., Statistical study on simultaneous monitoring of rebar corrosion rate and internal relative humidity in concrete structures exposed to the atmosphere. SCI proceedings, "Corrosion of reinforcement in concrete construction", 1995, Cambridge UK.

[4] Tuutti K., "Corrosion of steel in concrete", Swedish Cement and Concrete Institute", 1882, Stockholm.

[5] Morris W. “et al.”, "Practical evaluation of resistivity of concrete test cylinders using a Wenner array probe". Cement and concrete research Jour. 1996; 26 (12): 1779-1787.

[6] Holm T. “et al.”, "Carbonation of marine structural lightweight concrete", Concrete in marine environments, 1988; SP (109):667-676

[7] Baweja D. “et al.”, "Measurenments of corrosion of steel reinforcement under high chloride conditions", Fly ash, Silica fume, Slag and Natural Pozzolans in Concrete. ACI Detroit, IV Int. Conf. Malhotra ed. 1992; ACI SP 132, vol (II): 1543-1564

[8] Marchand J., Sellevold E., Pigeon M., The Deicer Salt Scaling Deterioration of Concrete-An Overview, Durability of Concrete Third International ACI Conference, Nice France, 1994; pp. 1-46,

[9] Peterson K. “et al.” Observations of chloride ingress and calcium oxychloride formation in laboratory concrete and mortar at 5 ^{o}C. Cement and Concrete Research, 2013; 45: 79-90.

[10] Sutter L, “et al.” Petrographic evidence of calcium oxychloride formation in mortars exposed to magnesium chloride solution. Cement and Concrete Research, 2006; 36: 1533-1541.

[11] Egüez H, De Belie N., De Schutter G., Proposed mechanism for the formation of oxychloride crystals during sodium chloride application as a deicer salt in carbonated concrete, Construction and Building materials, 2016; 109: 188-197.

[12] Coelho AA. Topas Academic Version 4.1, 2007. Available at: http://www.topas-academic.net. 2012.

[13] Snellings R, De Schepper M, De Buysser K, Van Driessche I, De Belie N., Clinkering Reactions During Firing of Recyclable Concrete. J Am Ceram Soc., 2012;95(5):1741-9.

[14] Borges PHR., Milestone NB., Costa JO. Carbonation of CH and C-S-H in composite cement pastes containing high amounts of BFS, Cement and Concrete Research, 2010; 40(2): 284-292.

[15] Battaglia, I., Muñoz., Cramer, S., 'Proposed Behavioral Model for Deicer Scaling Resistance of Slag Cement Concrete', Jour. of materials in Civil Engineering, 2010; 22 (4) 361-368.

CHAPTER 4. FREEZING PHENOMENA IN CONCRETE EXPOSED TO DEICERS.

4.1. Background

Some common salts preferred to melt ice in roads and bridges are the chlorides of sodium, magnesium or calcium. They are selected due to their high effectiveness and low cost, however the mentioned advantages that these salts provide are in contraposition with the notorious harm that they cause to concrete. The salt scaling damage has been well identified and consists of progressive exfoliating flakes released from concrete that has been partially saturated with salt solutions and subjected to freezing temperatures. The worst condition for damage occurs at moderate salt concentration, usually 3% by weight.

There are several proposed ideas that explain the reasons of the deterioration of concrete exposed to frost with deicing salts. Powers [1] (published in 1945, but later withdrawn by Powers himself), explains the effect that hydraulic pressure exerts on a saturated concrete. When the water freezes inside the concrete it increases 9% in volume, but the some remains of unfrozen water are expelled to the remaining pores exerting pressure. Besides, as water freezes, concentration gradients are generated in the residual unfrozen solution; this mechanism is also believed to provoke osmotic pressures that further contribute to the damage.

Hansen [2] proposed the mechanism of salt solution oversaturation in larger pores. At these sites salt crystals start to form and keep attracting more salt during their growth. The continuing salt crystallization intensifies inner pressures in the concrete microstructure.

Snyder [3] proposed that the surface and inner layers of concrete are initially frozen leaving an unfrozen high concentration solution in-between these two layers. When this latter layer starts to freeze, the

remaining unfrozen water exerts pressure on the top layer causing scaling.

More recently Valenza II and Scherer [4] presented a mechanism to explain the scaling. It was called the Glue-Spall theory in which the salty ice attached to the underlying concrete, at temperatures below its freezing point, undergoes higher contraction than the latter material due to its thermal expansion coefficient which is about 5 times larger. The stresses to which ice is submitted produces cracks; these cracks are further propagated to the concrete which exfoliates producing flakes.

Aforesaid mechanisms are mainly physical and consider the condition of ice formation for the damage. However, they do not explain scaling damage that has been observed to occur at low temperatures but some degrees above 0 °C. The deleterious mechanism of chloride attack on cementitious materials at low temperatures from a chemical point of view has not been clearly proposed. Moreover, the amplified damage that chloride attack could develop in combination with carbonated materials is not very well understood.

There are several forms in which chlorides react with cement compounds to form other salts. Some of the products are considered beneficial to concrete as the formation of Friedel's salt (FS) $3CaO.Al_2O_3.CaCl_2.10H_2O$ which chemically binds chlorides and somehow keeps them from reaching the steel [5]. Another form of chloride binding is in Kuzel's salt $3CaO.Al_2O_3.{}^1/_2\ CaSO_4.{}^1/_2\ CaCl_2.10H_2O$ and a modified form of iron containing FS, $3CaO.(Al,Fe)_2O_3.CaCl_2.10H_2O$) [6]. Other chlorides can be bound as calcium oxychloride with a general formula $3Ca(OH)_2.CaCl_2.nH_2O$ (3:1: n, where n=13,10 or 11), depending on temperature [7]. A similar mineral where n=12, is cited in the bibliography by Robbins [8]. Several investigators identified oxychloride of n=15 as being responsible for concrete damage after being exposed to $CaCl_2$ attack [9-11] (eq. (4-1)):

$$3Ca(OH)_2 + CaCl_2 + 12\,H_2O \leftrightarrow 3CaO \cdot CaCl_2 \cdot 15\,H_2O \qquad (4\text{-}1)$$

At temperatures just above freezing this reaction progresses fast; under these conditions the solubility of the oxychloride mineral is considerably diminished assuring mineral stability. Besides, high chloride concentration is a requirement to form oxychloride.

Many studies about oxychloride formation and its deleterious role on deicing scaling damage to concrete have been performed on pure OPC materials. Partial information on this matter is found for BFS/OPC blends. Also, the leading part that carbonation has in catalyzing the attack is not well understood. This research tries to match relations between the two damaging mechanisms.

4.2. Sample preparation and exposure conditions.

Four concrete mixtures without special properties regarding deicing resistance (the general purpose of the research was to obtain comparative behaviour of the materials without analysing specification compliance) were prepared for this investigation. Mix proportions, some obtained basic fresh concrete properties, initial curing conditions and carbonation exposure, have been described in the previous chapter.

At least 18 cylinders (diam. 100 mm, h. 100 mm) representing each type of concrete were exposed to a 10 % CO_2 concentration in a carbonation chamber, while a similar number were exposed to natural carbonation, in a climate controlled room. For both exposure conditions, the samples were maintained at 20 $\pm$ 2 ^{o}C and 60 $\pm$ 5 % RH until the time for testing. For each testing age, 3 cylinders were taken out from the curing place (accelerated and normal carbonation), each sawn parallel to the exposed surfaces into 2 half cylinders (diam. 100 mm, h. 50 mm) and the aluminum foil was removed. Three carbonated half cylinders representing each type of mix, were tested on the trowelled surface side (top face) for deicing scaling resistance according to the temperature cycle prescribed in CEN/TS 12390-9 Standard “Testing hardened Concrete-Part 9: Freeze-thaw Resistance-Scaling” (Fig. 4-1).

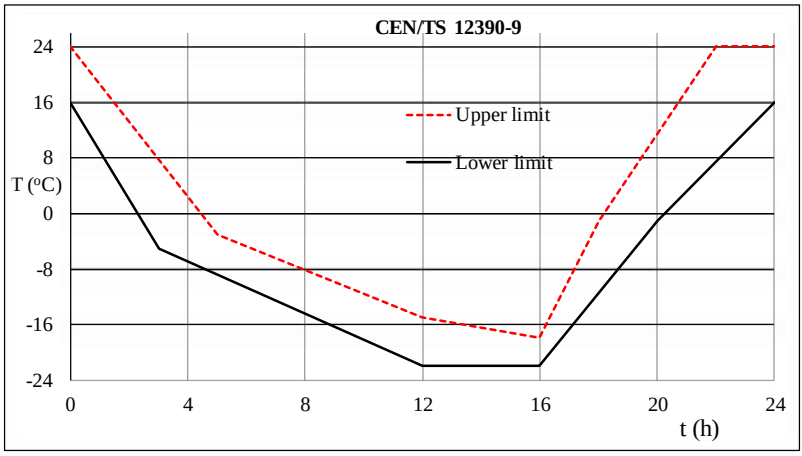

Figure 4-1: Temperature T (°C) limits vs. time t (h) prescribed in CEN/TS 12390-9 for ponding concrete with 3% sodium chloride solution.

Before starting the cycles the specimen is saturated by water ponding with a 3-mm deep layer of distilled water at 20° C on the top surface during 72 hours. Afterwards the 3-mm water layer is replaced by a 3% by weight NaCl solution. Then the specimen is subjected to the prescribed freeze-thaw cycle (Fig. 4-2). The scaled material is collected and a fresh solution is placed on the sample after 7, 14, 28, 42 and 56 cycles. The cumulative mass of scaled material related to the test surface in kg/m^2 for the prescribed cycles is then calculated.

Figure 4-2: Chloride solution ponding (left). Concrete samples in freeze and thaw chamber (right).

In addition to measuring the scaling loss for the different mixes, supplementary information was obtained from the samples that showed pronounced damage. It was decided to observe under the microscope the loose debris obtained from the samples, thus having an indication about the nature of the mineral assemblage that would be left over after the freeze and thaw attack in the presence of the combined action of carbonation and 3% sodium chloride. The sample was kept in the 3% salt solution to avoid any soluble mineral alteration; afterwards small remains of the scaled paste were transferred to a glass plate and while still being wet were immersed in a drop of ethylene-glycol while covering it with a thin glass plate. The immersion liquid was selected due to its polar nature; therefore, it easily wets the minerals and provides a good visualization under polarized light.

4.3. Experimental results

4.3.1. Scaling rate of carbonated concretes.

Fig. 4-3. shows the results of freeze and thaw action after 56 cycles performed on carbonated half cylinders (Ø 100 mm, h 50 mm).

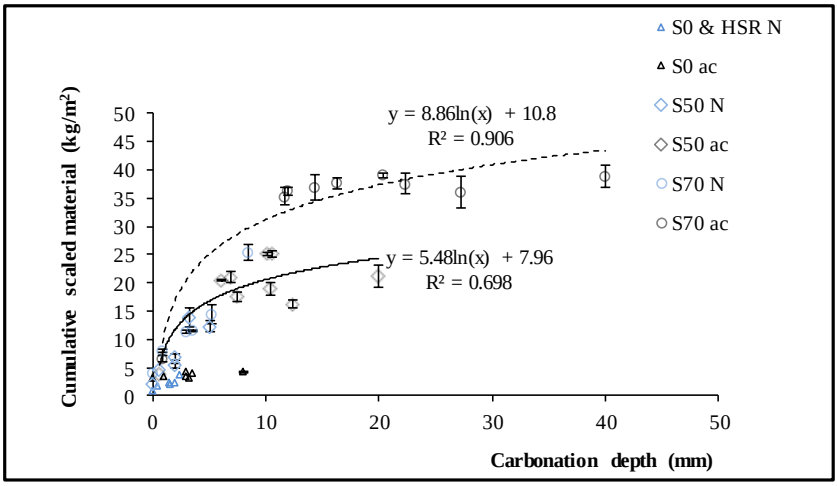

Figure 4-3: Scaling resistance of concretes (s/b = 0, 0.5, 0.7) exposed to 56 freeze-thaw cycles with 3% NaCl solution (CEN/TS 12390-9), after 10% (ac) and environmental (N) CO_2 exposure, (standard error, n=3).

From these results, it is noticed that carbonation influences the de-icing resistance of concretes. It was observed that scaling loss increases with the depth of carbonation for all the involved concretes until the amount of salt scaling does not significantly increase anymore. The slag concretes S50 and S70 showed comparable scaling loss up to a carbonation depth of about 5 mm; after 10 mm, the scaling loss for S50 reaches a steady level while for S70 flaking remains increasing and finally reaches a maximum constant value which remains invariable even for increasing carbonation depths. It was also noticed that for a similar carbonation depth greater than 10 mm the amount of concrete's damage increases with the amount of slag replacement.
At 8 mm carbonation depth S50 and S70 scaling rates were approximately 4 and 6 times greater respectively in comparison with the one quantified for S0.

4.3.2. Macro and microscopic observations on the scaling phenomena.

Some observations were made every time the scaled material from the samples was collected for weight registration and soon after the ice cover had melted, an unusual bubbling coming from the concrete interior was always observed (Figure 4-4). This behaviour was less pronounced in the pure cement concretes HSR and S0 and more intense in S50 and S70 samples and became more noticeable when removing the loose debris from the samples.

Figure 4-4: Loose fragment remains composed of exfoliating scales of cement paste, quartz gravel with little adherences of cement paste, and the presence of gas bubbles coming from the debris' interior, S70 by the end of the 56 days' cycle (CEN/TS 12390-9).

The collected debris coming from the most damaged concretes S50 and S70 showed gravel aggregates of which the surface was noticeably cleaner with little cement paste's adhesion, as shown in figure 4-4. This behaviour was not expected to occur from just mechanical disaggregation which normally leaves more remains of adhered paste.

Another observed detail was registered after the last F/T cycle (56 cycle). The pH from the attacking solution in contact with the concrete was measured. This solution had been replaced with a freshly prepared one (initial pH = 8.0), 14 days before in the 42th cycle; the following remaining pH values were found in the solutions: S70 (7.0 – 7.5), S50 (8.0 – 8.5), S0 (10.0), HSR (11.0-12.0) as shown in Figure 4-5.

Figure 4-5: pH remaining levels in the attack solution after the last defrost cycle (56 days). For S70 (upper left), S50 (upper right), S0 (lower left) and HSR (Lower right).

To identify the mineral assemblage produced on the damaged concrete, paste scales were analysed under the microscope shortly after they were obtained from the 56 days' cycle, it was decided to directly observe those flakes under the microscope without further treatment like used to prepare a polished thin section. Consequently, the potential dissolution of mineral associations is diminished.

Under polarized light, the presence of highly birefringent oxychloride crystals was observed as shown in Figure 4-6.

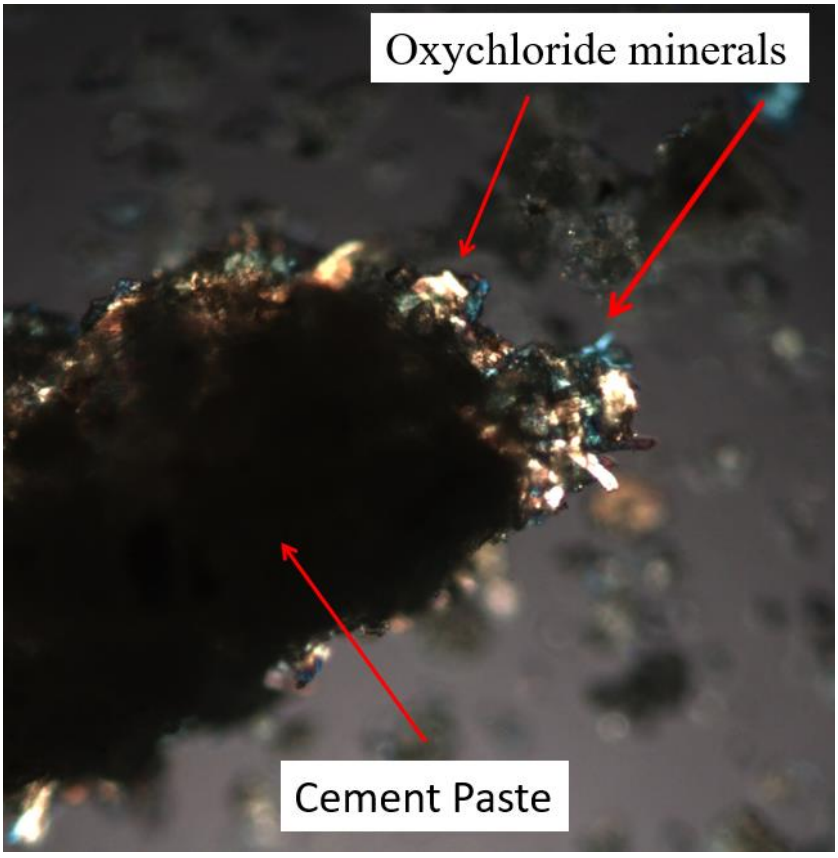

Figure 4-6: Highly birefringent Oxychloride minerals growing underneath exfoliated cementitious flake. Viewed under crossed polars. Accumulations of Rod-Prismatic-Platey crystal's type shapes are observed at the flake's borders. For scale reference of the flake size, refer to Figure 4-7 (b)

These minerals, were detected growing underneath the cement crust of the flakes. They were visible around the scales borders. Besides their high birefringence (Figure 4-7), some of these minerals show a prismatic habit with typical rounded edges, others have a slender rod shape, while others presented a platey form.

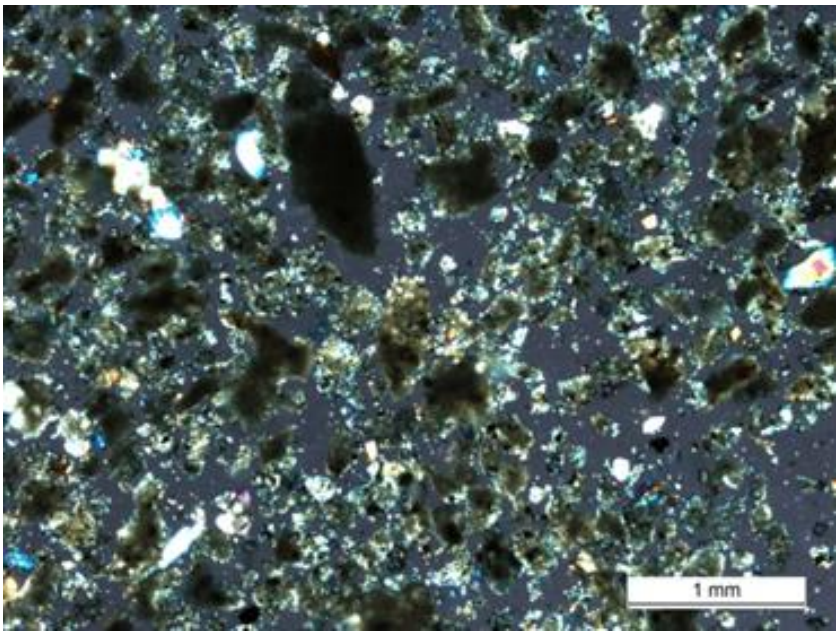

(a)

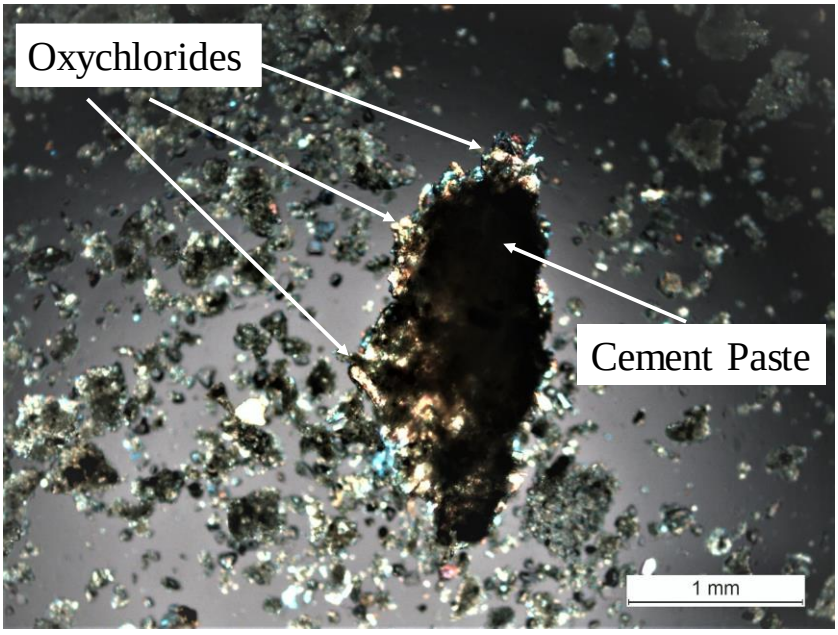

(b)

Figure 4-7: Scaled material from S70 concrete formed by tiny birefringent crystals highly disseminated (a). Prismatic and platey shaped oxychloride minerals growing underneath brown cement

paste (b) viewed with crossed polars, images taken from freshly obtained samples.

Very similar crystals have been identified in the work made by Peterson et al [12], (Figure 4-8).

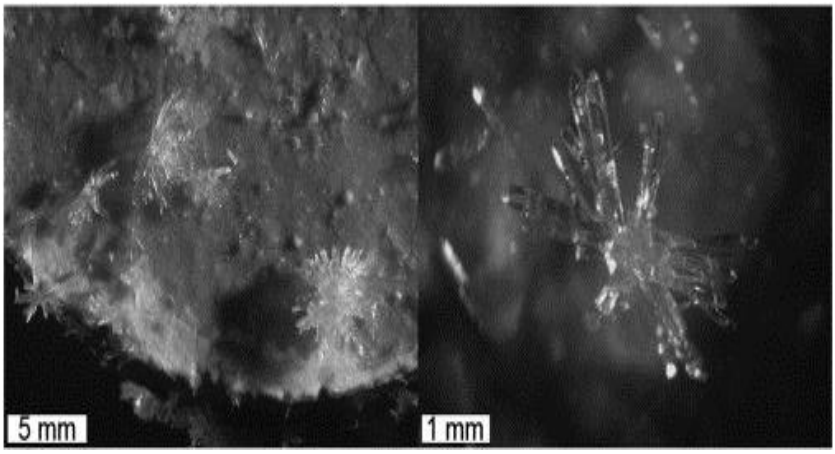

Figure 4-8: Prismatic calcium oxychloride minerals viewed under stereomicroscope. Corresponding to $3CaO \bullet CaCl_2 \bullet 15H_2O$ crystals at concrete surface after 500 days' exposure to 4.4 °C and high concentration $CaCl_2$ solution. Reprinted from Cement and Concrete Research, vol. 45/2013, K. Peterson, G. J. Betancourt, L. Sutter, R.D. Hooton, Daniel Johnston, "Observations of chloride ingress and calcium oxychloride formation in laboratory concrete and mortar at 5°C", page N° 86., copyright (2013), with permission from Elsevier."

To subsequently continue microscopic observations, the scaled material was stored in the 3% NaCl solution at 7 °C and investigated again after 48 hours. It was expected that the cold environment would not drastically change oxychloride mineralogy accordingly with most of the reported temperature conditions for its formation [12,13]. But contrarily, what was observed after the period in which these samples were stored, illustrates the ephemeral chemical stability these minerals have when they are exposed to slightly different conditions from those that created them. Figure 4-9 (left) shows a recently formed assemblage of oxychlorides growing underneath the cement

paste, Figure 4-9 (right) shows the found condition of a scale after 48 hours' storage at 7 °C in 3% NaCl bulk solution.

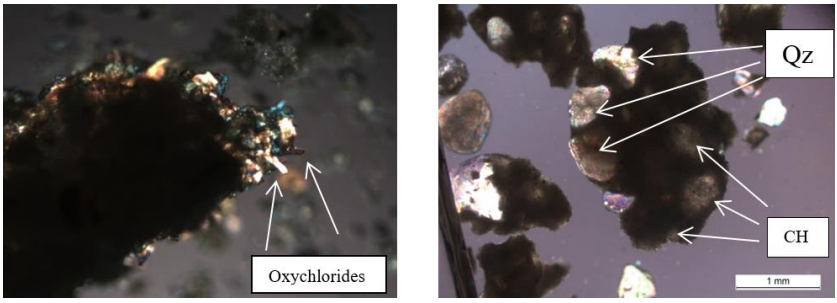

Figure 4-9: Freshly obtained oxychloride minerals on exfoliated flake, seen as highly birefringent crystals (left). Detail of scaled material after 48-hour storage in 3% NaCl solution at 7 °C, oxychlorides minerals have been dissolved, a smooth and clean surface is observed from the flake with some quartz grains (Qz) and portlandite pockets which show bright speckled appearance (CH), embedded in the matrix (right) viewed undercrossed polars.

In this later case, all oxychlorides minerals have been dissolved and the scale shows smoothly round and well defined borders with some inside pockets of brine remains containing tiny Portlandite minerals. Although most oxychloride minerals dissolved at this higher temperature; some of them may have been be protected from dissolution or rather possessed lower solubility, such as the one shown in figure 4-10.

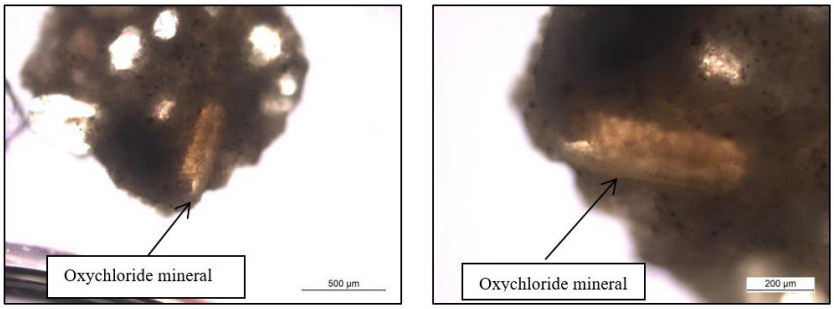

Figure 4-10: Prismatic oxychloride mineral protected by the cement paste from its dissolution, picture taken from scaled material of concrete S70 after 48-hour storage in 3% NaCl solution at 7 ^{o}C, some quartz grains are also embedded in the matrix, viewed under crossed polars.

4.3.3 Chloride penetration profiles at standard temperature

With the purpose of knowing how the chloride ion are distributed when they permeate the concrete, total chloride content profiles were obtained from the studied concretes. Thus, ground layers were obtained from the samples that had been exposed to a 3% NaCl solution for 1 year. Although the established procedures and obtained results will be presented in detail in the following chapter, it is important to offer in this section some partial results to understand the mechanism of deterioration that chlorides can potentially exert at freezing temperatures.

The distribution of total chlorides (acid soluble) for the samples S70-S50-S0 and HSR are presented in Figure 4-10. There, it is possible to compare the performance shown by blast furnace slag to restrain the penetration of these ions. All the concretes presented lower chloride contents near the surface and a high inner peak of chlorides located at 3-5 mm from the exposed surfaces. These low chloride contents at the near-surface region as well as the high content peaks, have been reported to occur in the so-called skin layer zones by some researchers

or in the convection zone by others, they have also been found in microcracked and carbonated zones of concretes [14-18].

Surface site density (surface charge of CSH) exerts a strong effect on the physical adsorption of chlorides. A rough evaluation of the surface site density of silanol sites on the paste at the inner peak was made. based on the correspondent total chloride content at that site. The work of Elakneswaran [19] was utilized to calculate the value.

Let's consider 0.276% (by weight of concrete) the highest chloride content for OPC in Figure 4-10. Therefore, 0.276/ (weight fraction of paste) = 0.276/(501/2357) = 1.29% (chloride content % by weight of paste). That value corresponds to a simulated surface site density value of approximately 10.9 sites/nm^2 [19]. It seems that BFS concretes provide higher values for surface site densities based on the higher peaks shown in the same Figure 4-11. Consequently, their capacity to adsorb chlorides should be higher. That property can also explain the steeper chloride profiles which represent much lower diffusivities in BFS concretes than in the pure Portland cement concretes.

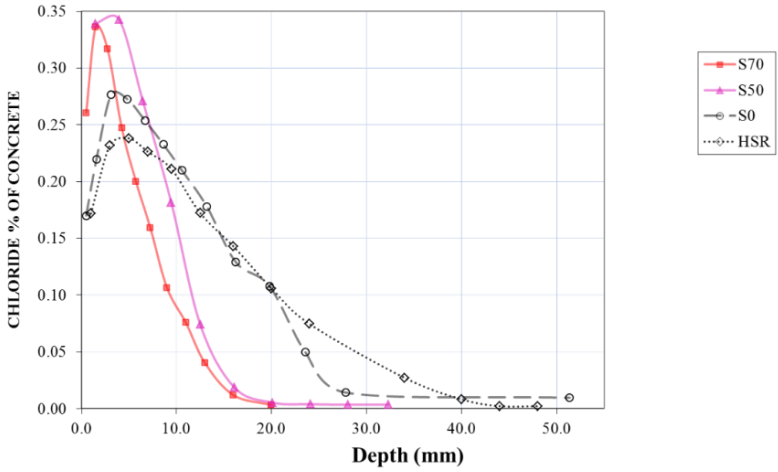

Figure 4-11: Acid soluble chloride content after 1 year 3% sodium chloride solution exposure, profiles obtained by grinding and chloride$^-$ potentiometric titration with silver nitrate (0.01 M).

4.4. Discussion

4.4.1 Chloride and the pore solution conditions in freezing medium

The environment found in concrete's nano and micro-pores transforms the physico-chemical characteristics of embedded solutions in these cavities, in such a manner, that its behaviour towards freezing differs from that found on a macroscopic scale. Additionally, salt presence in water further modifies this comportment. Boos and Giergiczny [18] suggest that the following aspects should be considered in this environment:

- Lowering of the freezing point due to the salt solutions
- Decrease of the freezing point due to surface forces
- Supercooling effects and vapor pressure differences.

As cited before and based on experimental evidence found by some researchers [10] it has been suggested that the severe deterioration of concrete exposed to chlorides deicers could be due to oxychloride formation. This damage has been proposed to occur even if concrete has not been exposed to temperatures below 0 ^{o}C. Recently, several laboratory tests have been conducted to elucidate conditions for its development. A main requisite for most of the oxychloride's crystals formation is a high concentration of chlorides and calcium ions. Thus, 4 mol/L of chloride is required for the 3:1:12 (CaO: $CaCl_2$: H_2O) and 9 mol/L for the 1:1:1 oxychloride type [11,20,21].

Several conditions have been studied during this research such as the usage of different types of binders (BFS, HSR, OPC), two types of carbonation exposures, a salt deicer attack at a fixed level of chloride of 0.5 M (3% by weight sodium chloride solution). The oxychloride formation has been identified to occur despite the relatively low chloride concentration [0.5 M] and the almost null presence of calcium ions from the water utilized to prepare the attacking solution. It is thought that actives surface sites present on the CSH from the cement's membrane play a crucial role in providing zones with high

chloride's levels. Besides, calcium ion is not provided by the attacking solution, but calcareous cementitious materials are a potential source of this element. Hence, somehow the conditions for oxychloride formation are met.

4.4.2.CO_2 equilibrium at low temperatures

CO_2 and its different chemical species play an important stability role in the pore solution, usually $CO_{2,aq}$ is continuously supplied to solution through diffusion from its gaseous form $CO_{2,g}$ coming from the atmosphere. Once in water, this species is in equilibrium with its aqueous species per the following temperature dependant equilibrium constants (equations 4-2 to 4-4) which manage the reactions. It is assumed that the cited correlations are also valid for the lower temperature range in a non-freezing salt solution; these values were taken from reference [22] where:

$$-log(K_1, K_2, K_h)\ at - 20℃\ are\ (6.95, 11.02, 0.69)\ respectively$$

$$-log(K_1, K_2, K_h)\ at + 25℃\ are\ (6.35, 10.33, 1.46)\ respectively$$

$$K_h = \frac{CO_{2aq}}{P_{CO_2}} \tag{4-2}$$

$$K_1 = \frac{(H^+)(HCO_3^-)}{CO_{2aq}} \tag{4-3}$$

$$K_2 = \frac{(H^+)(CO_3^{2-})}{(HCO_3^-)} \tag{4-4}$$

P_{CO_2} is the partial pressure of this gas and CO_{2aq}, HCO_3^- , CO_3^{2-} the aqueous and ionized species concentrations which are also pH and temperature dependent. Figure 4-12, shows the mole fraction distribution between the cited species as a function of the solution pH and temperature; to make the graph –20 °C was considered as the average lower expected temperature which is reached during the freezing cycle while the standard temperature of +25 °C was chosen as

a reference which is also close to the reached maximum temperature during the defrost cycle. To make this analysis it is assumed that the solution in the micro-pores is not yet or partially frozen during the freezing cycle and that the physically bound gel pore water does not freeze even until -43 °C [23,24].

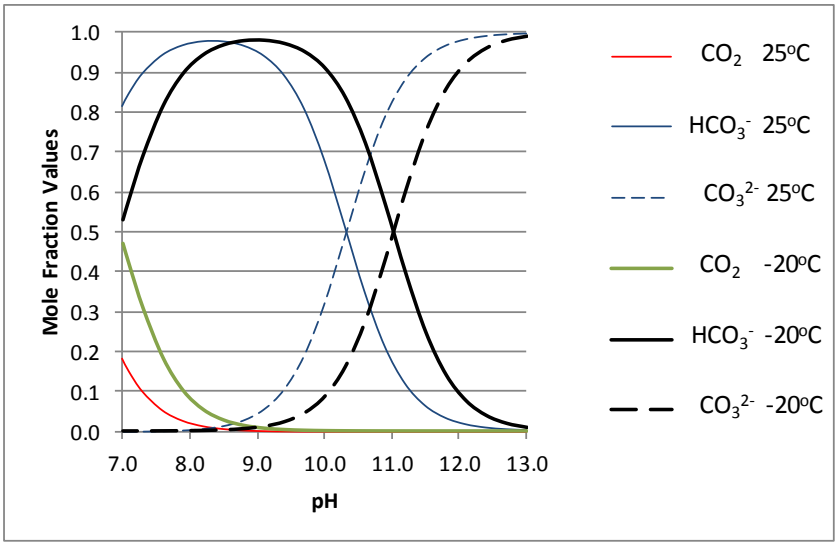

Figure 4-12: Distribution of CO_2 aqueous species as a function of temperature (at -20 and 25 °C) and solution pH.

When solution temperature drops from +25 towards -20 degrees, the equilibrium curves for the bicarbonate and carbonate species move towards higher pH values. The displacement is important, about 1 pH unit. This means that the system moves towards a more unstable condition for carbonate phases. In other words, during the low temperature cycle the carbonate minerals need higher pH values in the pore solution to avoid their dissolution. The other unstable state for carbonates is the noticeable increasing demand of aqueous CO_2 curve during the freezing cycle. In such condition, the system is willing to raise its CO_{2aq} content. Which, in normal conditions is usually replenished to the solution by direct diffusion from atmospheric air. However, the atmospheric diffusion mechanism is very slow in a saturated concrete medium, therefore the source of aqueous carbon dioxide the system is demanding is provided by rapid dissolution of

calcium carbonates (vaterite/calcite) available in the carbonated concrete. The CO_2 equilibrium responds as in a closed system. Thus, the increasing solubility of these two minerals which are usually reported at low temperatures [22], is only a consequence of the thermodynamic condition of the solution at reduced temperatures as discerned from Figure 4-12.

4.4.3. Conditions for Oxychloride crystals formation

We established an order of increasing sensibility to carbonation in our studied concretes. This was classified in table 3-3 (chapter 3) when comparing the increasing ratio of carbonation for CSH/CH in the cited concretes. The carbonation ratio was evaluated after 1 year of CO_2 exposures. At natural 0.03% and accelerated 10% CO_2 concentrations by volume. Thus, the following concrete mixtures were arranged in increasing carbonation sensibility order "HSR, S0, S50, S70". In these concretes 2 calcium carbonate polymorphs were identified. The metastable carbonate vaterite and the other identified phase calcite. During the low temperature cycle, the pore solution conditions are more unstable for carbonates. The pH in the pore solution is crucial for stability of these salts. Thus, the material whose paste assures to keep the higher alkaline conditions will provide stability towards these minerals. In that condition, pure Portland cement concretes have advantages compared to the high replacement BFS concretes.

Mineral solubility is increased at low temperature. The solution has a high demand of aqueous CO_2 and in very short time as explained in section 4.4.2. Consequently, carbonate minerals are dissolved per the following proposed reaction (4-5). This would happen unless a precipitation pH is guaranteed and the reaction keeps in its left-hand side by the common ion effect of OH^- ions:

$$4CaCO_3 + 4H_2O \rightarrow 4CO_{2aq} + 4Ca^{2+} + 8OH^- \quad (4\text{-}5)$$

This reaction occurs at the sites where carbonation took place. The freshly released calcium ions together with chloride ions are re-adsorbed on the silanol sites of CSH per reaction (4-6) [25]:

$$> SiOH + Ca^{2+} + Cl^{-} \leftrightarrow > SiOCaCl + H^{+} \quad (4\text{-}6)$$

It is believed that a chloride build up is produced and forms an inner chloride peak with high concentration of chloride.

It has been suggested that this type of adsorption is predominantly physical due to strong van der Waals forces [25]. Chloride adsorption takes place after calcium adsorption on CSH sites. Calcium ion acts as a surface activator and promotes chloride adsorption.

A new condition has been set where highly concentrated points of calcium and chloride ions are present on CSH sites. This condition together with low temperature pore solution provokes oxychloride formation. The following equations (4-7) (4-8), are proposed for reactions that take place at the solid-liquid interface:

$$4Ca^{2+} + 6OH^{-} + 2Cl^{-} + 12H_2O \leftrightarrow 3CaO \cdot CaCl_2 \cdot 15H_2O \quad (4\text{-}7)$$

$$4Ca^{2+} + 6OH^{-} + 2Cl^{-} + 9H_2O \leftrightarrow 3CaO \cdot CaCl_2 \cdot 12H_2O \quad (4\text{-}8)$$

Reactions (7)(8) and (9) evolve spontaneously as a response that seeks to nullify the effect generated by the products of reaction (6).

For spontaneous reactions, the change in Gibbs free energy (ΔG) for equations (4-7) and (4-8) and summarized in equation (4-10), should be negative under low temperatures.

$$\Delta G = \Delta H - T\,\Delta S \quad (4\text{-}9)$$

When a crystal is formed from a salt solution, the change of entropy of the reaction (ΔS) decreases and is negative. Therefore, the other term of equation 4-9 (enthalpy of the reaction ΔH) must take negative values. Consequently, oxychloride formation is an exothermic process. The process of oxychloride formation would be very much like water

freezing. The formation of ice when water is submitted to low temperatures, is also an exothermic process.

Sutter [26] identified two forms of these oxychloride minerals: a prismatic and a platey shaped one. The first was also identified by Peterson et al [12]. Its composition is closer to that shown in equation (4-7). It was also found more frequently in the carbonated zone than the platey shaped one. The latter corresponds more closely with the product of equation (4-8). It was found near an advancing point of deterioration. Both minerals are supposed to be stable at low temperature thanks to a decrease of their solubility [13]. Other researchers report oxychloride formation at 5 ^{o}C temperatures but at high chloride concentration (30 % $CaCl_2$) [26]. Harvie "et al." in their model [20] propose that oxychloride mineral 3:1:12 requires a high chloride concentration of almost 4 M for its formation.

In this work the 3:1:15 and 3:1:12 types of oxychlorides phases were found to co-exist. They were found intermixed in the analysed scales under the microscope (figures 4-6 and 4-7). These minerals have been formed despite the relatively low chloride concentration of 0.5 M (3% NaCl) from the bulk attacking solution; the only coherent explanation to this situation would be the presence of high concentration of chloride ions adsorbed on CSH sites. After calcium is released from the dissolving carbonated layer these ions are re-adsorbed on silanol surfaces from the gel or slag and contribute to an increase of the electrical double layer rising the chloride concentration level. This is believed to occur on the carbonated front boundary where OH^- is also available from the non-carbonated sites of the concrete or from carbonate dissolution. These sites, act as starting points for crystal growth.

The adsorption behaviour of chlorides and calcium depend on the type of binder [25]. In this research, it was noticed that the slag addition to concretes increased the concentration of chlorides in a place located near the surface of the exposed face. Thus, a higher chloride concentration peak was found in the slag concretes compared to that found in pure Portland cement ones. This peak was located

approximately between 3-5 mm from the surface exposed to chloride as shown in figure 4-11. The figure illustrates the contribution of the slag to the high chloride concentration in the proximity of the exposed surface. It appears that the location and magnitude of this chloride content peak is very important to define the relative susceptibility of materials to scaling. It is believed that the chloride's peak location shifts with carbonation, with the level of attacking bulk concentration and probably due to alterations on the microstructure (voids and cracks). Some researchers [28] who exposed concretes to higher chloride content (165 g/l, sodium chloride) have observed that the maximum chloride concentration values from the obtained profiles were located at the concrete surface. In such situation, oxychloride formation would be located predominantly at the surface without causing the typical scaling damage from the crystal growth. There have been reports of oxychloride presence located mainly on concrete's surface or in cracks when concretes were exposed to combination of high chloride concentration and low temperatures [12,26]. It seems like in these cases, the level of scaling was not as expected considering the high concentration of chloride utilized.

The previous analysis would explain why the worst condition for scaling occurs at a medium chloride bulk concentration which is generally around 3% (30 g/l) of salt solution. In this case, the high chloride concentration peak is located inward. In such condition a more severe damage is produced by oxychloride crystals which now start their growth underneath the surface and so concrete scaling is provoked.

After scaling has occurred, a new shift of the chloride's peak concentration towards inner zones is provoked, and the condition for the damage is reinstalled.

It was also observed that oxychlorides growing under the obtained flakes were not stable after storing them in 3% sodium chloride solution at 7 ^{o}C. The exact dissolution time of these crystals was not determined, but after 48 hours the minerals were already dissolved leaving Portlandite remains on the cement scales (Figure 4-9 right).

$Ca(OH)_2$ is the product after equations (4-7) and (4-8) reversal towards the left-hand side direction.

4.4.4. Some highlights about the potentially damaging mechanism to concrete by chloride deicers

Among the prerequisites that promote oxychloride harm are free calcium ions and low temperatures. At relatively low pH free Ca^{2+}species are available, while low temperatures promote oxychloride stability due to its decreasing solubility [21]. Conditions for low pH in concrete's pore system are found in carbonated concretes but also in concretes which have low capacity to withstand a reduction in their pore solution pH such as those prepared with high SCM's (supplementary cementitious materials) replacement. Even if these concretes have not been carbonated they are also likely to experience salt scaling damage. That would explain why several researchers have reported relatively high salt scaling deterioration levels in well prolonged cured uncarbonated concretes with high levels of SCM replacements [28-30].

High SCM replacement levels are commonly selected to stop chloride ingress and to avoid steel rebar corrosion. However, the application of such quantities to improve the scaling resistance of concrete could represent a risk.

More studies must be directed towards the high capacity for chloride adsorption these materials have and how the high chloride concentration peak located near the surface contributes to scaling. Related to this issue it was observed in this research that the utilized slag concretes showed the highest chloride peaks, as shown in figure 10. This property is considered good if the concrete's aim is to stop chloride from further ingress and so avoid rebar corrosion. But from a salt scaling resistance point of view perhaps it should be considered a risky property.

Besides of dissolving carbonates, the pore solution together with oxychloride salts at low temperatures could have a supplementary leaching effect on other cement components. This aggressiveness would also depend on the resistance of cementitious materials to the solution changes such as a reduction in the pH a resistance that also assures the stability of calcium bearing minerals. A quantification of the resistance capacity of concrete to a pH decrease was measured after the 56 F/T attacking cycles. The pH value was registered from the remaining salt chloride solution and the following values were found: S70 (7.0 – 7.5), S50 (8.0 – 8.5), S0 (10.0), HSR (12.0), thus S70 had the lowest resistance capacity to pH reduction while HSR showed the highest.

As a summary, it can be said that low temperatures reached during the freezing cycle promote pore solution aggressiveness towards calcium bearing cement minerals, specially to carbonates and Portlandite whose solubility is increased. The released aqueous CO_2 increases acidity of the pore solution and the free Ca^{2+} combines with chloride ions to form oxychlorides.

During the thaw cycle oxychloride minerals undergo dissolution releasing calcium hydroxide which either is leached away from the concrete after solution replacement, or remains in the solution awaiting to be again part of oxychloride formation in the next freezing cycle. Also, gaseous CO_2 escaped from the solution during the increasing temperature cycle.

The attack is pH dependent and is believed to be hindered by higher pH values in the solution or when binders in the concrete have a high resistance capacity to a pH reduction.

Due to the very high pH conditions found in the pore solution of pure OPC concretes the solubility of calcium carbonates is highly reduced and free Ca^{++} ion is no longer available to form oxychlorides and the damage is considerably reduced. However, this situation can be reverted and oxychloride minerals can still be formed, but the metal ions that promote their growth must be supplied in high

concentrations from an external source such as that found in former research [12,21,26].

4.5. Conclusions.

During this research, it was found that the damage caused by the deicing salt attack on carbonated concrete is not only physical in nature. A very strong combined destructive mechanism was observed, involving oxychloride salt formation and an aggressive pore solution during the freeze cycle that strongly contributes to the damage.

It was analyzed that during the freeze cycle the pore solution becomes aggressive towards carbonates driving them towards their dissolution. Oxychloride formation further increases its aggressiveness. The combined attack consists in a disruptive damage caused by oxychlorides together with a continued leaching of calcium ions from the cement paste in every cycle. This reaction progresses at a relatively low pH of the pore solution, a condition that is usually found in carbonated concrete or at high replacement levels of cement by SCM.

The attack is thought to be hindered at high pH values of the pore solution, a condition usually available in pure uncarbonated Portland cement pastes.

References

[1] Powers TC, A working hypotheses for further studies of frost resistance of concrete. Journal of American Concrete Institute. 1945;16(4):245-272.

[2] Hansen WC, Crystal Growth as a Source of Expansion in Portland-Cement Concrete. American Society for Testing and Materials (ASTM), Proc.1963;63:932-945.

[3] Snyder MJ, Protective coatings to prevent deterioration of concrete by deicing chemicals. National Cooperative Highway Research Program Report 16. Washington DC:Transportation Research Council (U.S.);1215.

[4] Valenza II J, Scherer G. Mechanism for Salt Scaling. J. Am.Ceram. Soc. 2006; 89(4): 1161-1179.

[5] Brown P, Bothe J. Jr. The system $CaO-Al_2O_3-CaCl_2-H_2O$ at 23 + 2 ^oC and the mechanism of chloride binding in concrete. Cement and concrete research. 2004;34(0):1549-1553.

[6] Csizmadia J, Balazs G, Tamas F, Chloride ion binding capacity of aluminoferrites, Cem. Concr. Res. 2001; 31(0): 577-588.

[7] Demediuk T, Cole W, Hueber H. Studies on magnesium;and calcium oxychlorides. Aust. J. Chem. 1955; 8(0): 215-233.

[8] Robbings C (Ed.). Phase diagram for ceramists. American Ceramic Society. Westerville, OH. 1964; vol. 1: Figure 2061.

[9] Monosi S, Collepardi M. Research on $3Ca(OH)_2.CaCl_2.15H_2O$ identified in concretes damaged by $CaCl_2$ attack. Il Cemento .1990; 87(0): 3-8.

[10] Collepardi M, "et al." Durability of concrete structures exposed to $CaCl_2$ based deicing salts, in: V.M. Malhotra (Ed.), Durability of Concrete ACI SP-145, 3rd CANMET/ACI International conference, Nice, France. 1994; 107-115.

[11] Glasser F, Marchand J, Samson E. Durability of concrete-degradation phenomena involving detrimental chemical reactions. Cem. Concr.Res. 2008;38(2):226-246.

[12] Peterson K. “et al.” Observations of chloride ingress and calcium oxychloride formation in laboratory concrete and mortar at 5 ^{o}C. Cement and Concrete Research. 2013; 45: 79-90.

[13] Abate and Sheetz quoting F.A.H. Schreinemakers and T. Figee, Het Stelsel: H_2O-$CaCl_2$-$Ca(OH)_2$ bej 24^{o}C, Chem Weebl 3. 1911; 683-688.

[14] Malheiro R. et al, Effect of Carbonation on the Chloride Diffusion of Mortar Specimens Exposed to Cyclic Wetting and Drying, Proceedings XIII International Conference on Durability of Building Materials and Components, Sao Paulo-Brasil Sept. 2014, 482-489.

[15] Lee C.S., Yoon I.S., Prediction of deterioration process for concrete considering combined deterioration of carbonation and chlorides ions, Journal of the Korea concrete Institute, 2003; 15 (6): 902-912.

[16] Chunhua Lu et al, Experimental Analysis of Chloride Penetration into Concrete Subjected to Dying-Wetting Cycles. Journal Mater. Civ. Eng. 2015; 27 (12), 04015036-(1-10).

[17] Chunhua Lu et al, Effect of Transverse Crack on Chloride penetration into Concrete Subjected to Dying-Wetting Cycles. 4th International Conference on the Durability of Concrete Structures.Purdue University, West Lafayette, IN, USA. 2014; 169-175.

[18] Andrade C., et al, Mathematical Modeling of a Concrete Surface "Skin Effect" on Diffusion in Chloride Contaminated Media, Institute of Construction Sciences "Eduardo Torroja" of the CSIC. 1997: 39-44.

[19] Elakneswaran Y, Iwasa A., Nawa T, et al, Ion-cement hydrate interactions govern multi-ionic transport model for cementitious materials, Cem Con Res. 2010; 40: 1756-1765.

[20] Harvie C, Moller N, Weare J. The prediction of mineral solubilities in natural waters: the Na-K-Mg-Ca-H-Cl-SO_4-OH-HCO_3-CO_3-CO_2-H_2O

system to high ionic strenghts at 25 ^{o}C.Geochim. Cosmochim. Acta 48. 1984;723-751

[21] Brown P. The system Na_2O-CaO-SiO_2-H_2O. Am. Ceram. Soc. 1990; 73: 3457-3463.

[22] L. Plummer, Busenberg E. The solubilities of calcite,aragonite and vaterite in CO_2-H_2O solutions between 0 and 90 ^{o}C, and an evaluation of the aqueous model for the system $CaCO_3$-CO_2-H_2O. Geochimica et Cosmochimica Acta.1982;46:1011-1040.

[23] Powers T.C. A working hypothesis for Further Studies of Frost Resistance of Concrete. J. ACI Proceedings.1945;41: 245-272.

[24] Helmuth R.A. Investigations of the Low Temperature Dynamic Mechanical Response of Hardened Cement Paste. 1974; Dept. of Civil Engineering, Stanford University, Technical Report 154.

[25] Elakneswaran Y, Nawa T, Kurumisawa K. Zeta potential study of paste blends with slag. Cement & Concrete Composites. 2009; 31: 72-76.

[26] Sutter L, “et al.” Petrographic evidence of calcium oxychloride formation in mortars exposed to magnesium chloride solution. Cement and Concrete Research. 2006; 36: 1533-1541.

[28] Van den Heede Ph., Durability and Sustainability of Concrete with High Volumes of Fly Ash. Ph.D. thesis, Ghent, Ghent University; 2014.

[29] Battaglia I, Munoz J, Cramer S. Proposed Behavioral Model for Deicer Scaling Resistance of Slag Cement Concrete. J.Mater. Civ. Eng. 2010; 22 361-368.

[30] Gruyaert E. Effect of Blast-Furnace Slag as Cement Replacement on Hydration, Microstructure, Strenght and Durability of Concrete. Ph.D. thesis, Ghent, Ghent University; 2011.

IV CHLORIDE INGRESS IN MECHANICAL LOADED CONCRETE

CHAPTER 5. TEST METHODS TO DETERMINE DURABILITY OF CONCRETE UNDER COMBINED ACTIONS AND MECHANICAL LOAD – FINAL REPORT OF RILEM TC 246-TDC

Chapter 5 presents the results performed by members of committee TC 246-TDC from RILEM, during almost 5 years of experimental work. Their effort is greatly acknowledged.

As a member of TC 246-TDC, the author has been responsible for the experiments at UGent and he has made the comparative analysis of the data from the different participating laboratories.

This chapter has been published as: YAN YAO; LING WANG; FOLKER H. WITTMANN; NELE DE BELIE; ERICK SCHLAGEN; CHRISTOPH GEHLEN; ZHENDI WANG; HUGO EGUEZ ALAVA; YIN CAO; BALQUIS MD YUNUS; JUAN LI. (2017). Recommendation of RILEM TC 246-TDC: Test methods to determine durability of concrete under combined environmental actions and mechanical load. Test method to determine the influence of applied stress on chloride diffusion. Materials and structures, 50:123, 13p.

This work also aimed in defining a relevant test method for chloride ingress under loading

5.1. Introduction

Design of load bearing structures has a long history in civil engineering. In Europe it is now based on Eurocode 2 [1]. Similar codes for structural design exist in other regions (see for example [2-4]). More recently a Model Code for service life design [5] has been set up in an analogous way, compared to Eurocode 2. In this document the stress is replaced by environmental actions such as carbonation, chloride penetration, and freeze-thaw attack with and without de-icing agents and mechanical resistance is replaced by resistance of concrete against environmental actions such as carbonation, chloride penetration or freeze-thaw cycles.

Based on this concept the following limit states can be formulated: (1) corrosion initiation induced by chloride ingress or carbonation, (2) cracking due to steel corrosion, (3) spalling of concrete cover due to

steel corrosion, and (4) structural collapse due to corrosion of reinforcement. The Model Code suggests four different options for service life design: (1) full probabilistic approach, (2) semi-probabilistic approach, (3) deemed to satisfy rules, and (4) avoidance of deterioration. Based on this Model Code the safety of structures under the influence of environmental actions can be expressed in terms of a reliability index β in a similar way as it is common practice for structural design.

The actual service life of reinforced concrete structures and of bridges in particular, is in many cases significantly shorter than the designed service life (see for instance ASCE 2013 Report Card [6]). According to this document more than 20 % of bridges in the United States are structurally deficient or functionally obsolete. In many industrialized countries, a similar situation exists. As a consequence, it has become difficult to keep pace with the growing costs for maintenance and repair of aging infrastructure.

The Model Code for service life design [5] may be considered to be a significant step forward, as durability and service life of reinforced concrete structures can be taken into account during the design stage. According to the Model Code, the necessary material parameters such as the inverse carbonation resistance or the chloride migration coefficient have to be determined under well-defined laboratory conditions. More recently, however, it has been shown that these parameters also depend on an applied stress. Rate of chloride penetration for instance can be doubled [7, 8] under the influence of an applied tensile stress. Hence, if the influence of an applied stress is not taken into consideration prediction of service life will not be realistic.

Before relevant comparative tests were started by members of the TC 246-TDC the state-of-the-art of this topic was carefully investigated. As a result, a comprehensive annotated bibliography could be published in 2013 [9]. These publications served as a starting point for the investigations described in what follows.

5.2. Experiments and materials

5.2.1 Preparation of specimens

Research groups of five laboratories participated in the comparative test series: (1) Chinese Building Materials Academy (CBMA), (2) Ghent University (UGent), (3) Delft University of Technology (TU Delft), (4) Technical University of Munich (TUM), and (5) Dalian University (DALIAN U.) They were asked to prepare concrete with identical geometry and dimensions. It was suggested that Portland cement Type I, corresponding to Chinese National Standard GB 175 [10], EN 197 [11] or ASTM shall be used. All groups were asked to add the necessary amount of polycarboxylate superplasticizer to the fresh concrete in order to reach a slump of approximately 15 cm.

With the fresh concrete, prisms with the following dimensions: 100 x 100 x 400 mm, were produced for tests under compression and dumbbell specimens as shown in Fig. 1 were produced for tests under tension.

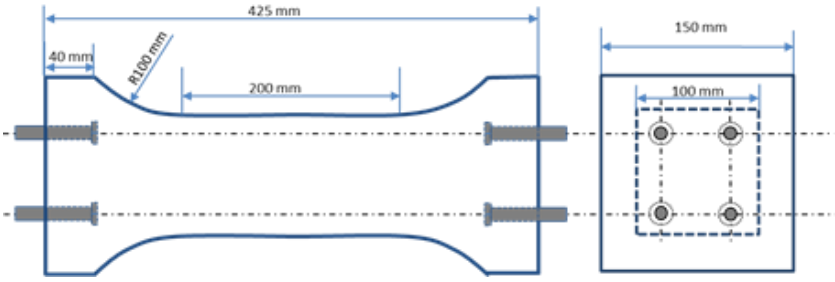

Fig. 5-1: Shape and dimensions of dumbbell specimen for tests under tension.

The compressive strength of the concrete prisms was usually determined at an age of 28 days. Results are shown in Tab. 5-1. The tensile strength of the dumbbell specimens at an age of 28 days as determined at CBMA was found to be 3.3 MPa. As can be seen a wide range of compressive strengths is covered.

Tab. 5-1: Compressive strength at 28 days of concrete as prepared in five different laboratories.

Laboratory	CBMA	UGent	TU Delft	TUM[1)]	DALIAN U.
Prism Strength (MPa)	36.6	56.9	40.7	34.0	26.2

[1)]: Prism strength of TUM was determined at an age of 146 days, just before the prisms were subjected to the combined loading regime (mechanical load and chloride loading).

The internal faces of all moulds were covered with a thin Teflon film to avoid the water repellent effect of demoulding oil. After casting, the specimens were stored under plastic sheets in a room maintained at 20 °C and at a relative humidity of about 95 % for 24 h. Then, the samples were de-moulded and further cured in tap water at 20 °C until testing.

The specimens were taken out from the water bath and the free water on the surfaces was removed with a clean dry towel, then the surface was immediately sealed with two layers of self-adhesive aluminium foil. A window with dimensions 80 x 160 mm^2 on one moulded side surface was left open, but the free surface was protected temporarily from drying until the salt solution tank was attached. A plastic tank with the inner dimensions of 80 x 160 x 50 mm was adhered or clamped to the specimens, covering the open window. As soon as the plastic tank was filled with salt solution, chloride could penetrate into the concrete by diffusion. Due to incomplete saturation and further hydration of cement, capillary absorption could not be totally avoided. Nevertheless, the diffusion coefficient obtained from chloride profiles in this experiment characterizes the diffusion of chloride in saturated concrete. For prediction of chloride penetration into real concrete structures the environmental climatic conditions have to be taken into consideration.

5.3. Test methods

5.3.1. Specimens under compression

Compressive stress was applied on the prismatic concrete specimens using a test rig as shown in Fig. 2, which fulfils the requirements of the Appendix of RILEM TC 107-CSP [12]. The chosen compressive stress

ratio, which is the ratio of applied stress to the compressive strength, is to be 0, 30, and 60 %. A 3 *wt.* % aqueous sodium chloride solution was circulated through the applied plastic tank with a pre-defined speed of 5±1 ml/s. The concentration of the solution was checked regularly at least once a week during the whole exposure period, and the chloride solution was isolated from the atmosphere by a lid on the reservoir to avoid evaporation and contamination. The specimens were unloaded after an exposure time of 2, 6, 18 and 36 weeks, or any other designed duration, after which the specimens were ready for chloride profile determination.

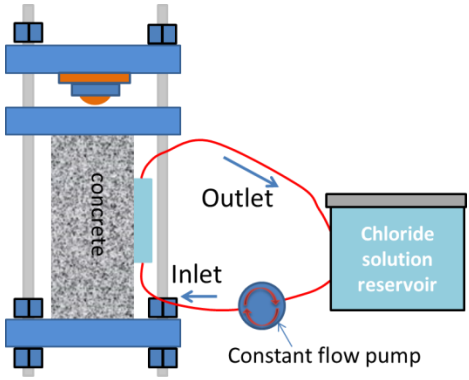

Fig. 2: Experimental setup for determination of chloride diffusion into concrete under compression

5.3.2. Specimens under tension

In order to be able to connect the dumbbell specimens with the testing rig, 4 bolts were fixed at each end of the mould before casting (see Fig. 1). A special test rig was designed for application of a predetermined tensile stress. Two steel joint plates served as a link between the 4 bolts on both ends of the dumbbell specimens with the spherical hinges of the test rig (see Fig. 3). In this way eccentricity of the tension specimens could be essentially avoided. Similar test rigs following the same principle can also be used. The following tensile stress ratios, which are the ratios of applied tensile stress to the ultimate tensile stress, were chosen: 0, 50 and 80 %. The operation of the tensile setup is described in more detail in Ref. [13]. A similar set up for circulation of the chloride solution on the concrete surface as shown in Fig. 2 was applied on the open windows of the dumbbell specimens. The flow

speed was the same as for the tests under compression. The circulation of the salt solution was stopped and the dumbbell specimens were unloaded after an exposure time of 2, 6, 18 and 36 weeks. After the fixed periods, the chloride profiles in the concrete specimens were determined. For specific applications other periods of chloride penetration under tensile stress can be chosen.

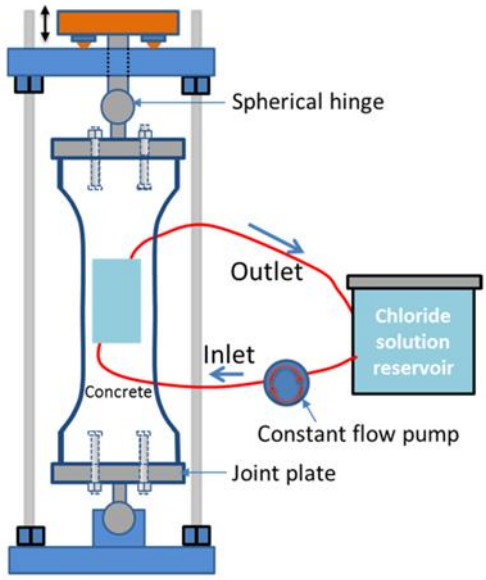

Fig. 3: Sketch of experimental setup for tension tests

5.3.3. Determination of chloride profiles

First the plastic tank was removed from the unloaded specimens. Care must be taken that the concrete surface is protected from drying before the milling process can begin, as drying will modify the chloride profile. Powder samples from the exposure surface of all specimens were obtained by stepwise milling layers with a thickness of 1 to 2 mm. The number and thickness of the layers was adjusted according to the expected chloride profile. A minimum of eight measuring points should be distributed on the descending branch of the profile. In order to avoid edge effects and an influence of the glue of the self-adhesive aluminium foil on the test results, sampling was performed on an area with a distance of 10 mm from the border of the exposure zone. Particles with a diameter of more than 1 mm may exist in powder

which is obtained by milling or crushing with subsequent grinding. In this case special care has to be taken to assure sufficient extraction time of the chloride from the powder. The chloride content dissolved in acid is to be determined by chemical analysis according to EN 14629 [14]. It is recommended that the tests shall run at least in triplicate, and average values of chloride ion diffusion coefficient shall be determined.

5.4. Test results

5.4.1 Influence of compressive stress

5.4.1.1 Chloride profiles as measured under stress ratios of 0 and 30 %

Chloride profiles obtained in different laboratories at stress ratios of 0 and 30 % are presented in Fig. 4 to Fig. 7. Results obtained at UGent are shown separately (Fig. 4 for 0 % and Fig. 5 for 30 % stress ratio), because of the different exposure times and higher number of data points obtained per profile. The latter was considered to be important especially for longer diffusion periods and for high loading ratios. In addition, from these figures the scatter of values obtained in one laboratory can be estimated, because profiles obtained on two similar samples are shown.

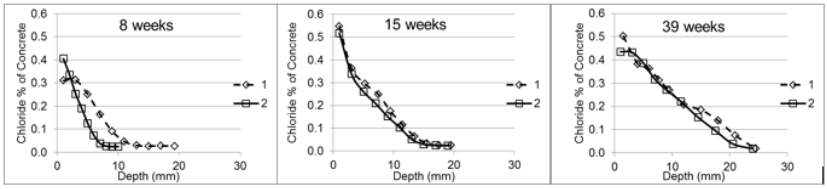

Fig. 4: Chloride profiles as obtained at UGent after 8, 15, and 39 weeks on similar concrete samples without applied stress

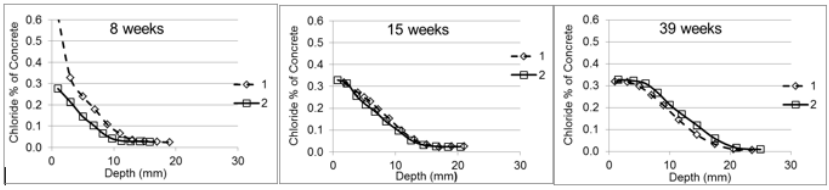

Fig. 5: Chloride profiles as obtained at UGent after 8, 15, and 39 weeks on similar concrete samples at a stress ratio of 30 %

As seen from Fig. 4 and 5, all chloride profiles show a smooth decrease of the chloride content with increasing distance from the surface. Near the surface, however, more scatter is observed. At longer exposure times a sort of plateau is observed. This observation clearly underlines the well-known fact that chloride penetration cannot be explained by pure diffusion. A series of different transport mechanisms, such as capillary absorption, chemical reactions with the porous matrix, sorption processes on the huge surface of hydration products, all contribute to the transport of ions into the pore space of concrete. But it can be seen that significantly less chloride penetrates into concrete under the influence of an applied compressive stress.

In Fig. 6, the chloride profiles as obtained on unloaded specimens by the other four laboratories involved in the comparative test series are shown. Fig. 7 shows the chloride profiles as obtained on concrete prisms under stress ratio of 30 % from the other four laboratories. It is not really astonishing that a wide scatter of the chloride profiles is observed, since the compressive strengths of the tested concrete samples are different. In addition, values from DALIAN U. represent water soluble chloride content, while the other values were obtained by acid extraction.

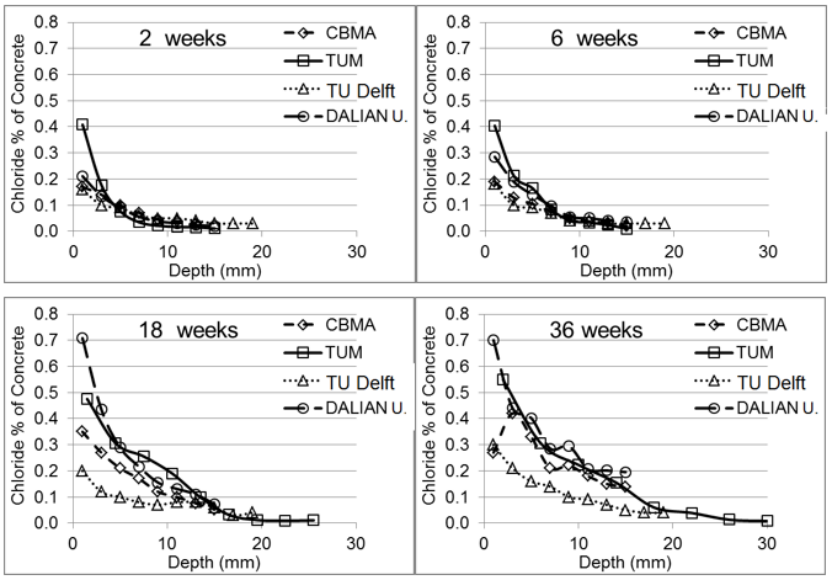

Fig. 6: Chloride profiles as obtained in four different laboratories after exposure times of 2, 6, 18 and 36 weeks on unloaded specimens

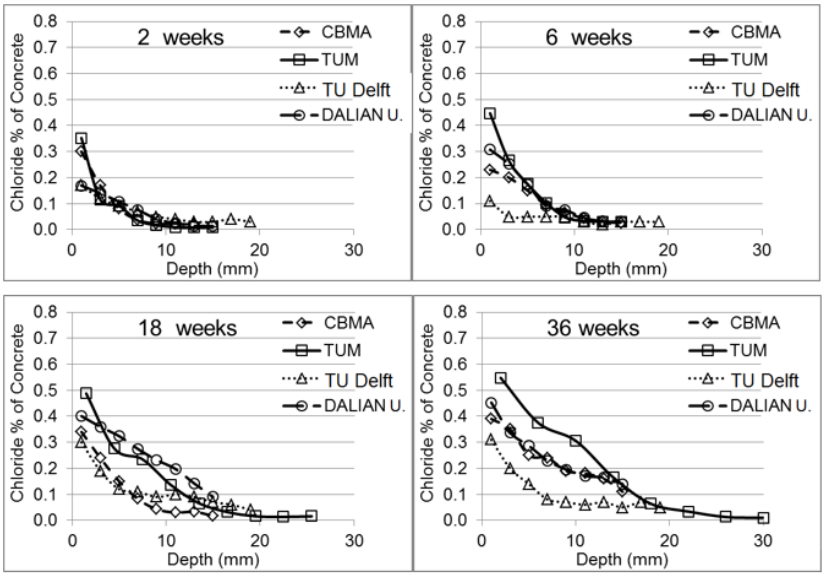

Fig. 7: Chloride profiles as obtained in four different laboratories after exposure times of 2, 6, 18 and 36 weeks at a stress ratio of 30 %

5.4.1.2 Chloride profiles as measured under 60 % stress ratio

Fig. 8 shows typical profiles as determined at UGent under a stress ratio of 60 %. At later exposure times in particular, chloride profiles as shown in Fig. 8 differ from the usually observed shape. A plateau is built up at low distances from the surface. This cannot be described by a simple diffusion process. One may call this surface near zone a convection zone. Most authors suggest using the values behind the convection zone only for determination of an apparent diffusion coefficient. Values right of the vertical lines may then serve as a basis for fitting the error function, erf.

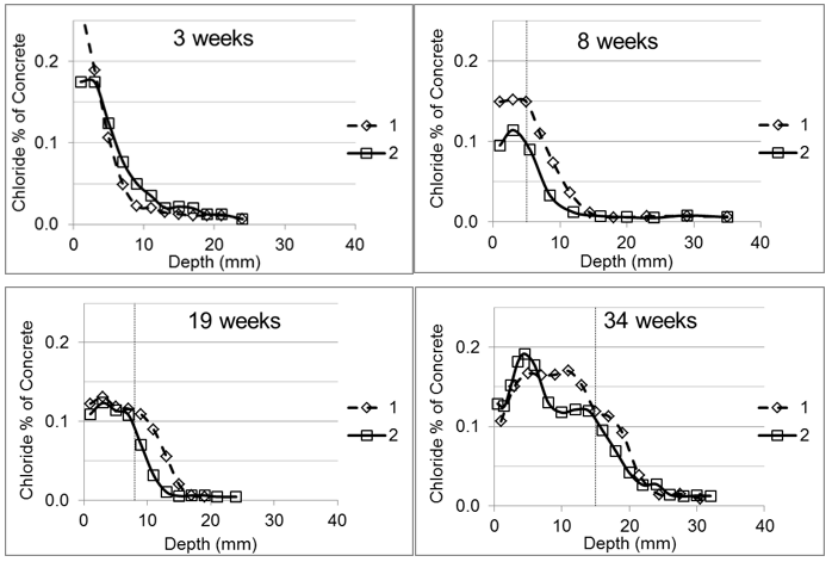

Fig. 8: Chloride profiles as obtained at UGent after exposure times of 2, 8, 19 and 34 weeks under a stress ratio of 60 %

Results shown in Fig. 8 underline again the fact that chloride penetration is not a pure diffusion process. Determination of a diffusion coefficient is a simplification of a complex process. The values obtained may nevertheless be used for comparison of different types of concrete.

Chloride profiles as determined by the four other groups under an applied stress ratio of 60 % are shown in Fig. 9. A wide scatter of the obtained chloride profiles is observed. This is among other influences due to the different quality of the concretes, which were tested (see Tab. 1). Nevertheless, fitting the data with Fick's second law may be

considered to be a reasonable approximation. Information on how to perform the fitting procedure is given in EN 12390-11: 2015 Annex F [15], recommendation and how to present and evaluate the chloride profiles is described in the Recommendation of RILEM TC 246-TDC Influence of Applied stress on Chloride Diffusion [13].

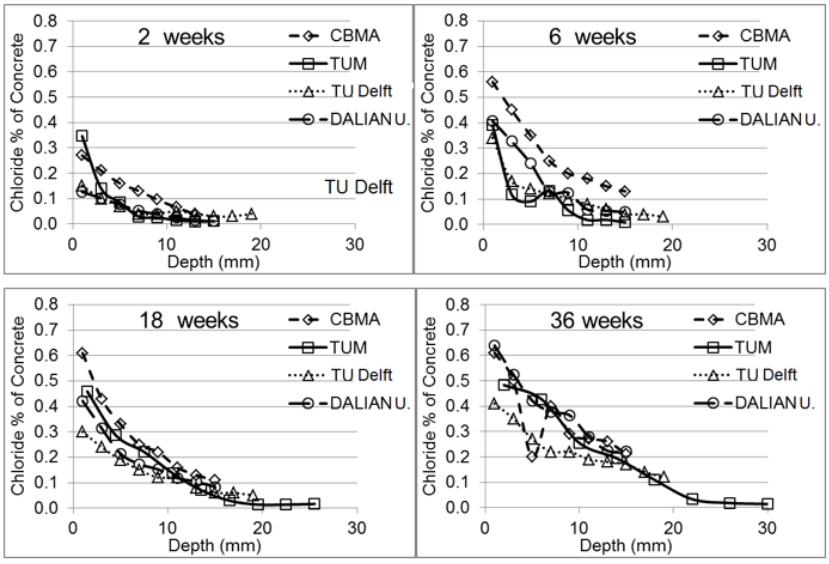

Fig. 9: Chloride profiles as obtained in four different laboratories after exposure times of 2, 6, 18 and 36 weeks under a stress ratio of 60 %

5.4.1.3 Diffusion coefficients and surface concentrations as obtained from profiles determined in five different laboratories

The diffusion coefficient D and the surface concentration C_s as obtained by the five participating laboratories: UGent, CBMA, TU Delft, TUM, and DALIAN U. are shown in Fig. 10. Diffusion coefficients and calculated surface concentrations were determined by curve fitting according to EN 12390-11: 2015 Annex F [15]. The large scatter of the values is mainly due to the fact that the quality of the tested concrete was not the same.

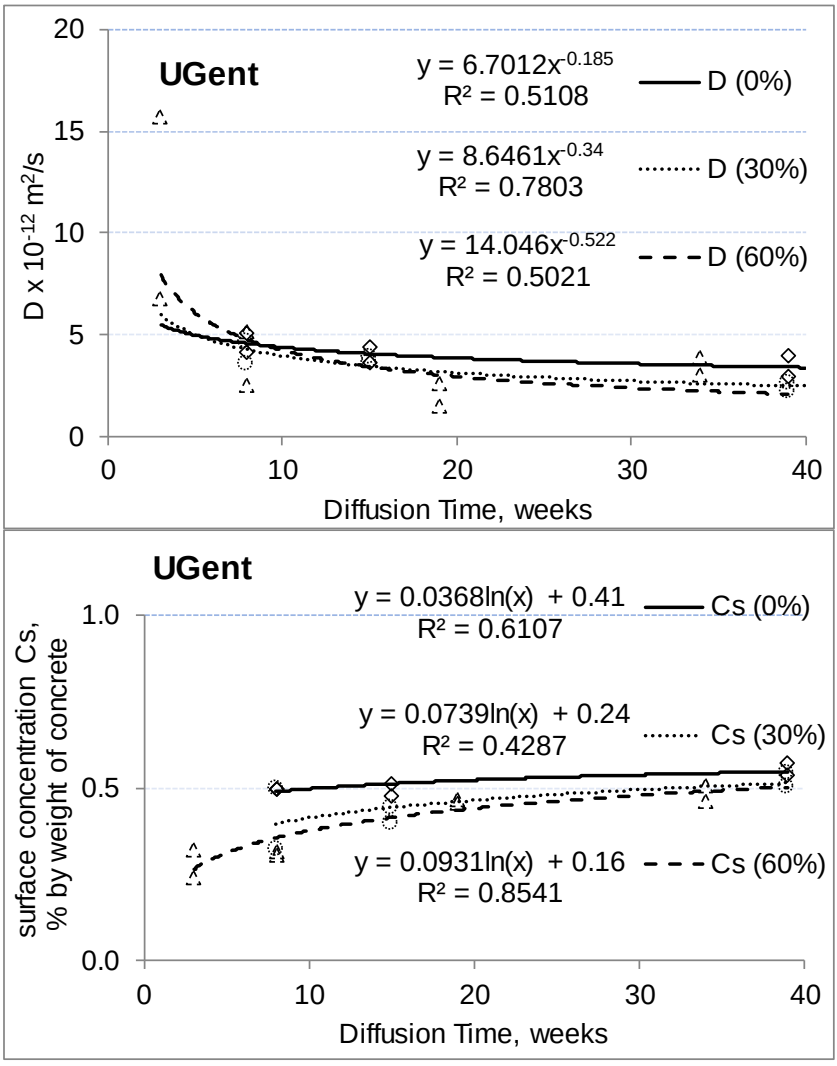
UGent
y = 6.7012x-0.185
R² = 0.5108
D (0%)
y = 8.6461x-0.34
R² = 0.7803
D (30%)
y = 14.046x-0.522
R² = 0.5021
D (60%)
D x 10-12 m²/s
Diffusion Time, weeks
UGent
y = 0.0368ln(x) + 0.41
R² = 0.6107
Cs (0%)
y = 0.0739ln(x) + 0.24
R² = 0.4287
Cs (30%)
y = 0.0931ln(x) + 0.16
R² = 0.8541
Cs (60%)
surface concentration Cs, % by weight of concrete
Diffusion Time, weeks

10 (a) UGent

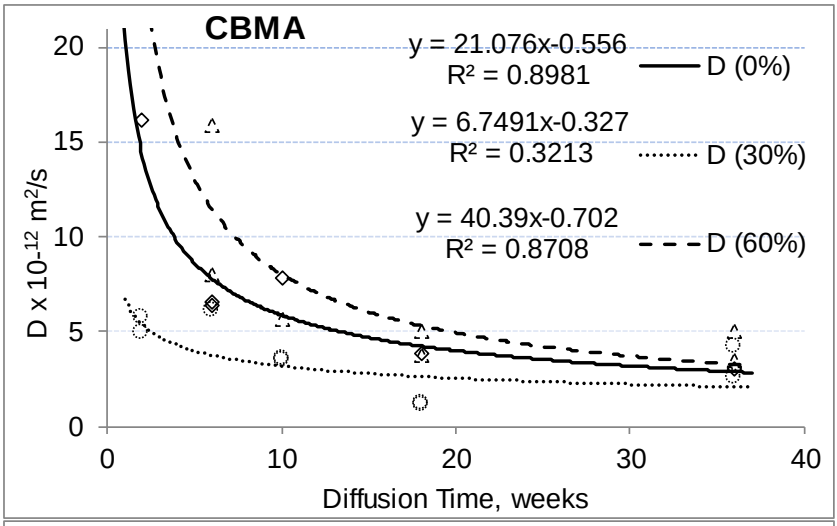
CBMA
y = 21.076x-0.556
R² = 0.8981
D (0%)
y = 6.7491x-0.327
R² = 0.3213
D (30%)
y = 40.39x-0.702
R² = 0.8708
D (60%)
D x 10-12 m2/s
Diffusion Time, weeks

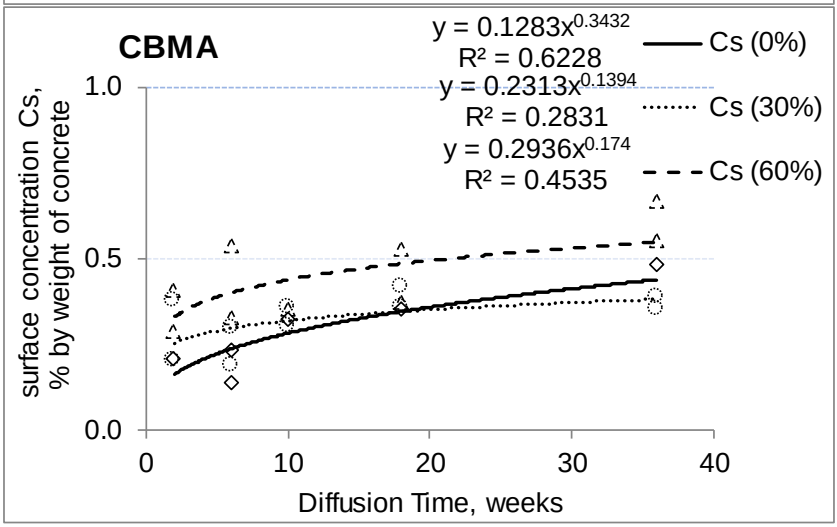
CBMA
y = 0.1283x0.3432
R² = 0.6228
Cs (0%)
y = 0.2313x0.1394
R² = 0.2831
Cs (30%)
y = 0.2936x0.174
R² = 0.4535
Cs (60%)
surface concentration Cs, % by weight of concrete
Diffusion Time, weeks

10 (b) CBMA

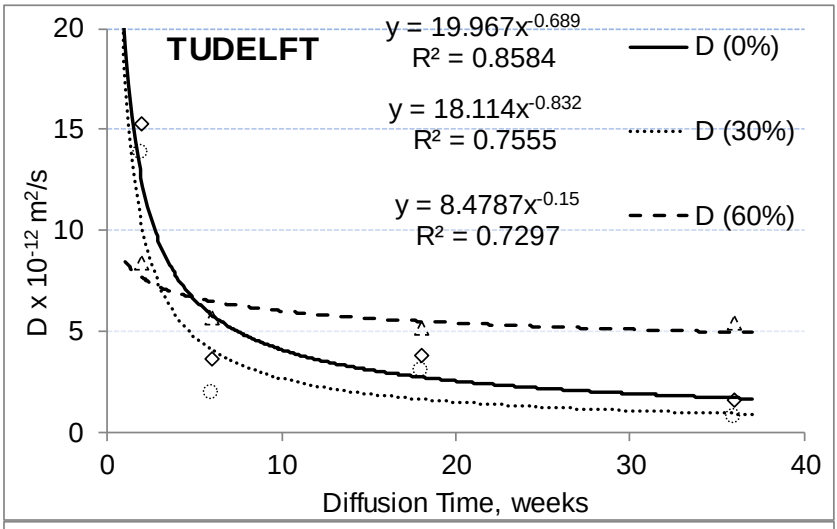
TUDELFT
y = 19.967x^-0.689
R² = 0.8584
D (0%)
y = 18.114x^-0.832
R² = 0.7555
D (30%)
y = 8.4787x^-0.15
R² = 0.7297
D (60%)
D x 10^-12 m²/s
Diffusion Time, weeks

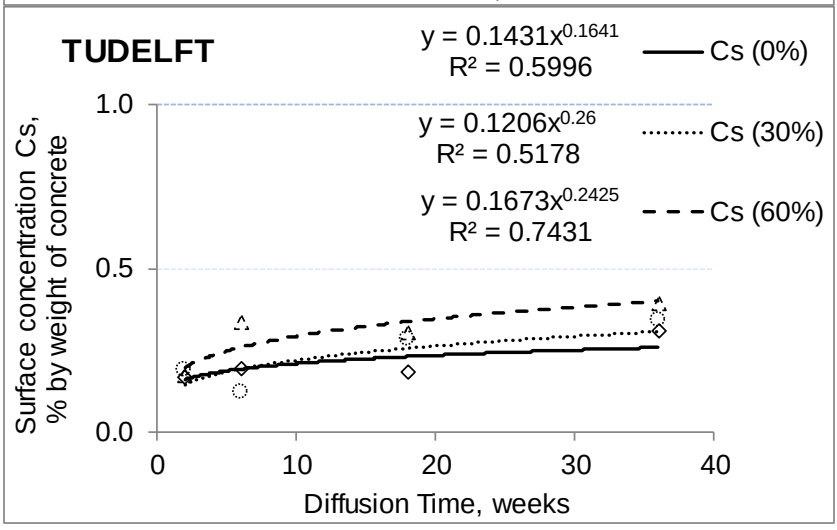
TUDELFT
y = 0.1431x^0.1641
R² = 0.5996
Cs (0%)
y = 0.1206x^0.26
R² = 0.5178
Cs (30%)
y = 0.1673x^0.2425
R² = 0.7431
Cs (60%)
Surface concentration Cs, % by weight of concrete
Diffusion Time, weeks

10 (c) TU Delft

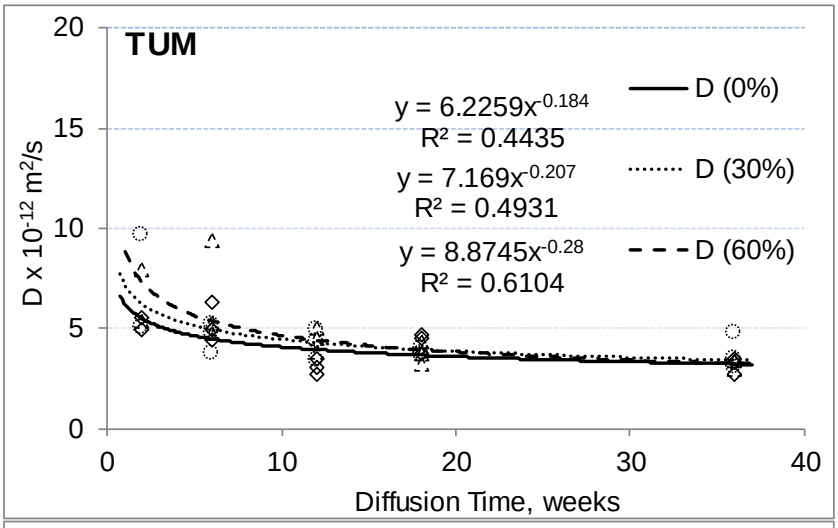
TUM
y = 6.2259x^-0.184
R² = 0.4435
y = 7.169x^-0.207
R² = 0.4931
y = 8.8745x^-0.28
R² = 0.6104
D (0%)
D (30%)
D (60%)
D x 10^-12 m²/s
Diffusion Time, weeks
0
5
10
15
20
0
10
20
30
40

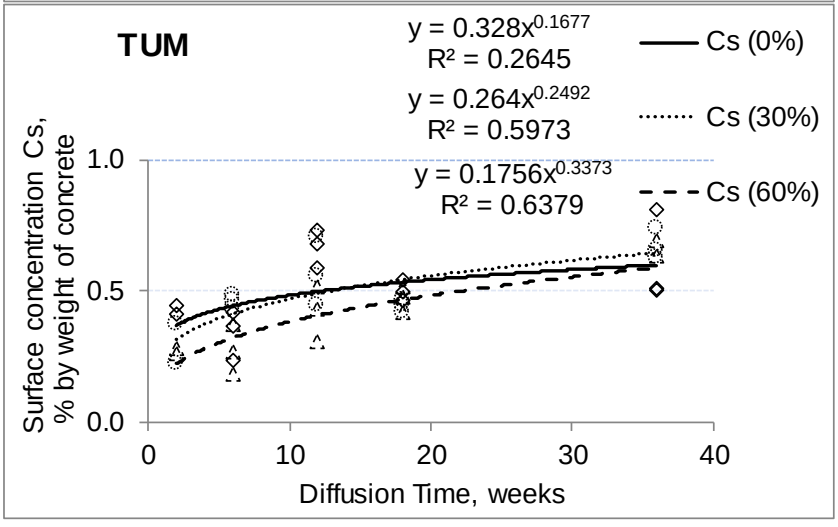
TUM
y = 0.328x^0.1677
R² = 0.2645
y = 0.264x^0.2492
R² = 0.5973
y = 0.1756x^0.3373
R² = 0.6379
Cs (0%)
Cs (30%)
Cs (60%)
Surface concentration Cs, % by weight of concrete
Diffusion Time, weeks
0.0
0.5
1.0
0
10
20
30
40

10 (d) TUM

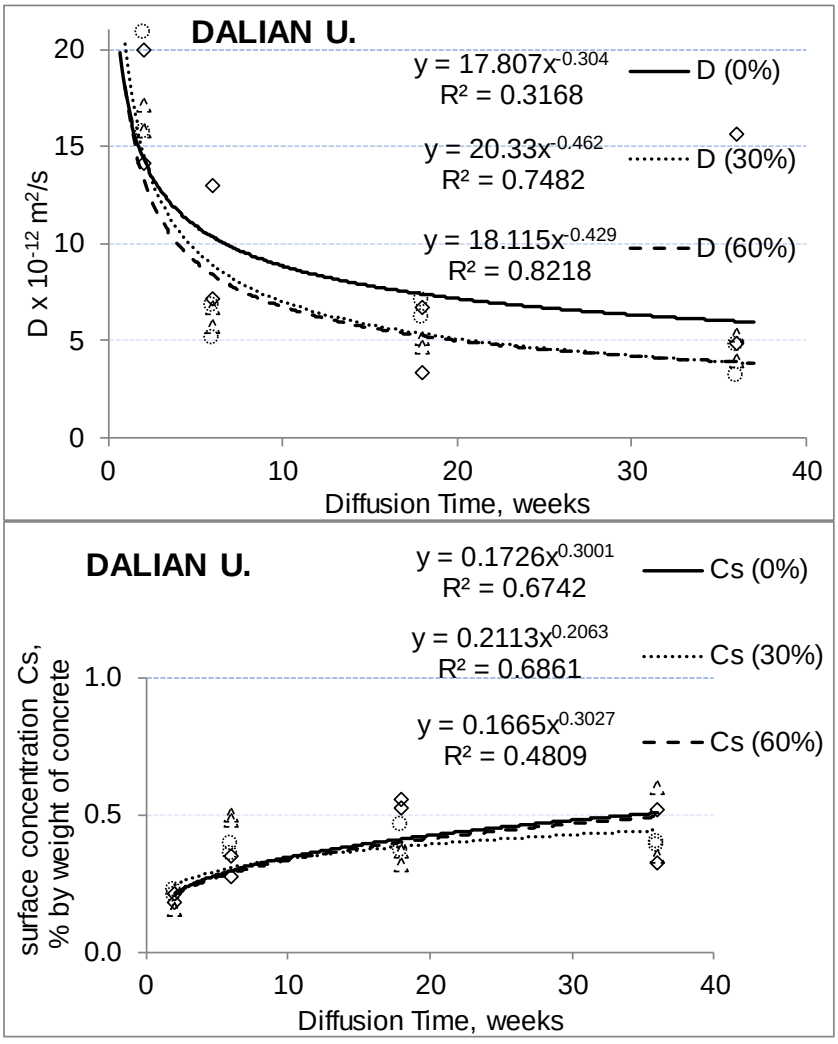

10 (e) Dalian

Fig. 10: Chloride ion diffusion coefficients and surface concentrations as determined from experimental data obtained by 5 laboratories

From Fig. 10 it can be concluded that the diffusion coefficients tend to decrease with exposure time while the calculated surface

concentrations increase. All the values for the diffusion coefficients tend to stabilize at values approaching (3~4) × 10^{-12} m^2/s for long exposure time (36 weeks). The calculated surface concentration stabilizes around 0.5 % for the same exposure age.

At a load of 30% of the ultimate failure load, the diffusion coefficients were mostly similar or lower than in the unloaded situation. At a load of 60% of the ultimate failure load, the situation was less clear, and in the different laboratories, similar, higher or lower diffusion coefficients were determined. In some cases, the formation of a convection zone near the surface was prominent, as shown in Fig. 8 and Fig. 9. The data therefore partly agree with literature, stating that chloride diffusion under moderate compressive load is slowed down, but it increases if the applied load overcomes half of the ultimate load [9].

5.4.2 Influence of tensile stress

5.4.2.1 Diffusion coefficients and surface concentrations measured under an applied tensile stress

Chloride profiles as determined on concrete specimens under tensile stress are shown in Fig. 11. Chloride profiles were determined after an exposure time of 2, 6, 10, 18, and 36 weeks. It can be clearly seen that the chloride content increases steadily with increasing exposure time. The chloride content at a given depth is increased significantly by an applied tensile stress. This result was expected as the pore space or the micro-cracks are widened under the influence of an applied tensile stress

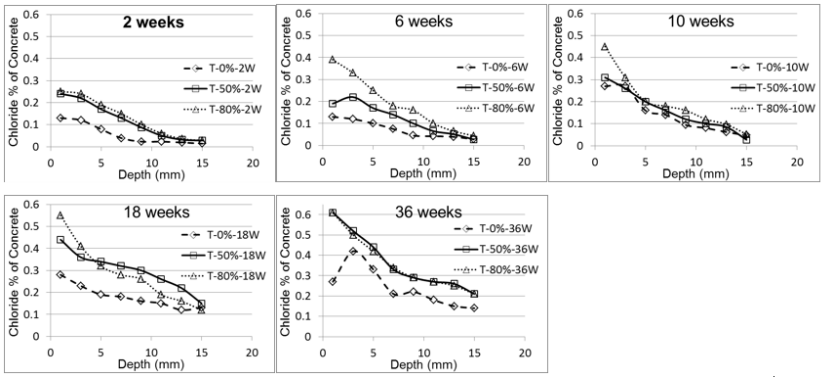

Fig. 11: Chloride profiles as determined after 2, 6, 10, 18 and 36 weeks under tensile stress with a stress ratio of 0, 50, and 80 %

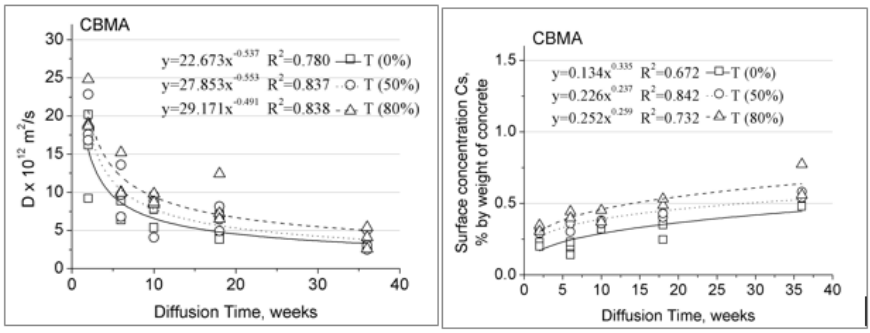

Fig. 12 Chloride ion diffusion coefficients and calculated surface concentrations of concrete under tension

Fig. 12 shows that the diffusion coefficient of concrete under tension increases with increasing stress ratio, but it decreases significantly with exposure time. Application of tensile stress accelerates chloride diffusion in concrete. Despite the wide scatter, it can be seen that the calculated surface concentration increases slightly with increasing exposure time.

5.5. Modelling and prediction

5.5.1 Modelling

Reinforced concrete structures which are exposed to de-icing salt or seawater could be damaged by chloride induced reinforcement corrosion. The fib Model Code for Service Life Design, fib bulletin 34 [5], provides a transport model for predicting the time-dependent probability that reinforcement corrosion is initiated. The transport model considers when a critical chloride content at the depth of the reinforcement is reached in dependence of the concrete characteristics and chloride impact. Further explanations on relevant input data and example calculations are given in fib bulletin 76 [16]. According to [5] and [16], transport of chlorides into concrete can be modelled utilizing Equations 1, 2 and 3, cp. [16]. Here, Equation 2 was extended by a so-called stress factor k_I, which takes investigated stress condition of the structural member into account.

$$C(c_{nom}, t_{SL}) = C_i + (C_s - C_i) \cdot \left[\operatorname{erf}\left(\frac{c}{\sqrt{D_{app,A}(t_0) \cdot t}} \right) \right] \quad (1)$$

$$D_{app,A}(t) = k_e \cdot k_l \cdot D_{app}(t_0) \cdot \left(\frac{t_0}{t} \right)^{\alpha_A} \quad (2)$$

$$k_e = \exp\left(b_e \cdot \left(\frac{1}{T_{ref}} - \frac{1}{T_{real}} \right) \right) \quad (3)$$

where c_{nom} is the nominal concrete cover; t_{SL} is the design service life; C_i is the initial chloride content; C_S is the chloride content at the concrete surface; c is the concrete cover; $D_{app,A}$ is the apparent chloride diffusion coefficient; t_0 is the reference point in time; t is the time; k_e is the transfer parameter; α_A is the aging exponent; b_e is the temperature coefficient; T_{ref} is the reference temperature; T_{real} is the temperature of the structural element or the ambient air.

In the following study the service life or the time to corrosion initiation respectively is presented for concrete components under unloaded condition compared to concrete components under compressive as well as under tensile stress.

The study corresponds to a case study already presented in [16], Table A.2-15 which has been considered due to its similarity in concrete material (CEM I-concrete of w/c = 0.45, unloaded). The case study of fib bulletin 76, which is re-calculated here for loaded concrete members, represents a typical XS2-exposure (member immersed in seawater) in Portugal (Europe). Most of model input parameters, especially the variables characterizing the environmental load, were taken from the aforementioned Table A.2-15 of fib bulletin 76. However, input variables which do characterize the concrete material ($D_{app}(t)$) were derived from the aforementioned experiments. Material data used in the re-calculation was average data of all 5 labs (CBMA, UGent, TU Delft, TUM and DALIAN U.) participating in the experimental program. Averaged diffusion coefficients determined after 6 weeks (t_0 = 0.115 years) of unloaded samples were considered to be the (unloaded) reference value (mean was 6.52 x 10^{-12} m^2/s, standard deviation was 2.88 x 10^{-12} m^2/s), cf. Tab. 2. All other load conditions were referenced with a stress factor k_l, in which k_l = 1 for the reference, k_l = 0.80 for stress ratio 0.3 (compression), k_l = 1.17 for

stress ratio 0.6 (compression), k_l = 1.25 for stress ratio 0.5 (tension) and k_l = 1.53 for stress ratio 0.8 (tension).

For the determination of an age exponent, the exposure time should be as large as possible (minimum 2 years). In this study, the maximum exposure time was only 36 weeks. In total 15 series were investigated (5 labs, 3 different stress levels), consequently 15 “short term” age exponents, cp. Fig. 10, could be calculated according to [16], approach A. Tab. 2 contains not only information on α_A but also shows the general input parameters in accordance with [5].

Tab. 2 Input parameters for the service life prediction

Parameter	Unit	Distribution type	Mean	Standard deviation	a	b
$D_{app}(t_0)$	$\cdot 10^{-12}$ m^2/s	Normal	6.52	2.88	-	-
α_A	-	Beta	0.39	0.18	0	1
t_0	years	Constant	0.115	-	-	-
t	years	Constant	50	-	-	-
T_{ref}	K	Constant	293	-	-	-
T_{real}	K	Normal	288	5.0	-	-
b_e	K	Normal	4800	700	-	-
$C_{S,\Delta}$	M.-%/c	Lognormal	3.0	1.0	-	-
Δx	mm	Constant	0	-	-	-
C_{Crit}	M.-%/c	Beta	0.6	0.15	0.2	2.0
c	mm	Normal	50	6	-	-

5.5.2 Prediction

The reliability of chloride exposed concrete members in unloaded conditions, under compressive stress and under tensile stress respectively, is given in Fig. 13. All calculations of this exemplifying case study are performed by utilizing the software STRUREL [17].

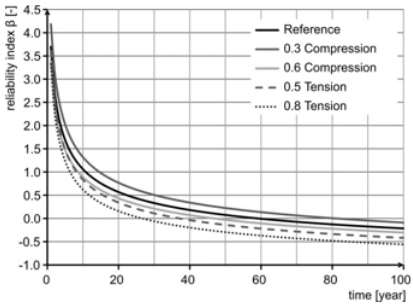

Fig. 13 Calculated reliability of chloride exposed concrete members, unloaded, and under compression and tension stress (two different ratios)

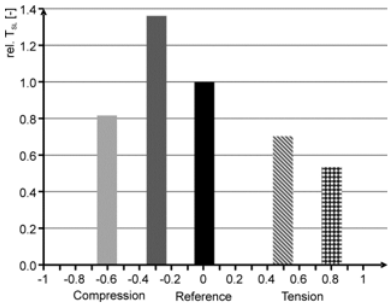

Fig. 14 Relative service life (rel. T_{SL}) of chloride exposed concrete members, unloaded (reference), compression and tension loaded (two different ratios)

In order to give numbers on the influence of loading on service life, the end of service life was defined to be reached when reliability drops below the defined minimum reliability of β = 0.5. Based on this definition, service life was determined for each of the five presented calculations and referenced on the unloaded case respectively, cf. Fig. 13 and Fig. 14. Fig. 14 shows that the service life of elements loaded by 30 % of compressive strength was on average prolonged by a factor of 1.36 compared to the reference; the service life of elements loaded by 60 % of compressive strength was on average shortened by the factor of 0.82 in comparison to unloaded elements. It is remarked, that at compressive stress ratio of 60 % only two out of five labs found a remarkable increase in diffusion coefficient (which is linked to shortened service life), others found a low decrease in diffusion coefficient. From the data presented here we may conclude that further tests will be needed to get more precise information on the influence of loading condition on service life of reinforced concrete elements. But it should be underlined in this context that the main aim of RILEM TC 246-TDC was to develop a suitable test method.

If tensile stress was applied, service life decreased compared to the reference. Service life was shortened by the factor of 0.70 (50 % of tensile strength stress) and 0.53 (tension, 80 % of tensile strength), respectively.

In conclusion, it is obvious that the concrete loading condition has an influence on the service life.

5.6. Conclusions and outlook

The main task of RILEM TC 246-TDC was to develop a test method to study the influence of applied compressive and tensile stress on the rate of chloride penetration. Results obtained are presented and discussed in this report. These results show that the state of stress should be taken into consideration to make durability and service life design more reliable.

As mentioned in the introduction of this report already, RILEM TC 246-TDC opened a new field of research, with the major aim to make design for durability and service life of reinforced concrete structures more realistic and more reliable by taking combinations of applied mechanical stress and environmental loads into consideration. It was initially clear that this task could not be finished within the duration of one single RILEM TC. Yet a beginning was made, which now asks for well-structured continuation. The influence of an applied stress on chloride diffusion was measured and a recommendation on the test method was formulated. Results obtained already allow an estimation of the influence of an applied stress on durability and service life of reinforced concrete structures exposed to a chloride containing environment. If the recommended test method is applied, specific behaviour of different types of concrete under the influence of stress can be taken into consideration.

In the future, more work will be necessary in order to investigate the influence of an applied stress, for instance on the rate of carbonation and on frost resistance. Results described in the final report of RILEM TC 246-TDC clearly show the need for follow-up investigations. Future technical committees could have the common task to establish a solid basis for taking the influence of an applied stress on durability and service life into consideration. Then only the actual situation of the built infrastructure in many countries can be substantially improved in a systematic way. The next step should be to run similar test series on concrete exposed to carbonation and to formulate a standard method that will allow determining the influence of an applied tensile or compressive stress on the rate of carbonation.

For a generally realistic and reliable service life prediction the influence of an applied cyclic stress has to be taken into consideration too. So far, however, only very limited data exist related to this topic [9].

In this report an experimental method to study the influence of mechanical load on chloride penetration into the pore space of cement-based materials is described in detail. In fact service life of reinforced concrete structures depends on a multitude of possible combinations of mechanical load and environmental actions, including freeze-thaw cycles. Frost action has been studied in detail by two RILEM TCs, TC 176-IDC [18] and TC 117-FDC [19]. Recommendations published by these two RILEM TCs were based on a series of comparative test series and results were evaluated according to ISO 5725 [20]. Now the essential results of these two TCs are part of European standardization. Cracks formed during freeze-thaw cycles and frost suction in particular will have to be taken into consideration in future tests of combined environmental and mechanical loading [21].

In order to achieve a better understanding and a systematic description of the influence of combined mechanical load with environmental actions on durability and service life of reinforced concrete structures, a numerical model of damage processes in the composite structure of concrete has to be developed. This model can be tested by comparison with measured data and it can be helpful to predict the behaviour under different load combinations.

In parallel to the experimental test series and numerical simulations, the actual method to predict durability and service life has to be further developed in order to enable easy use of the experimental data obtained for realistic service life prediction.

Acknowledgements

The financial support from the following four organizations is gratefully acknowledged: 1) National Natural Science Foundation of China (Grant No.51320105016), 2) the Ecuadorian National Secretary for Science and Technology "SENESCYT", 3) ESPOL University (Ecuador) and Magnel Laboratory for Concrete Research of Ghent University (Belgium), 4) Ministry of Higher Education Malaysia (MOHE) and Universiti Teknologi MARA (UiTM).

References

1. Eurocode 2 (2004) Design of concrete structures, Part 1-1: General rules and rules for buildings, EN 1992-1-1
2. ACI 318-14 (2014) Building code requirements for structural concrete and commentary
3. JSCE Guidelines for Concrete No. 15 (2007) Standard specifications for concrete structures –design
4. GB 50010 Chinese National Standard (2010) Code for design of concrete structures
5. Schießl P, Bamforth P, Baroghel-Bouny, V, Corley G, Faber M, Forbes J, Gehlen C, et al (2006) Model code for service life design. fib bulletin 34
6. ASCE (2013) 2013 Report card for America's Infrastructure
7. F. H. Wittmann, T. Zhao, F. Jiang, and X. Wan (2012) Influence of combined actions on durability and service life of reinforced concrete structures exposed to aggressive environment, Restoration of Buildings and Monuments 18 : 105-112
8. X. Wan, F. H. Wittmann, and T. Zhao (2011) Influence of mechanical load on service life of reinforced concrete structures under dominant influence of carbonation, Restoration of Buildings and Monuments 17: 103-110
9. Y. Yao, L. Wang, and F. H. Wittmann (editors) (2013) Publications on durability of reinforced concrete structures under combined mechanical loads and environmental actions, An Annotated Bibliography, RILEM TC 246-TDC
10. GB 175 Chinese National Standard (2007) Common Portland Cement
11. BS EN 197-1 Cement (2011) Composition, specifications and conformity criteria for common cements-part 1: cement
12. RILEM TC 107-CSP Recommendation (1998) Measurement of time-dependent strains of concrete, Materials and Structures 31: 507-512

13. Recommendation of RILEM TC 246-TDC: Influence of applied stress on chloride diffusion. Submitted to Materials and Structures

14. EN 14629 (2007) Products and systems for the protection and repair of concrete structures – Test methods – Determination of chloride content in hardened concrete

15. EN 12390-11 (2015) Determination of the chloride resistance of concrete, unidirectional diffusion

16. Gehlen, C.; Bartholemew, M.; Edvardsen, C.; Ferreira, M.; v. Greve-Dierfeld, S.; Gulikers, J.; Helland, S.; Markeset, G.; McKenna, P., Papworth, F.; Pielstick, B and Rahimi, A. (2015) Benchmarking of Deemed-to-Satisfy Provisions in Standards, fib bulletin 76: ISBN: 978-88394-116-8, May 2015

17. Structural reliability analysis software, http://www.strurel.de/

18. RILEM TC 176-IDC Recommendation, M. J. Setzer, P. Heine, S. Kasparek, S. Palecki, R. Auberg, V. Feldrappe, E. Siebel (2004) Internal damage of concrete due to frost action. Materials and Structures 31: 743-753

19. RILEM TC 117-FDC Recommendation (1996) CDF test - test method for the freeze thaw and deicing resistance of concrete - Tests with sodium chloride (CDF). Materials and Structures 29: 523-528

20. ISO 5725-1 (1994) Accuracy (trueness and precision) of measurement methods and results

21. M. J. Setzer, Development of the Micro-Ice-Lens Model, in M. J. Setzer, R. Auberg, R and H.-J. Keck (2002) Frost resistance of concrete. Proc. Intern. RILEM Workshop, Essen 2002. RILEM Proc. 24. RILEM Publ. S.A.R.L., Cachan-Cedex, France, pp 133-146

CHAPTER 6. CHLORIDE ATTACK IN LOADED CONCRETE

The development of section 6.3 has considered part of the content published by: HUGO EGUEZ ALAVA, ELENI TSANGOURI, NELE DE BELIE, GEERT DE SCHUTTER, " Chloride interaction with concretes subjected to a permanent splitting", Construction and Building Materials 127 (2016) 527 – 538

6.1. Background

Hardened concrete resists very well the applied compressive loads from external sources. However, this material has a low tensile strength which is about one tenth of its magnitude in compression. This renders it susceptible to cracking under tensile loads. Consequently, a steel reinforcement is needed in the structural element to carry the tensile stresses provoked by applied loads. The tensile strength of concrete is practically neglected from most structural designs. Thus, cracking is expected to occur in structural elements due to the loads applied during its service life. The designer's main goal is controlling the crack width and their distribution in the structural element. Cracks are not only originated by external loads, the volume change caused by the drying shrinkage of concrete may provoke cracking. This situation can happen when concrete volume change in the structural element is restricted and tensile stresses are generated.

Corrosion of reinforced concrete is amongst the main causes of concrete deterioration. Every year important expenditures are consumed worldwide to rehabilitate damaged structures affected by corrosion. Chlorides are amongst the main factors that cause corrosion in concrete structures. Chloride ingress to reinforced concrete is commonly found in pavement and bridges that have been exposed to deicing salts. Other examples of structures exposed to chlorides are found in marine structures and industrial chloride rich environments.

Chloride transport into concrete is governed by several mechanisms. Capillary suction, convection, migration, are some of the most common means of carrying chlorides. In saturated concrete, diffusion

is the predominant mode of transporting chloride salt. The concrete cover in concrete and its cementitious hydrated paste act as an electrochemical membrane in which ions interact [1-9]. In well cured concrete this concrete cover acts as a barrier retarding the diffusion of chlorides.

Chloride is immobilized by chemical reaction to form Friedel's salt. Among the factors that reduce the movement of these ions are the physical adsorption of ions on CSH and its charge generation, the gel pore size and the presence of an electrical double layer (EDL), and the surface site density of CSH [10]. The ionic transport in cement paste with low porosity is made through capillary pores that are connected to gel pores. At gel pores the EDL plays a main role in the ionic transport and controls it [10].

On the other hand, the lagging motion of the corresponding cations of chloride in the solution also contributes to a delay of the chloride ingress [2,3,4].

Nevertheless, in the same way that there are conditions that restrain the entry of chlorides, there are also processes that can accelerate this infiltration.

The micro-pore system of concrete is always changing in time. Its characteristics can be improved due to continued paste hydration or degraded due to its deterioration.

Concrete structures at field sites are exposed to mechanical loads in combination with aggressive agents. Thus, a mechanical load can modify the chloride transport into the structure.

Relatively recent research revealed that the chloride passage through concrete micro-structure is regularly reduced when concrete is subjected to compressive load lower than one third its maximum compressive loading capacity [11, 12]. The reduction of the attack has been perceived by the lower content of total chlorides observed in the diffusion profile of the samples subjected to a stress level of 30%. The

explanation for this drop has been accredited to a decrease in the concrete pore size due to the compression level.

Under direct tensile load the rate of chloride penetration increases progressively as the load is increased [11].

A contrary effect in the chloride intrusion and the damage, should be produced when the load exceeds certain limit. Some researchers attribute this situation to the critical stress level (CSL). At this stress level microcracks should start to develop. According to Choinka “et al.”, CSL was observed to occur in concretes subjected to an 80 % of the maximum compressive load [13]. On the other hand, Takafumi “et al.”, found this critical value in a range between 76 – 79% stress level for normal weight concretes and 82 - 89% for lightweight structural concrete [14]. However, it should be considered that critical stress level in concrete has been studied and determined in an inert environment. The combination of mechanical and corrosive loads may induce a threshold level for cracking at stresses lower than the defined CSL which is obtained in a corrosion free environment.

Stress-corrosion cracking (SCC) is a term used to describe service failures in engineering materials that occur by slow, environmentally induced crack propagation (15). The simultaneous combination of chemical-mechanical forces produces a synergetic effect that ends in crack propagation at stress levels lower than the critical.

Is generally agreed from the information available so far, that the chloride content in concrete is certainly reduced at 30 % stress level in compression. However, at a 60 % stress level the data are contradictory. Some results have shown an increase in the chloride profile, some other reports show no apparent influence in the chloride content while others describe a reduction on the chloride content level [12].

It seems that low chloride profiles are not an uncommon feature in concrete subjected to combined attack. Available research show some examples in concretes that have been previously carbonated, subjected to wetting and drying, or to combination of wetting and

drying plus cracking. All these concretes show a consistently lower chloride content specially located in its outermost zones [16-19]. Thus, a progressively formation of an altered "skin layer" seems to be generated by one or more of the previously mentioned combined factors. The difference in composition between this modified skin layer and the unaltered bulk may be the cause. Consequently, they could have different transport behaviour for chloride. Thus, different chloride contents as well as distinct diffusivity values can classify these zones [20]. The differences in the chloride interaction in these two zones can generate a chloride profile that deviates from error-function model.

This study tries to understand the chloride transport into concrete subjected to stresses below and near the critical stress level.

6.2. Chloride attack under compression

6.2.1 Concrete mixture, test samples and initial conditions.

A concrete mixture named OPC with a water/cement ratio of 0.45 was prepared for this investigation, as presented in Table 2-3. The purpose of the investigation was oriented to analyse a relative effect of compressive loading on chloride intrusion.

The aggregates were gravel and a natural sand of siliceous nature with gradings shown in Figure 2-1. An ordinary Portland cement (OPC), CEM I 52.5 N according to European Standards was used, its chemical composition is shown in Table 2-1. To improve the fresh concrete properties (slump about 160 mm) 1.1 L/m^3 superplasticizer (polycarboxylic ether based) was used.

After mixing, concretes prisms were cast in (100 X 100 X 400) mm^3 moulds. Subsequently, after 24 hours the prisms were demoulded and cured until 28 days at 20 $\pm$ 2 ^oC and RH > 95% RH.

At 28 days, the prisms were removed from the curing chamber and their surfaces were dried with a cloth from free water. A casted concrete face from one of the sides of the molds was chosen and polished with sandpaper to obtain a flat and homogeneous surface for

chloride exposure. Next, a solution tank (80 x 160 x 50) mm^3 was glued on this surface using black silicon (Figure 6-1). It is necessary to allow the silicon to harden before starting the process of vacuum saturation.

Figure 6-1: Concrete prisms with the solution tank and covered with black silicon to impermeabilize the sample.

6.2.2 Experimental setup in compression loading

The samples were placed under vacuum at 2.7 kPa during 2.5 hours. Next they were gradually saturated with tap water and the pressure was slowly released to atmospheric conditions and left for 24 hours. The saturated samples were then surface dried. Afterwards, an additional layer of black silicon was applied (Figure 6-1) to cover remaining areas of the solution tank followed by an aluminum foil protection. The solution tank was connected to an 8 litres stock solution tank provided with an aquarium pump with capacity to pump the solution at a flow rate of 23 l/h.

Before exposing the samples to the attacking solution, they were gradually loaded until reaching the test load as shown in Figure 6-2.

The load was transferred by a hydraulic jack which is connected to a pressurized cylinder which contains a nitrogen/oil mixture. Periodically check-ups were made to correct any load losses.

Figure 6-2: Two coaxially loaded prisms showing detail of the chloride stock solution and the loading rigs

6.2.3 Compressive strength values and digital image correlation (DIC) tests

At 28 days of age, 2 prisms were tested for compressive strength and their average value is shown in Table 6-1. The values for the loading corresponding to 30 and 60% of the ultimate load are also shown in this table.

Table 6-1: Permanent loading conditions for the compression test setup at 30 and 60% stress ratio.

Sample Denom.	Ave. Load (100%) kN	Variation Coeff. %	Compr. Strenght MPa	30% of Max. kN	60% of Max. kN
OPC	568.9	1.07	56.9	171	341

The previously acquired information was utilized to perform Digital image correlation (DIC) analysis. This technique consists of a stereoscopic camera system (two high-resolution cameras are placed facing the area under investigation) that, based on stereo-correlation and stereo-triangulation, reconstructs the 3D full-field deformation vector field on the material's surface. In practice, one of the samples'

side area (100 mm · 250 mm) was covered with high-contrast random speckle pattern as shown in Figure 6-3. The Vic-3D post-processing software tracked the speckles at the reference stage (sample without load) and through time as the samples were progressively loaded under compressive stresses.

Figure 6-3: Prismatic samples with the digital image correlation (DIC) pattern setup.

The strain field map was computed by numerical derivation of the deformation fields. The first principal strain maps, e_1 (%) are considered in this study. The principal strain e1 was derived by transformation of the e_{xx}, e_{yy} and e_{xy} normal strains (the Cartesian coordinates system is given in Figure 6-3. An incipient strain distribution was started to develop after 30% stress ratio. The samples were loaded until 80 % stress ratio to avoid complete failure. The strain distribution for the tested prism is shown in Figure 6-4.

Considering that the obtained overall strain distribution for the samples at 80% stress ratio would develop larger micro-cracks, it was decided to apply a stress level of 60% in the final experiment. That

stress level is considered high enough and can be maintained stable during a long sustained load application.

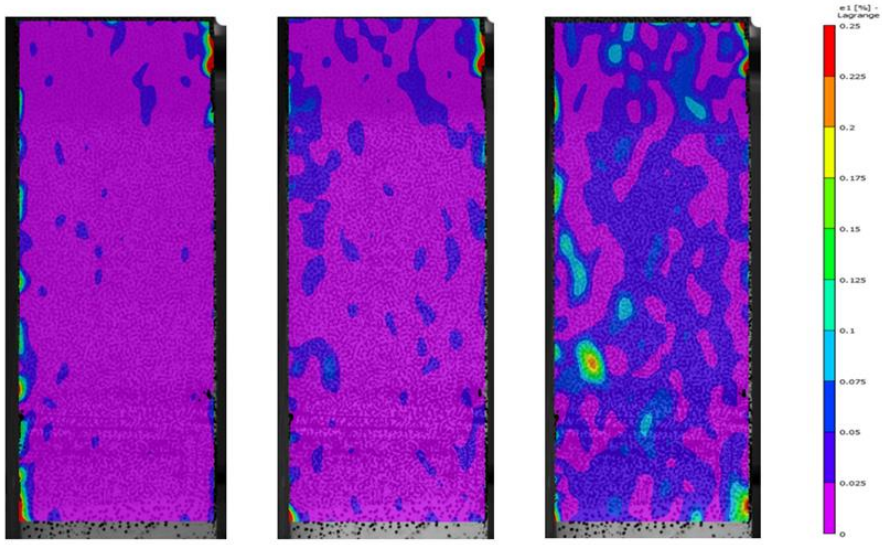

Figure 6-4: Principal strain distribution e1 (%) for S0 concrete subjected to 30, 60 and 80 % compressive stress level respectively.

6.2.4 Chloride profiling

For the 0 and 30% stress level exposure, the samples were taken out from the loading rigs after 8, 15 and 39 weeks for chloride profiling. On the other hand, for the 60 % exposure condition the samples were tested at 3, 8, 19, 34, and 64 weeks.

Considering the homogeneous distribution of strains shown in Figure 6-4, the powders were collected from a groove 10 mm wide by 30 mm long. The groove's long axis was aligned with the elongated axis from the prism. Special care was taken to extract the samples at least 10 mm from the exposure border. The grinding was done in layers of 1-2-3 or 4 mm thickness. The thickness of the layers increased as the depth progressed. The powder extraction was executed utilizing a 10-mm

diameter drilling bit placed in a fixed vertical shaft as shown in Figure 6-5. The sample was anchored to a table capable of a controlled and precise movement in two directions perpendicular to each other. The obtained indentation (10 x 30 mm, width x length) was filled with epoxy for continuing the investigation with the same specimen for later ages. Thus, the sample was subjected to an un-loading/loading cycle at each moment of chloride determination.

Figure 6-5: 10 mm wide by 30 mm long grooves for chloride powder extraction (left). Detail of the drilling tool provided with sliding table in 2 directions (right)

The obtained powders were treated with nitric acid to extract the total chloride content. The utilized technique is described in EN 14629 “Determination of chloride content in hardened concrete”. Chloride content determination was done by potentiometric titration with a 0.01 M silver nitrate solution Figure 6-6. It was utilized a potentiometric titrator model 702 SM Titrino (Metrohm) with a precision of $\pm$ 30 micro-liters. This allows the measure of chloride content with an error of $\pm$ 0.0005% by weight of concrete in the case that 2 grams of powdered sample is tested.

Figure 6-6: Extracted chloride solution from powdered samples with nitric acid digestion (left). Potentiometric titration of chloride with 0.01 M silver nitrate (right).

The chloride content in the concrete powdered sample is calculated with the following equation (6-1).

$$Cl^-(\%) = \frac{[Ag^+ - B]*M*35.45*100}{1000*W} \quad (6\text{-}1)$$

Where:

B = ml (blank obtained from the utilized de-minerilized water)

Ag^+ = titration volume (ml)

W = sample weigth (g)

M = silver nitrate molarity = 0.01 mole/L

CMW= Chloride molecular weigth (35.45 g/mole)

6.2.5 Thin section preparation for microscopic analysis

After the final chloride exposure, a rectangular concrete section (width = 30 mm, depth = 50 mm) was sawn from the specimen subjected to 60% stress level as shown in Figure 6-7.

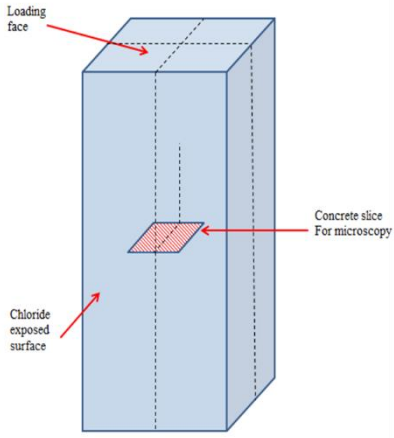

Figure 6-7: Schematic view of the concrete slice cutting location for microscopic examination

After fluorescent epoxy impregnation under vacuum, the sawn slice was ground and polished removing the excess of epoxy. Subsequently the finished surface was glued on an object glass. Finally, the concrete sample was cut parallel to the glass and the remaining slice was polished to obtain a 25 µm thin section of concrete for microscopic observation. Thin sections were analyzed using a petrographic microscope under fluorescent light excitation.

6.2.6 Results and discussion

6.2.6.1 Chloride profiles for non-loading conditions

Chloride profiles obtained at different stress levels and their evolution with time are shown in Figure 6-8.

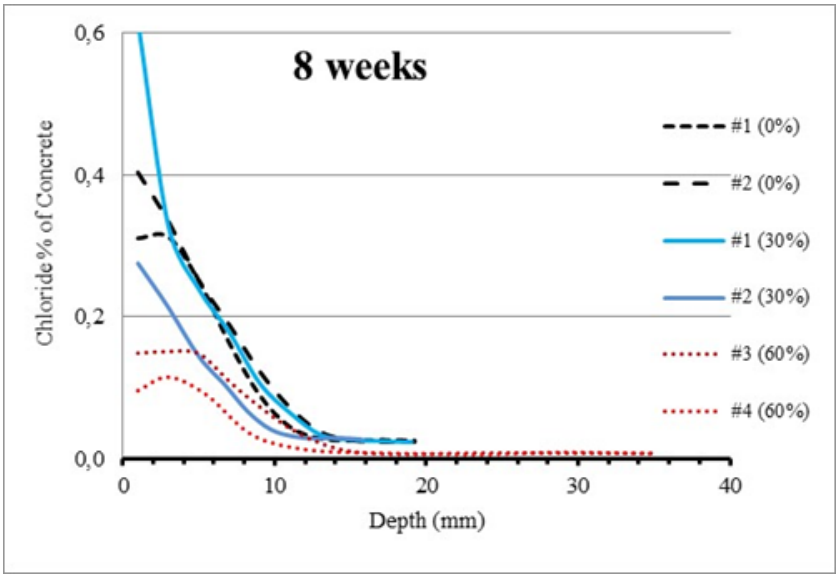
8 weeks
Chloride % of Concrete
0,6
0,4
0,2
0,0
0
10
20
30
40
Depth (mm)
#1 (0%)
#2 (0%)
#1 (30%)
#2 (30%)
#3 (60%)
#4 (60%)

(a)

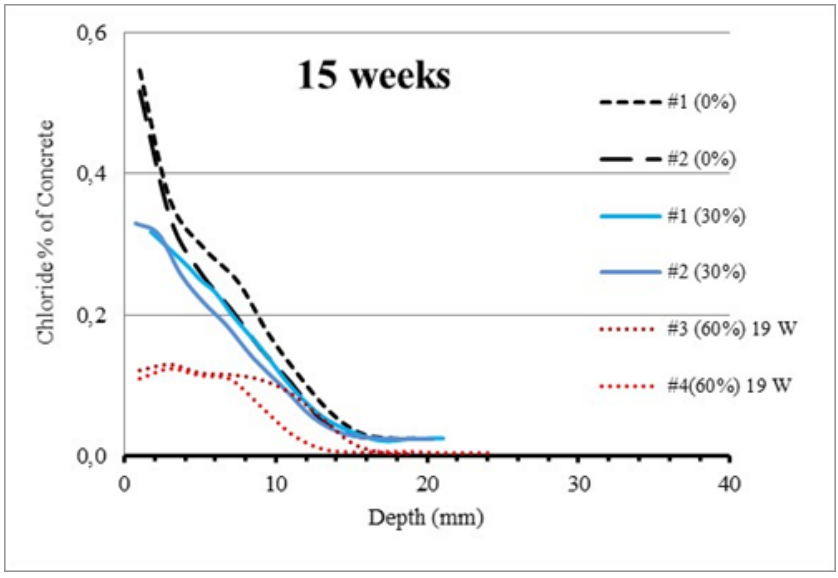
15 weeks
Chloride % of Concrete
0,6
0,4
0,2
0,0
0
10
20
30
40
Depth (mm)
#1 (0%)
#2 (0%)
#1 (30%)
#2 (30%)
#3 (60%) 19 W
#4(60%) 19 W

(b)

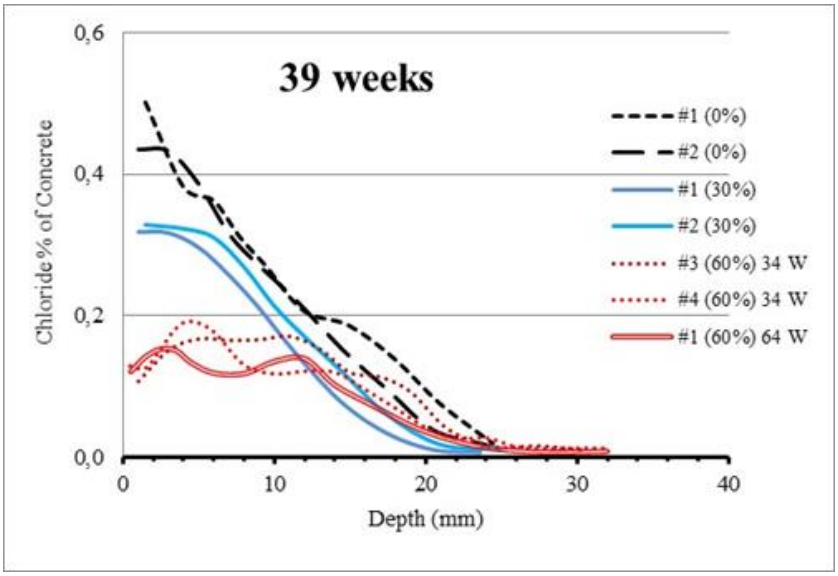

(c)

Figure 6-8: Total chloride content penetration profiles for OPC concretes subjected to combined attack of 3% sodium chloride solution by weight and permanent compressive loading corresponding to 0-30-60 % stress levels. The samples subjected to 60% stress level show the profiles obtained after 8-19-34 and 64 weeks of combined exposure.

The profile found for non-loaded concrete follows the regular error-function model which provides a smooth and progressive drop of chloride values as the depth increases. Some slight deviations from the model were observed near the exposed concrete surface. More pronounced deviations from error-function typical curve were found in the profiles under 30-60% load, especially in the near surface zones. However, for the higher stress level conditions results will be discussed in next sections.

Regarding the non-loading conditions, several researchers have witnessed near the concrete surface a decrease in the chloride values that do not follow the model trend. These deviations from the error function model are only restricted to areas very close to the exposed surface [16-19]. Some researchers have reported comparable behavior in hydrated cementing materials exposed to chlorides.

Elakneswaran et al [10] observed this behavior in OPC cement paste that was exposed to a simulated sea water solution. There is a high degree of minerals dissolution near the exposed surface. An important amount of calcium ions is dissolved in this zone. The concentration of calcium in the pore solution plays an important role regarding chloride adsorption on CSH sites. Adsorption of chlorides by Van Der Waals and electrostatic forces is considered physical binding. Physical adsorption of chlorides on hydrated cement pastes is dominantly taking place on the CSH phases.

One of the proposed mechanism for physical adsorption of calcium and chloride on the silanol sites from CSH is explained by equation (6-2)[10].

$$> SiOH + Ca^{2+} + Cl^{-} \leftrightarrow > SiOCaCl + H^{+} \quad (6\text{-}2)$$

The pH and calcium concentration of pore solution also influences surface equilibrium in equation (6-2). A minimum pH value of 11.15 and a calcium ion concentration greater than 1 mmol/L has been identified as a requisite to promote the adsorption in hardened cement pastes [10,22]. However, it seems that the ionic species that is adsorbed on these active sites is the first Hydroxy complex of calcium [$Ca\,(OH)^{+}$] which is increasingly present in a pH range between 11 and 13 for an amount of calcium of 1 mmol/L as shown in Figure 6-9, which was calculated based on data given in [23]. First hydroxy complex acts as a surface activator for chloride adsorption. According to Fuerstenau et al [24], Hydroxy complexes are such surface-active specie that they will adsorb even on positively charged surfaces.

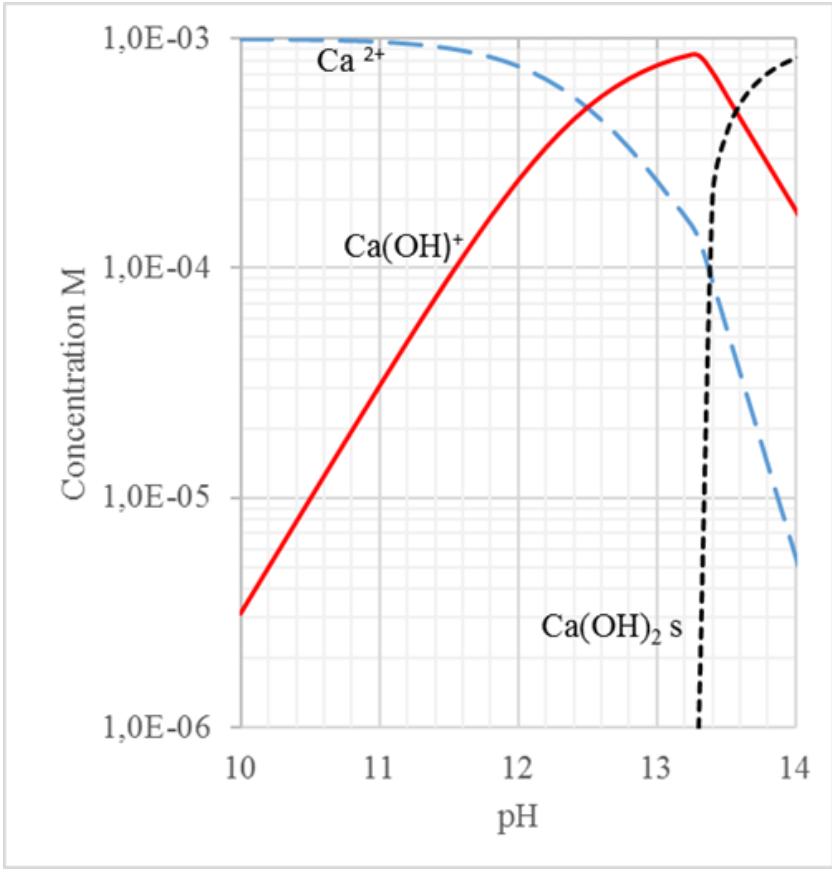

Figure 6-9: Concentration diagram in logarithmic scale for 1 x 10 $^{-3}$ M (mole/liter) of calcium equilibrium data from (23)

Therefore, an alternative mechanism for chloride adsorption in the presence of the first hydroxy complex of calcium is proposed in equation (6-3).

$$> SiOH + Ca(OH)^{+} + Cl^{-} \leftrightarrow > SiOCaCl + H_2O \qquad (6\text{-}3)$$

Close to the surface the sample is in contact with the chloride attacking solution (initial measured pH=8.0). Although Ca^{2+} concentration can be higher in this zone due to Portlandite dissolution near the surface [10], the conditions here are less favorable for chloride adsorption due to the absence of the 1st hydroxy complex of calcium at this low pH (Figure 6-9). This zone is more porous with the presence of capillaries. A porosity gradient has been reported for this outer zone, with higher

values at the surface and decreasing towards the concrete interior [25]. This zone is characterized by a low chloride content.

The parameters for non-loaded and loaded concretes were calculated by fitting the experimental data to the typical error functions equations (6-4 & 6-5), depending whether a skin layer develops or not.

$$C(x,t) = C_i + (C_s - C_i) * (1 - erf\left[\frac{x}{\sqrt{4Dt}}\right]) \quad (6\text{-}4)$$

$$C(x,t) = C_i + (C_{s\Delta x} - C_i) * (1 - erf\left[\frac{x-\Delta x}{\sqrt{4Dt}}\right]) \quad (6\text{-}5)$$

Where

$C(x,t)$ is the chloride content measured at average depth x and exposure time t for $x > \Delta x$, % by mass of concrete

C_i is the initial chloride content, % by mass of concrete

$C_{s\Delta x}$ is the calculated surface chloride content at the skin layer deepest boundary, % by mass of concrete

C_s is the surface concentration at x=0

(Δx) is the depth of the skin layer, m

D is the non-steady state chloride diffusion coefficient, $m^2\ s^{-1}$

x is the depth below the exposed surface to the mid-point of the ground layer, m

t is the exposure time, seconds.

Table 6-2 shows a first approach to calculate diffusivities and modeled surface concentrations "Cs" for all the loading conditions. A conventional error-function model was used for the calculation of the parameters, equation (6-4) The points that were out of the error function model and usually found in the first layers were not considered for the fitting and reported in the table. The obtained

information was used to plot the diffusion coefficients and modeled surface concentration variations in time as shown in Figure 6-10.

Table 6-2: Diffusion coefficients and modeled surface concentration for concrete exposed to 3% sodium chloride solution at 0 – 30 & 60% stress ratio. Obtained from equation (6-4)

Compression	Time	Sample	D x 10^{12}	Cl⁻ cont. % of Concrete		Eliminated	
Loading rate	Weeks	N°	m^2/s	C_s	C_o	points	R^2
	8	1	4.18	0.501	0.0220	1	0.986
	8	2	5.09	0.501	0.0220	1	0.993
0%	15	1	4.39	0.512	0.0170	1	0.979
	15	2	3.61	0.478	0.0170	1	0.990
	39	1	3.97	0.538	0.0176	2	0.972
	39	2	2.96	0.573	0.0176	2	0.985
	8	1	4.63	0.498	0.0220	1	0.995
	8	2	3.52	0.324	0.0220	0	0.995
	15	1	3.89	0.444	0.0170	1	0.987
30%	15	2	3.63	0.400	0.0170	1	0.994
	39	1	2.17	0.502	0.0061	2	0.984
	39	2	2.65	0.545	0.0061	2	0.986
	3	1	6.76	0.323	0.0332	0	0.996
	3	2	15.73	0.243	0.0332	1	0.976
	8	3	5.18	0.311	0.0332	2	0.994
	8	4	2.51	0.319	0.0332	2	0.999
60%	19	3B	2.60	0.467	0.0220	4	0.944
	19	4	1.51	0.460	0.0220	3	0.988
	34	3	3.91	0.511	0.0220	6	0.946
	34	4	3.01	0.464	0.0220	8	0.836

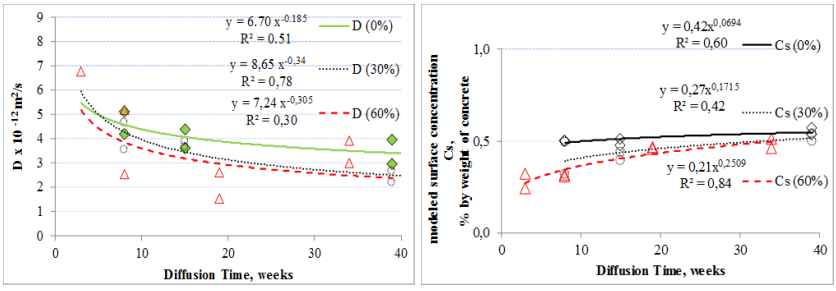

Figure 6-10: Diffusion coefficients and modeled surface concentrations obtained according to the conditions given in Table 6-2 and equation (6-4). C_s is the modeled surface concentration at x=0 replaced .

For the non-loaded concrete, the diffusion coefficient decreases over time from average values of 4.6 x 10^{-12} m^2/s at 8 weeks of exposure until reaching 3.5 x 10^{-12} m^2/s at 34 weeks. Similar decrease in diffusivities has been reported in other researches [12]. In the same way, "Cs" tends to increase until reaching a level slightly superior to 0.5% by weight of concrete. This theoretical value contrasts with the real lower values often found in skin layers and usually not considered for model fitting.

Finally, the comparative intrusion of chlorides into concrete under load is discussed in the next section.

6.2.6.2 Comparative results for chloride intrusion at 0-30 and 60% stress ratio.

Figure 6-8 shows the obtained chloride distribution from profiles obtained from OPC concrete samples that have been exposed in time to 0, 30 and 60 % permanent stress levels. The main observed characteristic in the profiles after stress application is the progressive formation of an altered skin layer. A reduction in the chloride values is observed in this layer as the load is increased. This zone of lower chloride concentrations starts at the exposure surface and a nearly constant chloride level is maintained towards deeper sites. The observed constant values in the chloride content suggest a zone where diffusivity is high and a steady state regime is quickly achieved. This region ends where the chloride profile takes again the smooth typical decrease in the curve which follows the error-function distribution as shown in Figure 6-11. The skin zone is characterized by a different paste composition, micro-structure (which may contain microcracks), or both. Hence, a difference is established between this outer region and the inner matrix, which will affect the chloride transport. Some other examples of skin zones are found in the surface layers of concrete where more paste is accumulated, in layers that have been carbonated, or in layers where brucite has been precipitated (20).

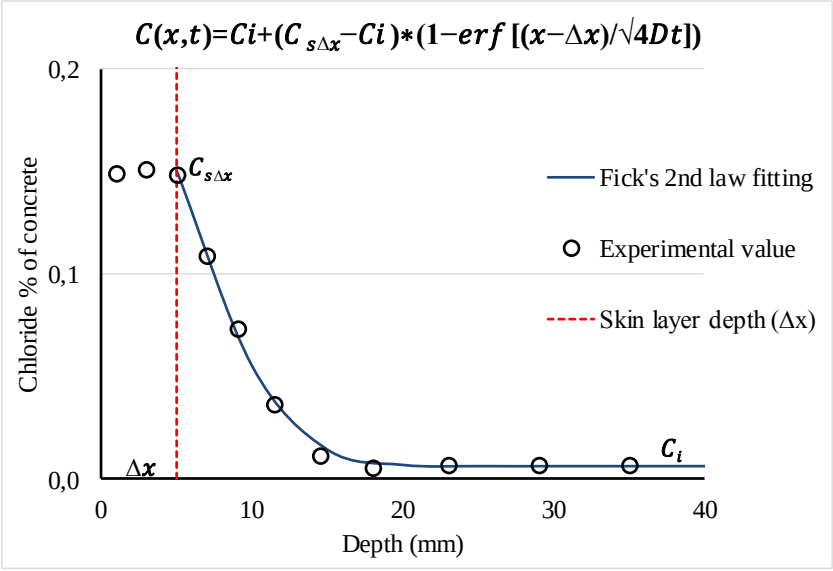

Figure 6-11: Chloride profile considering the development of a skin layer zone (Δx) and the chloride content at that point ($C_{s\Delta x}$) for concrete subjected to combined exposure of 60% stress level and 8 weeks in a 3% sodium chloride solution.

Within the skin layer, chloride values apparently do not follow the typical error-function distribution. On the other hand, the surface chloride content measured in the skin layer ($C_{s\Delta x}$) can be considered a more representative value that would represent the loss in the chloride adsorption capacity that a damaged hardened cementitious paste suffers during the combined attack. On the contrary, the typical surface concentration (C_s) which is obtained by Fick's model without consideration of a "convection zone" and discussed in the previous section represents overestimated values.

The growth of the skin layer as a function of the stress level and exposure time is shown in Figure 6-12. It was observed that the skin layer zone (Δx) grows with increased stress level and time.

For a stress level of 30% the skin layer depth (Δx) reaches 6 mm at 39 weeks of exposure, while for 60 % it reaches an average of 14 mm within that exposure age range. It appears that the growth of (Δx)

tends to stabilize at greater exposure times for the studied OPC concrete.

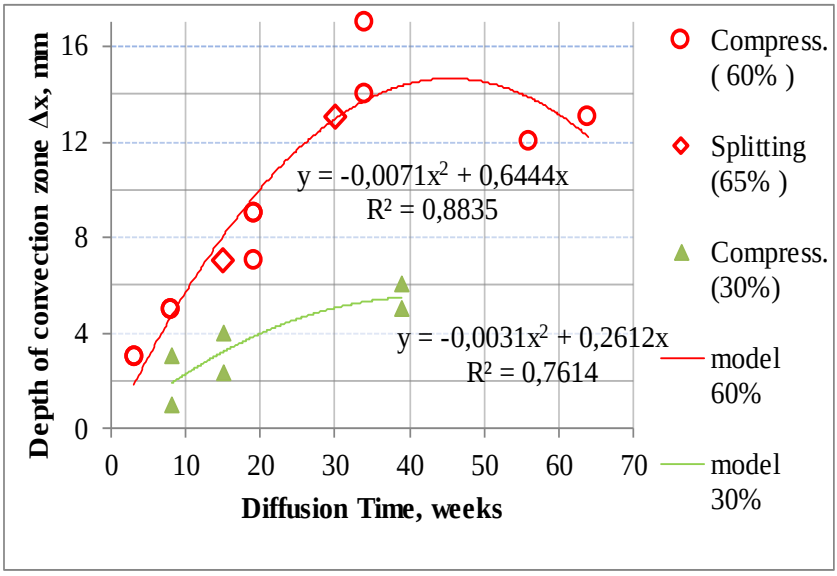

Figure 6-12: Skin layer growth, for OPC concretes subjected to a 3% sodium chloride solution and 30 and 60% compressive stress level. Including data obtained for OPC mixtures subjected to 65% stress level in splitting tensile tests [26].

The depths of the skin layers obtained under tensile stresses are also represented in figure 6-12. This information comes from earlier work [26], in which an OPC concrete of similar characteristic was subjected to a combined attack of chlorides plus a splitting tensile stress level of 65%. The growth trend of the skin layer zone in the splitting tensile tests coincides with the tendency found at 60% in compression. This suggests that both processes share a common deterioration mechanism.

The surface concentration ($C_{s\Delta x}$) and diffusion coefficient (D) for 30 and 60 % stress levels are presented in Tables 6-3 and 6-4 respectively. For the non-loading condition the data are shown in table 6-2.

Table 6-3: Diffusion coefficients and surface concentration at the skin layer for concrete exposed to 3% sodium chloride solution and 30% stress level, according to equation (6-5).

Sample N^0	Time weeks	Δx mm	Surf. Conc. at Δx (%)	D x 10 $^{-12}$ m^2/s	R^2
1	8	3.0	0.330	3.140	0.997
2	8	1.0	0.282	3.031	0.996
1	15	4.0	0,284	2.553	0.992
2	15	2.3	0.312	2.830	0.995
1	39	5.0	0.311	1.397	0.990
2	39	6.0	0.320	1.631	0.993

Table 6-4: Diffusion coefficients and modeled surface concentration at the convection zone for concrete exposed to 3% sodium chloride solution and 60% stress level. Using equation (6-5).

Sample N^0	Time weeks	Δx mm	Surf. Conc. at Δx (%)	D x 10 $^{-12}$ m^2/s	R^2
1	3	3,0	0,188	2,974	0,999
2	3	3,0	0,175	6,311	0,994
3	8	5,0	0,151	2,824	0,998
4	8	5,0	0,110	2,391	0,996
3A	19	9,0	0,130	0,828	0,998
3B	19	9,0	0,116	0,968	0,978
4	19	7,0	0,111	0,557	0,994
3	34	17,0	0,118	0,565	0,980
4	34	14,0	0,122	0,890	0,992
1	64	13,0	0,122	0,459	0,998

The influence of loading on the chloride attack can be clearly seen in Figure 6-13. Primarily, the diffusion coefficient (D) and the surface concentration at the skin layer depth ($C_{s\Delta x}$) decrease with load increment. Diffusion coefficients obtained at later ages (39-34 weeks) for 30 and 60 % stress levels respectively, are only 44 and 21 % with respect to the non-loading condition. On the other hand, the surface concentration at the skin layer zone for concretes loaded at 30 and 60 % also presented low values such as 56 and 21 % respectively, with respect to the non-loading condition.

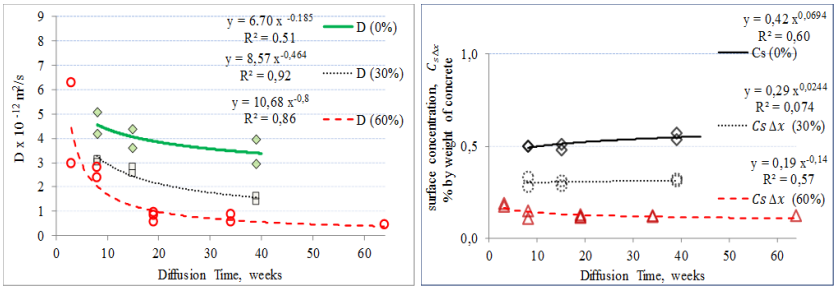

Figure 6-13: Diffusion coefficient evolution for 3 stress level exposure (left). Chloride surface concentration evolution at the skin layer zone for 0-30-60% stress level (right). For OPC concretes subjected to combination of compressive strengths and 3% sodium chloride solution.

6.2.6.3 The two-layer model for the chloride diffusion.

A bi-layer diffusion model for the 60 % stress level was proposed. It was considered only the samples that developed a significant skin layer with enough number of chloride's points in the chloride profile to perform calculations to fit an equation. The model was taken from the work of Andrade "et al." [20] who applied the formerly diffusion model of Crank (1975) to concrete.

The following expression (6-6) taken from Crank (1975) was utilized to fit the experimental results.

(6-6)

$$c_1 = C_0 \sum_{n=0}^{\infty} \alpha^n \left\{ \operatorname{erfc} \frac{(2n+1)l+x}{2\sqrt{(D_1 t)}} - \alpha \operatorname{erfc} \frac{(2n+1)l-x}{2\sqrt{(D_1 t)}} \right\},$$

$$c_2 = \frac{2kC_0}{k+1} \sum_{n=0}^{\infty} \alpha^n \operatorname{erfc} \frac{(2n+1)l+kx}{2\sqrt{(D_1 t)}},$$

where

$$k = (D_1/D_2)^{\frac{1}{2}}, \qquad \alpha = \frac{1-k}{1+k}.$$

C_1 is the chloride content measured at average depth x and exposure time t, for x within the skin layer "l", % by mass of concrete.

C_0 is the surface chloride content, % by mass of concrete.

C_2 is the chloride content measured at average depth x and exposure time t, for x beyond the skin layer "l" (in the matrix), % by mass of concrete.

D_1 and D_2 the corresponding non-steady diffusivities in the skin and matrix zones, $m^2\ s^{-1}$

"l" the skin layer depth, m

"t" the exposure time, seconds

Figures 6-14, 6-15 and 6-16, show the experimental and modeled results obtained for the 19, 34 and 64 weeks of combined exposure. Additionally, Table 6-5 gives a summary of the parameters found in the bi-layer model.

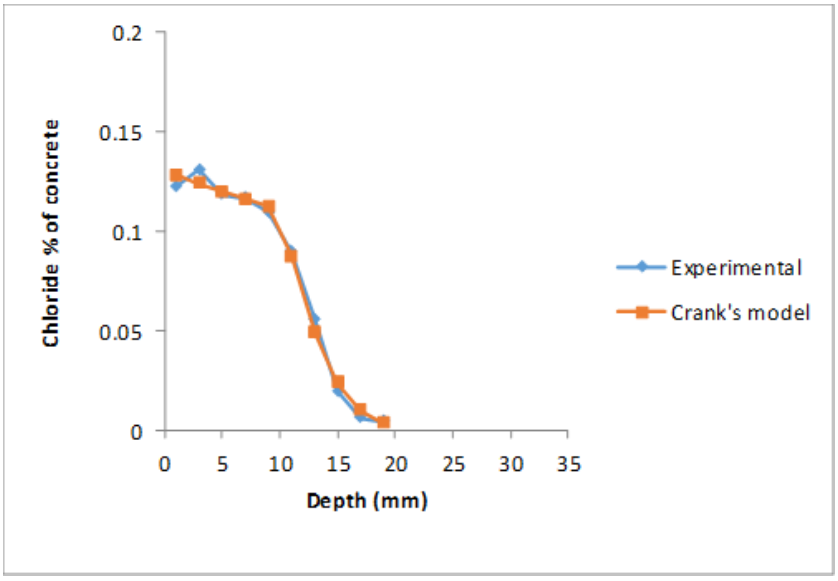

a)

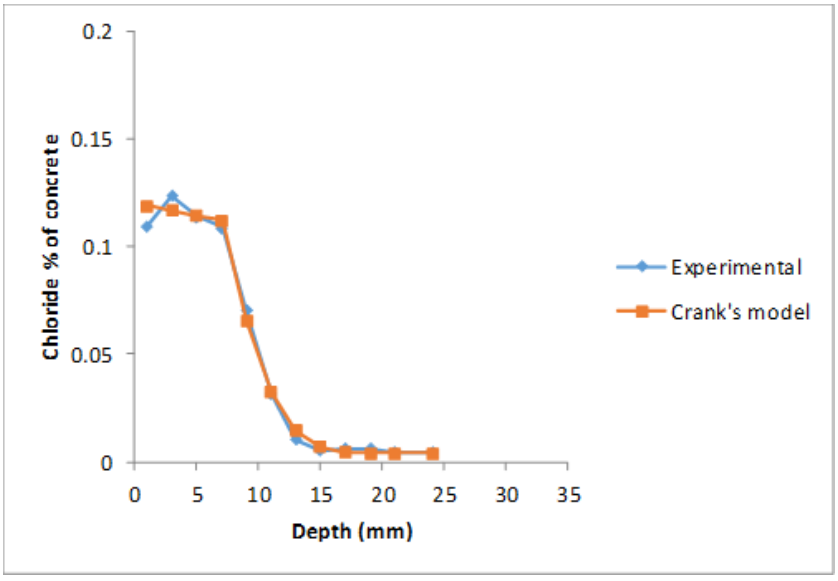

b)

Figure 6-14: Bi-layer model of diffusion (20), for samples 3 (a) and 4 (b), exposed during 19 weeks at 60 % stress level in compression and 3 % sodium chloride solution.

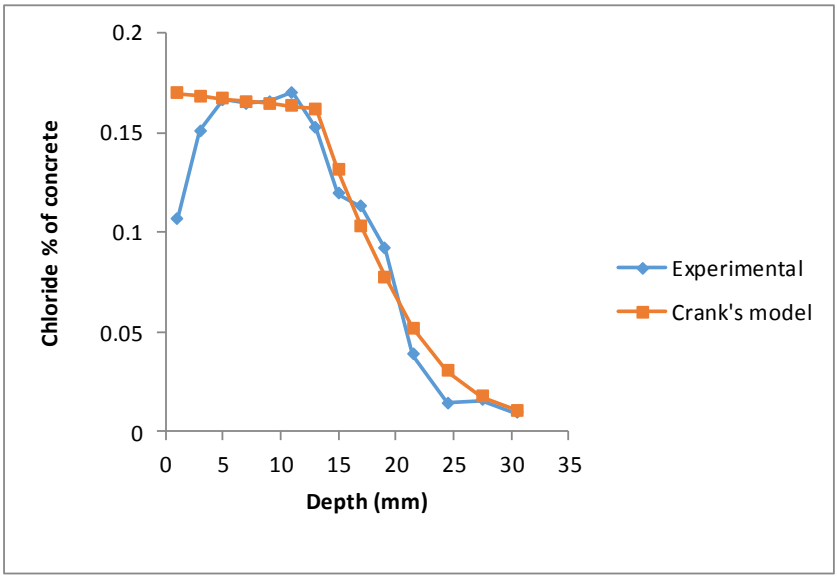

a)

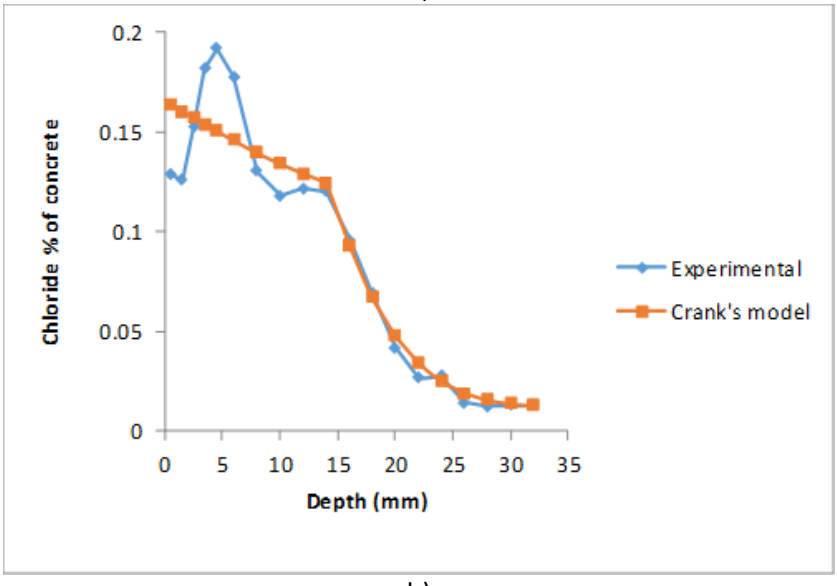

b)

Figure 6-15: Bi-layer model of diffusion (20), for samples 3 (a) and 4 (b), exposed during 34 weeks at 60 % stress level in compression and 3 % sodium chloride solution.

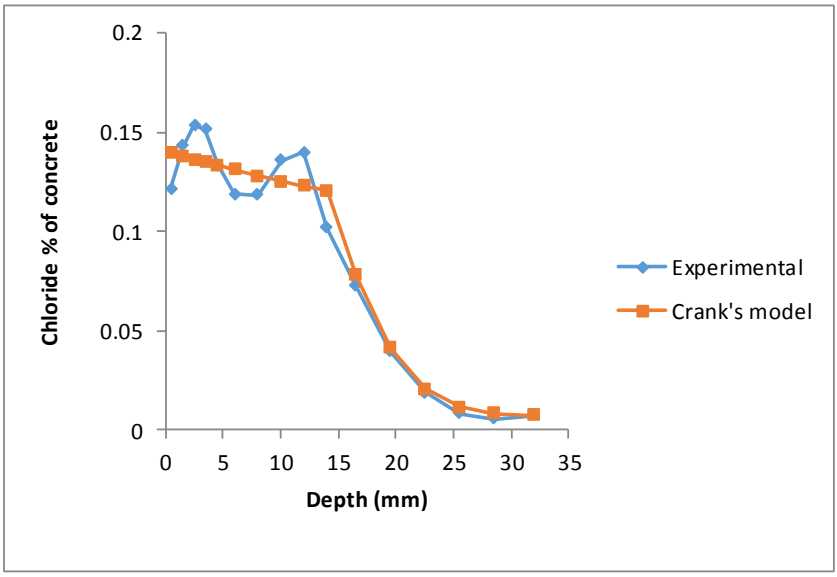

Figure 6-16: Bi-layer model of diffusion (20), for sample 1, exposed during 64 weeks at 60 % stress level in compression and 3 % sodium chloride solution.

Table 6-5: Diffusion coefficients and surface concentrations obtained using the Bi-layer model (20) equation (6-6), for concrete exposed to 3% sodium chloride solution and 60 % stress level.

Sample N^0	Time weeks	D1	D2	D1/D2	C_0 (%)	Ci (%)	l (mm)	Sum.Cuad.Err.
		X 10 $^{-12}$ m^2/s						
4	19	16.4	0.7	23	0.120	0.004	7	2.0E-04
3	19	15.7	1.0	16	0.130	0.005	10	1.6E-04
3	34	48.9	1.9	26	0.170	0.005	13	4.8E-03
4	34	11.7	1.5	8	0.165	0.012	14	6.3E-03
1	64	9.0	0.6	16	0.140	0.007	14	1.9E-03

What can be noticed from the results is the marked differences in diffusivities between the skin layer and the bulk inner zone. The values found in the skin layer are between 8 and 26 times higher than the ones found in the bulk. This suggests a rapid transport of chloride ions in this zone.

6.2.6.4 Influence of loading on the chloride adsorption.

The hydroxy complex of calcium plays a fundamental role in the surface equilibrium of hydrated cement paste. As proposed in equation 6-3, it promotes the chloride physical binding on silanol sites from sound non-loaded pastes. A pH higher than 11.15 and calcium ion concentration greater than 1 m mol/L is needed to promote the adsorption [10,22]. The diagram presented in Figure 6-9 was plotted for an assumed total calcium concentration of $1x10^{-3}$ M which seems to be a common average concentration in the pore solution of mature OPC pastes [27]. At a pH value of 11.15, the total ionic concentration for calcium is distributed in the following manner: Ca^{2+} = 0.95 m mol/L and $CaOH^{+}$ = 0.05 m mol/L, Figure 6-9. As the pH is increased, the 1st hydroxy complex becomes more abundant. Big hydrated molecules like $CaOH^{+}$ have lower hydration energy than small ions like Ca^{2+}. This means that the first hydroxy complex dehydrates and attaches to the CSH surface more easily than Ca^{2+} . On the other hand, this latter ion decreases as the pH increases.

According to the ionic distribution shown in Figure 6-9, the ionic species adsorbed on CSH for the pH range 11.15 – 13.3 would be the first hydroxy complex.

In undisturbed cement pastes the calcium bearing minerals are in equilibrium with a Ca^{2+}pore solution. However, the solubility of the cement minerals may be increased in presence of chloride [28-31] and it is enhanced under certain conditions. Consequently, this equilibrium may be altered in chloride's presence.

Another factor that alters the surface equilibrium of CSH is leaching. Calcium leaching starts at the concrete's surface. De Weerdt and Justnes [31] exposed OPC pastes to sea water and they found CH depletion and CSH decalcification in the outermost layers due to the solution aggressiveness. If CH is consumed, a disequilibrium is created in the pore system. Calcium must be provided by CSH to restore equilibrium but the CSH decomposition generates porosity and as consequence mechanical deterioration of the paste. Choi "et al." [32],

observed a significant worsening of the mechanical properties of calcium leached concrete. But, they found a better resistance to chloride penetration in previously leached OPC concrete than in concrete with slag or fly ash replacements.

If chlorides alter the chemical equilibrium at CSH's surface when concrete is not under load, a synergistic increase in deterioration would be expected when a mechanical load acts simultaneously.

A mechanism that has been proposed to explain cementitious materials deterioration under combined chemo-mechanical loads is the so-called stress corrosion cracking of concrete. Schneider "et al.", proposed that Ca^{2+} dissolution is facilitated from calcium silicate structural units when the material is subjected to stresses [33].

The simultaneous combination of chemical attack and fracture behavior of concrete seems to be a complex topic, and has not attracted the attention of researchers very much until now.

The influence of a sustained compressive stress of 60% on the chloride ingress into OPC concrete is summarized in Figure 6-17. For contrast, the profiles for non-loaded concrete at two reference ages (8 and 39 weeks) were plotted in the graph. The chloride profiles of concrete subjected to load present a flattened form, that extends from the surface of exposition up to a profundity that we have called skin layer depth (Δx). The chloride content differences between loaded and non-loaded concrete described by the triangular shape that is indicated in Figure 6-17 could be partially connected with a reduced capacity of the matrix to adsorb chlorides when it is under load.

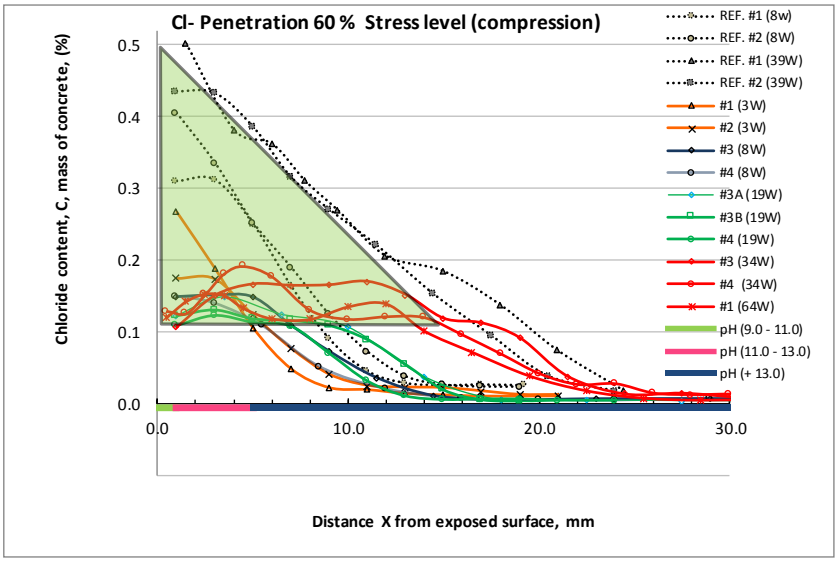

Figure 6-17: Chloride profiles in concretes subjected to permanent 60 % stress level in compression and 3% sodium chloride solution. Exposure times: 3-8-19-34-and-64 weeks. Also, shown non-colored curves for reference samples at 8 and 39 weeks' exposures. Shadowed area resembles the reduction of chloride binding capacity of stressed concretes. pH measurements were taken at 64 weeks' exposure.

If calcium minerals are being dissolved from CSH sites due to stressed conditions, pore solution should become rich in calcium and hydroxy ions as well. It has been recognized that the pore solution of mature hydrated OPC pastes has low levels of Ca^{2+} ions and high levels of OH^{-} [27]. In that conditions, recently dissolved calcium ion may locally face high pH values and a re-precipitation could be imminent probably at less stressed zones. Also at these high pH, the CSH's silanol sites ionize due to deprotonation and their surfaces become negatively charged as shown in equation (6-7) [10,22].

$$> SiOH \leftrightarrow > SiO^{-} + H^{+} \qquad (6\text{-}7)$$

Chloride ions cannot be adsorbed on such negatively charged surface. The localized very high pH conditions would decrease the first hydroxy complex of calcium as shown in Figure 6-9. Therefore, the mechanism shown in equation (6-3) cannot proceed. That would also explain the

low flattened chloride surface found in the skin layer zone. Under the cited conditions, it is believed that free chloride content should predominate in the pore solution and the total chloride content of concrete should decrease.

Relatively recent research on concrete exposed to long-term creep suggests internal dissolution-precipitation mechanisms to explain the deformation under sustained load at a relative humidity greater than 50% [34]. This mechanism is active at nanoscale grain contacts. It is believed that the dissolution of calcium bearing minerals could be the most obvious mechanism when concrete is under sustained stress and saturated condition. In this scenario, calcium responds by dissolving from the solid state to relieve stressing conditions.

Another significant parameter influencing the ingress profile of concrete when it is under load is the surface concentration. The increase on chloride penetration due to cracking is counteracted by a reduced concentration gradient. Then, the flat development of the chloride profile in the skin layer is a natural result, and similar chloride contents are found in inner concrete where deterioration due to cracking is much lower. The reasons for the reduction of the surface concentration are unclear. Similar results have also been found by Wang “et al.” when they permanently exposed loaded specimens to a salt fog (Wang “et al.” 2011) [35], but not when they exposed specimens to wetting and drying cycles (Wang “et al.” 2016) [36]. In this second case, it seems that the wick action contributes to the penetration of chlorides into concrete into a more cracked concrete. When no contribution of convection phenomena is involved in the penetration of chlorides, the reduction of the surface concentration due to the loading ratio of concrete could be related to a physical-chemical modification of the electrical double layer. If the loading ratio can increase the ionic strength of the pore solution, then the effect of the electrical double layer would be increased and the surface concentration will reflect this change (Nguyen and Amiri, 2014) [37].

6.2.6.5 Petrographic observations

To investigate the micro-structure of the concrete exposed to the combined attack, samples were taken for thin section microscopy. Special care was taken to obtain a rectangular section extracted from the middle of the exposed surface and parallel to the loading plane as shown in Figure 6-7.

Figure 6-18 shows a thin section of OPC concrete subjected to combined attack at 60% stress level after 34 weeks. The weakest points for dissolution appears to be along the aggregate's interface and its continuation in formed microcracks that bridge aggregates through the paste.

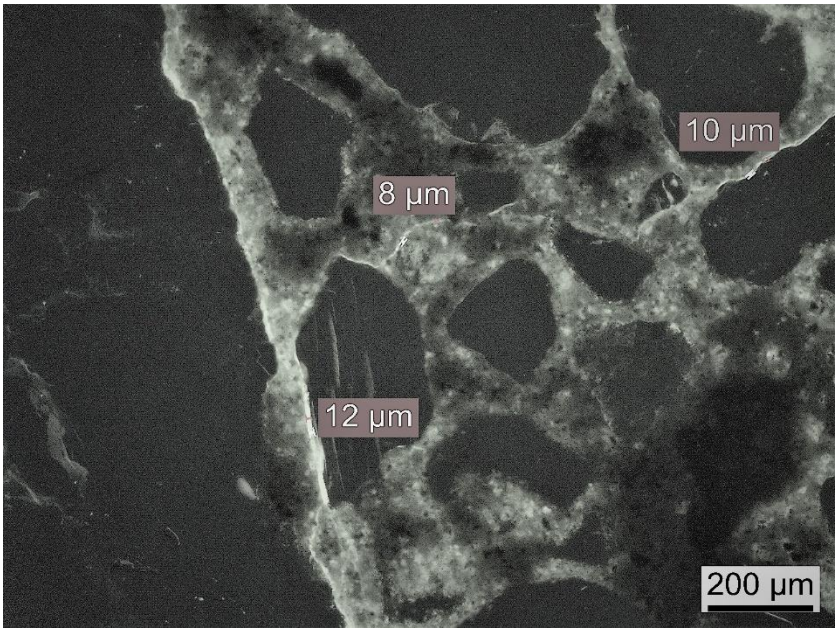

a)

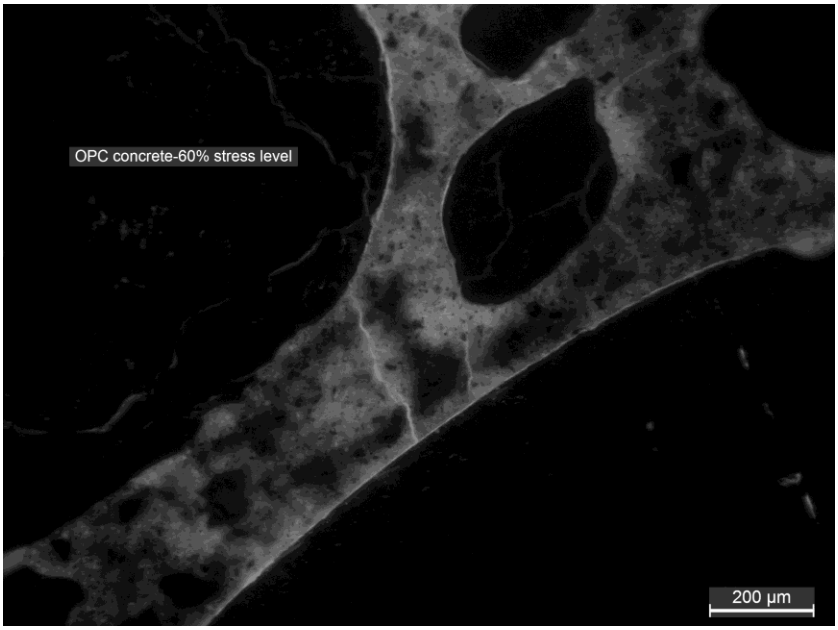

b)

Figure 6-18: Thin section micro-photography of OPC concrete after 34 weeks combined attack exposure of 3% sodium chloride solution and 60% stress level. Under fluorescent light (Grey tones (a)). showing microcracks (12 – 1 µm) bridging between aggregates and surrounding aggregates interface (b).

In other locations, it was observed that some of the cracks develop a sub-parallel orientation with the exposed surface. This pattern is not always constant and some irregular orientation has also been observed. The width of the micro-cracks is finer and its frequency lower than those observed in the splitting test presented in previous work [26]. The widest showed an average width of 8 – 10 µm, reducing to 1-3 µm opening at the ends.

The microcracking pattern observed for 60% loading ratio sustains the formation of a skin layer with a significantly increased diffusivity.

6.2.6.6 Conclusions.

OPC concrete mixtures were exposed to combined sodium chloride solution plus 2 levels of compressive stresses. The following aspects regarding the attack were observed:

- A progressive decrease in the chloride profiles was noticed when the load was gradually increased. This is mostly connected with a reduced chloride surface concentration caused by the loading ratio. The reasons for this influence are not clear at this stage, and they can relate to an influence of the loading on the ionic strength, the electrical double layer and micro-structure changes.

- The low chloride levels found in the loaded samples suggest that the chloride adsorption capacity of hardened cement paste is affected by the combined attack.

  A skin layer zone with rather constant chloride content is formed with the increase in load. It initiates at the surface and grows inward over time. Two different diffusion rates can be identified for this outer skin layer and the inner zone, showing that the application of load mostly results in an affectation of the external layer of concrete regarding chloride ingress, with minor effects in the inner concrete.

- For the highly loaded specimens, the observed constant values for the chloride content in this skin layer, suggest a zone where diffusivity is increased to such a level that a steady state regime is quickly

achieved. Although total chloride content decreases in this zone, future research should focus on the effective influence of the load on the free chloride content in the pore solution, which might be increased by the application of load.

- The skin layer depth and its rate of growth increases with increasing stress level.

  Propagation of sub-critical stress microcracking is initiated from zones near the surface, and this defines the extension of the skin layer.

6.3. Chloride attack under splitting tensile loads

6.3.1 Concrete mixture, test samples and initial conditions.

Four concrete mixtures without special properties regarding durability characteristics (the research purpose was to compare materials behaviour without analysing specification compliance) were prepared for this investigation, as presented in Table 2-3. The aggregates were gravel and a natural sand of siliceous nature. The utilized binders are presented in Table 2-1 and are composed of an ordinary Portland cement (OPC) with no special durability properties and a high sulphate resistant cement (HSR), both materials complying with type CEM I 52.5 N according to European Standards. A (ground granulated) blast furnace slag addition was also used to replace 50 and 70 % by weight of the OPC. To improve the fresh concrete properties (slump between 160-210 mm) a superplasticizer (polycarboxylic ether based) was used in amounts between 0.2 – 0.4 % by weight of the total binder content.

After mixing, concrete was cast in cubical molds (h.=150 mm). Subsequently 7 days of wet curing at 20 ^{o}C and RH > 95% was applied and additionally, 21 days at 20 $\pm$ 2 ^{o}C and 60 $\pm$ 5 % RH. A schematic view of the experimental procedure is presented in Figure 5-19.

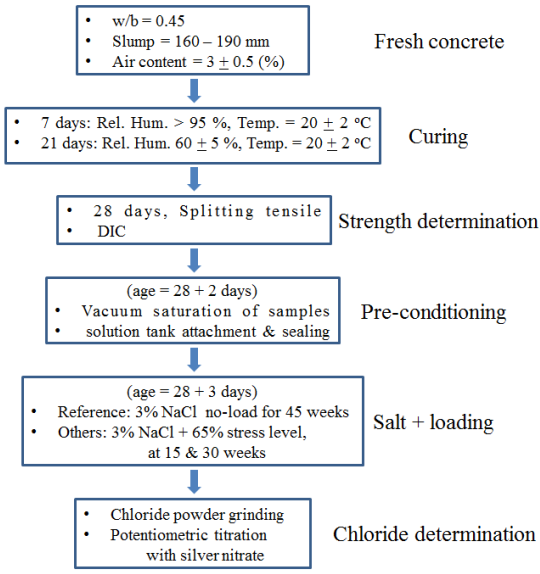

Figure 6-19: Schematic view of experimental procedure

6.3.2 Splitting tensile strength values and digital image correlation (DIC) tests.

At the age of 28 days 3 cubes for each one of the S0, S50, S70 and HSR mixtures were tested for splitting tensile strength. The procedure stated on ASTM C496M-04 standard was followed but applied to cubic concrete samples. A schematic view of the test that was also used for the experimental setup is shown in Figure 6-20 (left). The obtained splitting strength average values that represent each mix are shown in table 6-6.

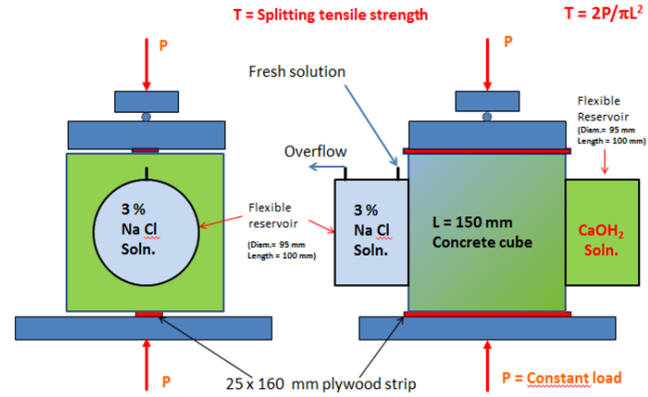

Schematic view of chloride and sustained load attack to concrete

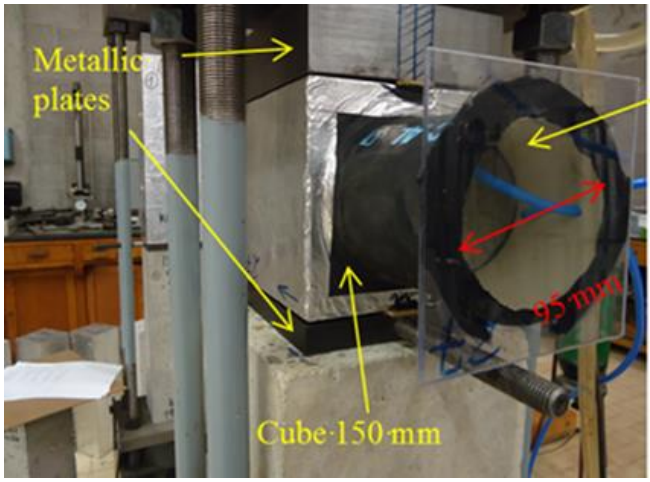

Figure 6-20: Schematic view of the combined test setup, 3% NaCl solution and 65 % stress ratio.

Table 6-6: Permanent loading conditions for the splitting test setup at 65% stress ratio.

Sample #	Ave. max. Load kN	Var. Coeff. %	Splitt. Strength MPa	65% of max. kN
S0	145.5	1.9	4.1	94.6
S50	142.5	4.9	4.0	92.6
S70	124.0	1.8	3.5	80.6
HSR	168.7	1.8	4.8	109.6

The previously acquired information was utilized to perform Digital image correlation (DIC) analysis. This technique consists of a stereoscopic camera system (two high-resolution cameras are placed facing the area under investigation) that, based on stereo-correlation and stereo-triangulation, reconstructs the 3D full-field deformation vector field on the material's surface. In practice, one of the samples' side area (150 mm * 150 mm) was covered with high-contrast random speckle pattern as shown in Figure 6-21. The Vic-3D post-processing software tracked the speckles at the reference stage (healthy sample) and through time as the samples were progressively loaded under splitting tensile stresses.

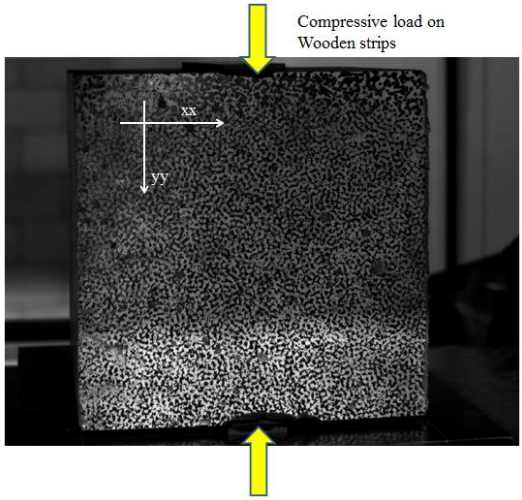

Figure 6-21: High contrast random speckle pattern in cubic sample subjected to splitting tensile load. Pattern setup.

The strain field map was computed by numerical derivation of the deformation fields. The first principal strain maps, e_1 (%) are considered in this study. The principal strain e1 was derived by transformation of the e_{xx}, e_{yy} and e_{xy} normal strains (the Cartesian coordinates system is given in Figure 6-21. For most of the samples the development of a perceptible strain distribution was noticed along the splitting plane after 50% stress level. The samples were loaded until 80 % stress ratio to avoid complete failure. The strain distribution for S0 at 0-50 &80% is shown in Figure 6-22.

Considering that the obtained overall strain distribution for the samples at 80% stress ratio will develop larger micro-cracks, it was decided to apply a stress level of 65% in the setup, which is an intermediate value. Furthermore, the potential effects on the microstructure provoked by the combined action of a sustained load and an aggressive solution was scrutinized.

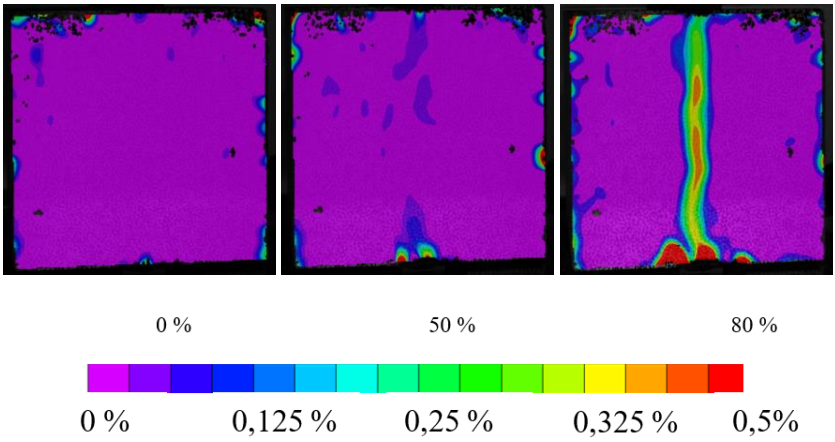

Figure 6-22: Principal strain distribution e_1 (%) for S0 concrete subjected to 0, 50 and 80 % splitting stress level respectively.

6.3.3 Sample preconditioning and experimental setup.

Two cubes representing each mix were placed under vacuum at 2.7 kPa during 2.5 hours. Next they were gradually saturated and the pressure was slowly released to atmospheric conditions and left for 24 hours. The saturated samples were then surface dried. The non-exposed faces were covered with black silicone and aluminum foil leaving two opposite open faces on which the solution reservoirs were positioned. One 640 cm^3 capacity reservoir is glued to each one of the opposite faces. One of them is selected to contain the attacking salt solution. It is connected to an 8 litres stock solution tank provided with

an aquarium pump with capacity to pump the solution at a flow rate of 23 l/h. On the other face a similar capacity reservoir is placed, filled with saturated $Ca(OH)_2$ solution whose function is to keep the sample saturated, provide calcium ions in case of leaching and to check for any unexpected chloride infiltration.

Before exposing the samples to the attacking solution, they were gradually loaded until reaching 65% of the splitting tensile breaking load. The cubes were subjected to a permanent splitting stress in the middle of the loading faces. This was achieved by 2 opposed and parallel aligned plywood strips 160 mm in length, 25 mm wide and 3 mm of thickness. The wooden strips rest between the metal plates of a mechanical rig and the loading faces of the cubes as shown in Figure 6-20. The load is transferred by a hydraulic jack which is connected to a pressurized cylinder which contains a nitrogen/oil mixture.

6.3.4 Chloride profiling.

After 15 and 30 weeks of the combined exposure the samples were taken out from their respective rigs. Subsequently they were subjected to profile grinding starting from the chloride exposed face. Special care was taken to grind the samples making grooves of 10 mm width, 30 mm long, and layers of 1 - 2 – 3 or 4 mm depth. the magnitude of the layers increases as the depth progressed. The groove alignment was always parallel to the splitting plane as shown in Figure 6-23 - left. For each age, at least 3 equally spaced chloride profiles were taken starting from the centre and on parallel planes from the splitting plane at 0-20-40 mm deviation. This was done to observe any variation in the chloride profile at different distances from the loading plane.

Figure 6-23: 10 mm wide by 30 mm long grooves for chloride powder extraction (left). Detail of the drilling tool provided with sliding table in 2 directions (right).

The powder extraction was done utilizing a 10-mm diameter drilling bit placed in a fixed vertical shaft as shown in Figure 6-23 - right. The sample was anchored to a table capable of a controlled and precise movement in two directions perpendicular to each other. The obtained groove (10 x 30 mm, width x length) was filled with epoxy for continuing the investigation with the same specimen for later ages. Thus, the sample was subjected to an un-loading/loading cycle at each moment of chloride determination. The concrete samples were subjected to 2 loading cycles during this research.

The obtained powdered layers were treated with nitric acid to extract the total chloride content. The utilized procedure is described in EN 14629 “Determination of chloride content in hardened concrete”. Chloride content determination was done by potentiometric titration with a 0.01 M silver nitrate solution.

Preliminary results shown good repeatability in the chloride content obtained from the 2 replicate samples. This was specially observed for the layers obtained beyond the convection (Skin layer) zone. The chloride level within the convection zone showed the same trend although slight dispersion among replicate samples. Therefore, to reduce the alteration in the concrete that could be caused by the grooves after grinding, it was decided obtaining the profiles three at a time in one sample and the other sample was considered for the following age.

6.3.5 Thin section preparation.

After 30 weeks' exposure, a rectangular section (width = 30 mm, depth = 50 mm) centered around the splitting plane and perpendicular to it was obtained.

After fluorescent epoxy impregnation under vacuum the sample was ground and polished removing the excess of epoxy. Subsequently the finished surface was glued on an object glass. Finally, the concrete sample is cut parallel to the glass and the remaining slice is polished to obtain a 25 µm thin section of concrete for microscopic observation.

6.3.6 XRD analysis.

According to Elakneswaran et al [10], calcium ion and pore solution pH play an important role for chloride adsorption on CSH sites. It is well known that CH mineral acts as a buffer and is a source of calcium ion in pore solution. Therefore, no-carbonated pastes were extracted from the concrete samples at 1 year of age. Then the amount of Portlandite in the concretes was measured by XRD technique. A more detailed description about sample preparation and the utilized procedure has been described by the authors in previous paper [21]

6.3.7 Results and discussion.

6.3.7.1 Chloride profiles in non-loading conditions.

Chloride profiles with their respective diffusion coefficient, calculated surface chloride content at the convection zone, depth of the convection zone and correlation coefficient are shown in Figure 6-23 and table 6-7 correspondingly. This information was obtained after 45 weeks of 3% chloride exposure and non-loading conditions.

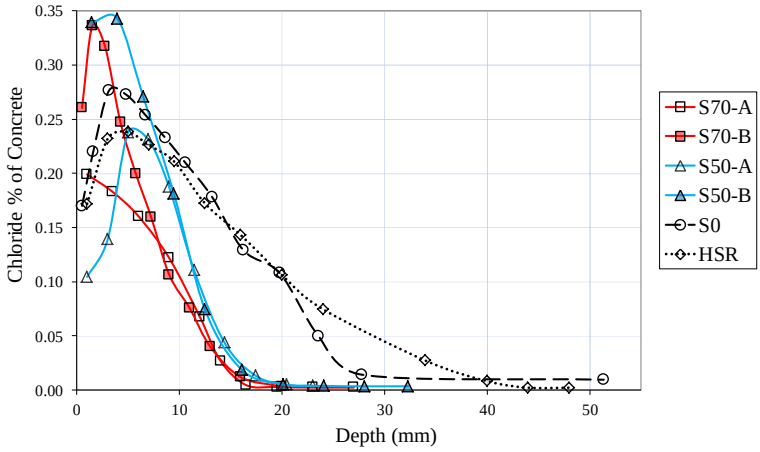

Figure 6-23: Acid soluble chlorides profiles for no-loaded concretes exposed to 3% sodium chloride solution after 315 days (45 weeks) exposure.

This exposure time was considered to be long enough to be used as a reference point for this study. The difference in chloride penetration resistance is noticeable for every type of mix and binder. Nevertheless, some common details were also observed. For instance, the samples showed a reduction of the chloride content near the exposed surface.

Table 6-7: Diffusion coefficients and modeled surface concentration for concrete exposed to 3% sodium chloride solution during 45 weeks.

Sample denom.	Δx mm	Surf. Conc. at Δx (%)	D x 10^{-12} m^2/s	R^2
S0	3.0	0.301	4.7	0.975
S50	4.0	0.354	0.9	0.991
S70	2.0	0.341	0.9	0.998
HSR	4.0	0.260	6.5	0.995

Some researchers have found similar behavior in hydrated cementitious materials exposed to chlorides. Elakneswaran et al [10] observed this phenomenon near the surface through simulated and experimental tests on OPC cement paste exposed to sea water.

According to his experience there is a high degree of dissolution of elements near to the exposed surface. Amongst several elements calcium is dissolved in this zone. Changes in calcium concentration in the pore solution also affect the adsorbed chloride content on CSH sites.

Chloride can be physically adsorbed on silanol sites where calcium has been adsorbed according to equation (6-2)[10].

Elakneswaran et al [22] also found that calcium adsorption is considerably enhanced on hydrated OPC cement paste above pH = 11.15.

Reaction (6-2) is pH dependent and it seems that close to the surface where the sample is in contact with the chloride attacking solution (initial measured pH=8.0) there is a less favorable condition for chloride adsorption. Conversely chloride adsorption is enhanced at deeper sites where conditions favor adsorption. At deeper depths, the pH is reestablished to higher values. Hence the adsorption of calcium and chloride is again favored and a high chloride's content peak is reached on these sites. Several researchers have noticed the presence of an inner higher peak in the chloride profile for concretes subjected to carbonation [16,17]. Others also found this behaviour in concrete exposed to drying-wetting cycles [18]. While others have also noticed this conduct in cracked concrete [19].

According to the behavior of the chloride profiles shown in Figure 6-23, two replicate samples from the same mixture can display dispersion between each other on the chloride content. This spreading is especially found up to a depth of 4 mm. in the samples that have been exposed for 45 weeks. Beyond that zone it seems that a common microstructure with similar adsorption characteristics is developed and from there on these replicate samples present more or less the same chloride profile. The surface layer is usually enriched with cement paste. This zone is more heterogeneous with the presence of a higher w/b ratio. Here the capillaries are more frequent specially when bleeding was present. In this near surface zone a porosity

gradient has been observed, with higher values at the surface which decreases towards the concrete's interior [25]. The dominant transport here is by convection. The experimental points obtained in this zone usually do not follow Fick's second law profile and should not be taken into account for this model. Only the layers located beyond the convection zone were included for the profile fitting.

A remarkable difference in the chloride penetration resistance can be noticed between OPC, HSR and S50, S70. The mixes with BFS replacement showed a much better resistance to chloride ingress in non-loaded conditions. This is also concordant with the lower diffusion coefficients of about 1 x 10^{-12} m^2/s for these materials as shown in table 6-7. On the contrary the values found for OPC and HSR were 4.7 x 10^{-12} m^2/s and 6.5 x 10^{-12} m^2/s respectively. The parameters presented in Table 6-7 were calculated fitting the experimental data to Fick's second law equation (6-5)

6.3.7.2 Chloride profiles at 65% stress level

According to the strain distribution for concrete subjected to splitting tensile stresses (as seen in Figure 6-22) a major chloride transport is expected along the vertical plane where a large strain concentration is observed.

Figures 6-24 through 6-30 show the chloride profile for all the mixes exposed to 3% chloride solution and permanent 65% splitting tensile stress level during 15 and 30 weeks (Only S70 shows a profile at 7 weeks instead of 15).

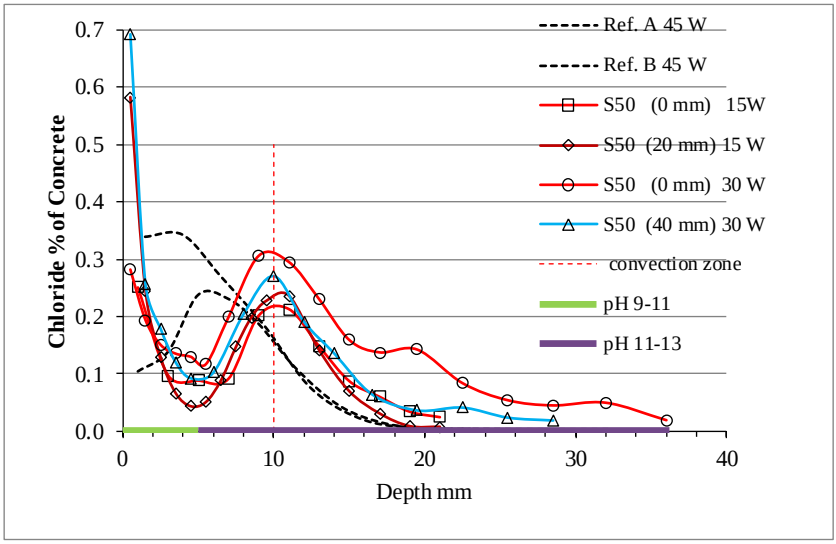

Figure 6-24: Total chloride content penetration profiles ground parallel to the loading axis (deviation distance from axis in parentheses), for S50 exposed to 65% permanent splitting tensile stress level and 3% chloride solution at 15 and 30 weeks (ref. samples 0% stress level, 45 weeks). Dashed vertical line shows the location of the convection zone (Δx). pH change, determined by rainbow indicator on powder extracted from ground layer (0 mm deviation) at 30 weeks.

It was expected to find a larger concentration of chloride at the splitting plane but unlike, it was found a homogeneous distribution of this ion which spreads towards wider areas. The profile obtained at every plane parallel to the splitting one, shows similar trend. This suggest a transverse connection between the parallel planes to the splitting plane for the chloride transport.

The presentation of chloride distribution in just 1 dimension (depth) is more difficult for interpretation. Thus, a surface graph that links the obtained profiles with a second dimension (2D) which shows the deviation from the splitting plane was added. The 2D & 1D results show the following common features between the studied mixes:

- Firstly, at the exposed surface the chloride distribution (in 2D graphs) looks like a V-shaped trench with its lowest value located

at 0 mm deviation (splitting plane). Chloride values steadily increase towards the sides when moving away from the center. This feature is more enhanced for the BFS mixtures and less for the HSR and OPC samples.

- The shape of the chloride content also forms a “valley”. It decreases from a relatively higher value at the exposed surface towards the interior of the concrete until a lowest chloride level is reached. Next there is a continuous increase of chloride values until a peak is reached. This place demarcates the extension of the convection zone (10 mm approx. for S50). The magnitude of this “valley” is reduced in the neat cement mixtures and increases with BFS addition.
- After the highest peak value the chloride content progressively decrease and more or less follows a Fick’s model shape.

Every mix has its particular response related to its chloride distribution. Hence, an individual analysis is presented below.

6.3.7.3 Chloride distribution in S50.

As can be seen in Figure 6-24 the place for the convection zone does not move with time. Only higher chloride content values were found at longer exposure ages.

Table 6-8 shows the diffusion parameters corresponding to the profiles shown in Figure 6-24.

Table 6-8: Diffusion coefficients and modeled surface concentration at the convection (skin layer) zone for concrete with 50% BFS replacement (S50) exposed to 3% sodium chloride solution and 65% stress level during 15 and 30 weeks. Profiles ground in parallel planes at 0 – 20 – 40 mm deviation from the splitting plane.

Time	Axis dev.	Δx	Surf. Conc.	D x 10^{-12}	
weeks	mm	mm	at Δx (%)	m^2/s	R^2
15	0	10	0.258	1.26	0.890
15	20	10	0.295	0.87	0.998
30	0	10	0.290	3.46	0.952
30	40	10	0.266	0.89	0.984

The largest value for the diffusivity is obtained at the splitting plane. In this zone, the values for this parameter and for the surface concentration at the convection zone are D = 1.26 x10^{-12} m^2/s and $C_{s\Delta x}$ = 0.26% respectively for 15 weeks' exposure. These parameters show an important increase after 30 weeks' exposure reaching D = 3.46 x10^{-12} m^2/s and $C_{s\Delta x}$ = 2.90%. Consequently, this noticeable increase of both factors suggests a sustained expansion of the damage within this period.

Figure 6-25 shows the 2D distribution of chlorides for S50 concrete. Here the progressive ingress of chlorides can be observed specially at the location of the splitting plane. The homogeneous chloride distribution towards the sides of the splitting plane is also noticed. Other typical features are the V-shaped trench and the chloride depression "valley", located close to the exposed concrete surface. The location and geometrical orientation of these 2 noticeable features are strongly influenced by the presence of the splitting plane. The inner chloride peak that limits the extension of the convection zone is also shown.

Finally, another important feature is mentioned, the chloride content at the exposed surface increased remarkably when moving away from the splitting plane. Although this behavior was also observed in the Portland cements, S50 & S70 mixtures showed in this zone a more than 3 times higher level of chloride compared to S0 & HSR. This could suggest that, if BFS mixtures are free of cracks, their capacity to bind chlorides is superior to that of S0 or HSR.

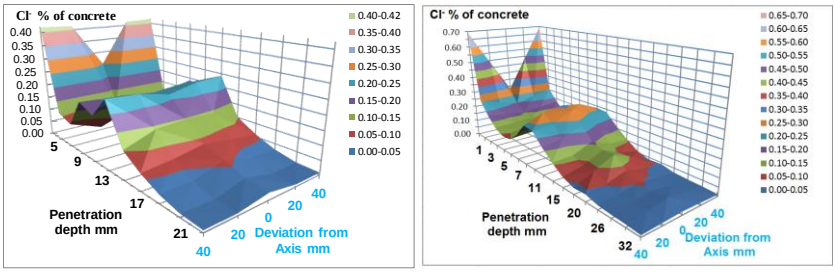

Figure 6-25: 2D Total chloride content penetration profiles ground parallel to the loading axis (at 0-20-40 mm deviation), for S50 exposed to 65% permanent splitting tensile stress level and 3% chloride solution after 15 weeks (left) and 30 weeks' exposure (right).

6.3.7.4 Chloride distribution in S70.

Figure 6-26 and Table 6-9 show the chloride distribution and the calculated diffusion parameters for the mix with 70% BFS replacement. The chloride distribution at the exposed surface also looks like a V-shaped trench. But in this case its growth is more pronounced inward and develops at early age (7 weeks). The presence of the first chloride peak is highly reduced at 0 and at 20 mm deviation. The values at 30-week exposure for $C_{s\Delta x}$ are 0.16 and 0.10 % respectively. The small amount of chloride measured on this peak located at the loading plane decreases in time. Also, high diffusivities were noticed, D = 23 and 37 x10 $^{-12}$ m^2/s for 0 and 20 mm deviation respectively at 30 weeks of exposure.

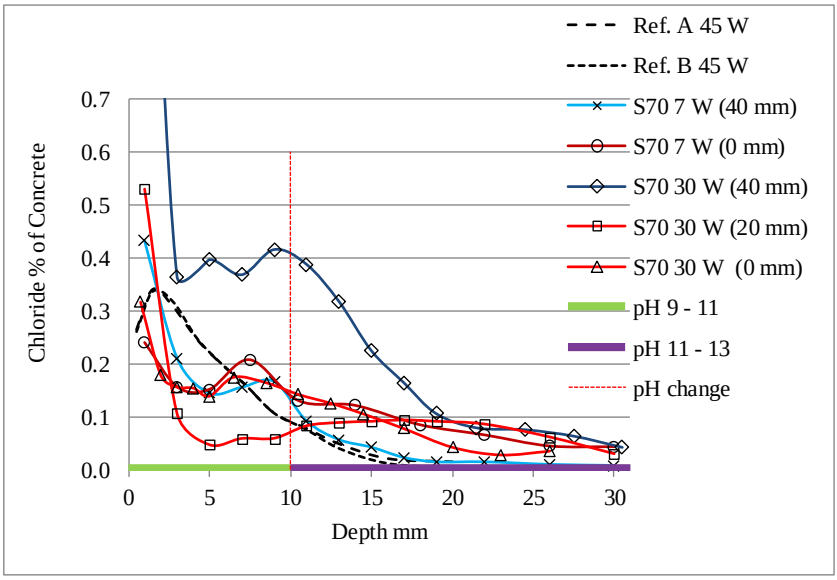

Figure 6-26: Total chloride content penetration profiles ground parallel to the loading axis (deviation distance from axis in parentheses), for S70 exposed to 65% permanent splitting tensile stress level and 3% chloride solution at 15 and 30 weeks (ref. samples 0% stress level, 45 weeks). Dashed vertical line shows the location of pH change, determined by rainbow indicator on powder extracted from ground layer (0 mm deviation) at 30 weeks.

Conversely the chloride content increases at 40 mm deviation from the loading plane. At this position, there is a significant chloride build up within the 7 & 30-week period where $C_{s\Delta x}$ changes from 0.18 to 0.40 %, respectively. The diffusivity in this zone is lower than in the loading plane.

Table 6-9: Diffusion coefficients and modeled surface concentration at the convection zone for concrete with 70% BFS replacement (S70) exposed to 3% sodium chloride solution and 65% stress level during 7 and 30 weeks. Profiles ground in parallel planes at 0 – 20 – 40 mm deviation from the splitting plane.

Time	Axis dev.	Δx	Surf. Conc.	D x 10^{-12}	
weeks	mm	mm	at Δx (%)	m^2/s	R^2
7	0	7.5	0.179	24.8	0.970
7	40	10.5	0.120	1.4	0.975
30	0	6.5	0.160	23.0	0.912
30	20	15.0	0.100	37.2	0.876
30	40	10.0	0.400	9.6	0.974

The 2D graphs from Figure 6-27 show that 0 and 20 mm deviation planes are the most aggressive zones which promotes chloride desorption with time and probably high free chloride mobility. An explanation for the high diffusivity found at the 20-mm plane could be that this zone is located very close to the wooden strip edge that is used for loading. Consequently, some shear stresses could be acting parallel to the splitting plane and provoking a high diffusion zone.

On the contrary the external layers located at 40 mm deviation would allow chloride adsorption and limit the mobility of free chlorides.

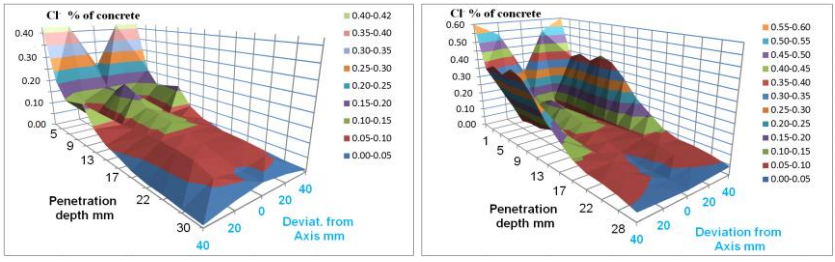

Figure 6-27: 2D Total chloride content penetration profiles ground parallel to the loading axis (at 0-20-40 mm deviation), for S70 exposed to 65% permanent splitting tensile stress level and 3% chloride solution after 7 weeks (left) and 30 weeks' exposure (right)

6.3.7.5 Chloride distribution in S0

Figures 6-28 and 6-29 (left) show the 1D and 2D chloride profiles respectively for S0. Some of the characteristics found in the other mixes are visible as well in this sample. Although the V-shaped chloride trench and the valley located before the first chloride peak are of a reduced magnitude than those found in the previous slag mixtures.

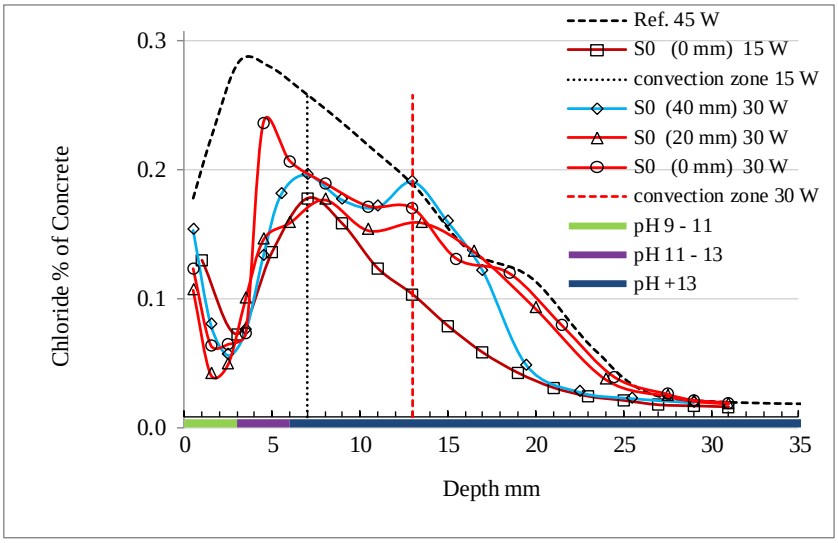

Figure 6-28: Total chloride content penetration profiles ground parallel to the loading axis (deviation distance from axis in parentheses), for S0 exposed to 65% permanent splitting tensile stress level and 3% chloride solution at 15 and 30 weeks (ref. sample 0% stress level, 45 weeks). Dashed vertical lines show the location of the convection zone (Δx) with time. pH change, determined by rainbow indicator on powder extracted from ground layer (0 mm deviation) at 30 weeks.

The convection zone expands with time. Thus, the level of chlorides obtained at the end of the 1st convection zone remains constant in depth until a 2nd boundary is reached after 30 weeks of exposure. This would mean that chlorides continue traveling deeper into concrete through micro-cracks and on their way, are being adsorbed by the paste. Later, they reach a zone where the chemical interaction

between paste and chlorides overcomes the damage provoked by mechanical load. Afterward the microstructure response performs like in sound concrete and chloride ingress is decelerated as is observed in the normal diffusion profile at the end.

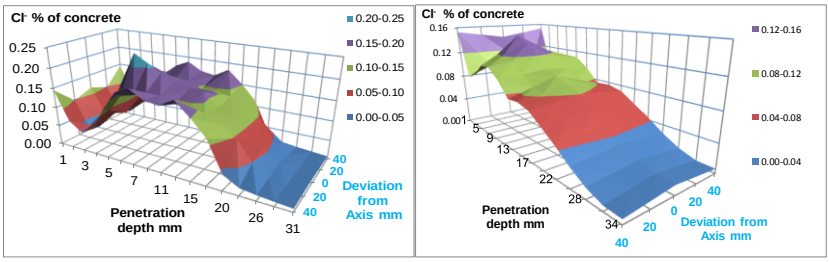

Figure 6-29: 2D Total chloride content penetration profiles ground parallel to the loading axis (at 0-20-40 mm deviation), exposed to 65% splitting tensile stress level and 3% chloride solution. S0 after 30 weeks (left) and HSR at 15 weeks' exposure (right)

According to the chloride diffusion coefficient obtained and shown in table 6-10

Table 6-10: Diffusion coefficients and modeled surface concentration at the convection zone for OPC concrete (S0) exposed to 3% sodium chloride solution and 65% stress level during 15 and 30 weeks. Profiles ground in parallel planes at 0 – 20 – 40 mm deviation from the splitting plane.

Time weeks	Axis dev. mm	Δx mm	Surf. Conc. at Δx (%)	D x 10^{-12} m^2/s	R^2
15	0	7	0.176	4.01	0.995
30	0	13	0.166	2.15	0.969
30	20	13	0.142	2.57	0.925
30	40	13	0.193	0.87	0.976

the largest values are obtained at 0 & 20 mm deviation. The magnitude of the diffusivity decreases towards the sides at 40 mm away from this plane suggesting more chloride adsorption and chloride ingress retardation. The magnitude of the diffusion coefficient and surface concentration obtained at the splitting plane (D = 2.15 x10^{-12} m^2/s & $C_{s\Delta x}$ = 0.17%) are the lowest of all the samples.

6.3.7.6 Chloride distribution in HSR

Figure 6-29 (right) and 6-30 show the distribution of chlorides after 15 and 30 weeks' exposure. The HSR mixture presents similarities with the behavior shown by S0 concrete. It shows a small "valley" shaped profile before the first chloride peak is reached. The V-shaped trench close to the surface is also limited. The convection zone shown in Figure 12 (left) moves inwards from the 7-mm observed at 15 weeks to approximately 18 mm perceived at 30 weeks. This suggests a progressing mechanical damage. The shape of the chloride profiles beyond the convection zones show a gentle slope which suggests a deep ingress of chloride ions.

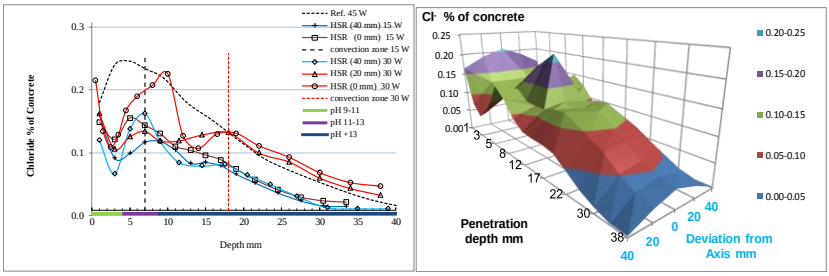

Figure 6-30: Total chloride content penetration profiles ground parallel to the loading axis (deviation distance from axis in parentheses), for HSR exposed to 65% permanent splitting tensile stress level and 3% chloride solution at 15 and 30 weeks (ref. sample 0% stress level, 45 weeks).

Finally, Table 6-11 confirms the limited ability of HSR mixtures to stop chlorides. High chloride diffusivities (D = 6.95/4.95 x10 $^{-12}$ m^2/s & $C_{s\Delta x}$ = 0.13/0.12 %) where determined correspondingly at 0 and 20 mm deviation after 30 weeks of exposure.

Table 6-11: Diffusion coefficients and modeled surface concentration at the convection zone for high sulfate resistant concrete (HSR) exposed to 3% sodium chloride solution and 65% stress level during 15 and 30 weeks. Profiles ground in parallel planes at 0 – 20 – 40 mm deviation from the splitting plane.

Time weeks	Axis dev. mm	Δx mm	Surf. Conc. at Δx (%)	D x 10^{-12} m^2/s	R^2
15	0	7	0.138	10.90	0.982
15	40	7	0.119	10.10	0.955
30	0	18	0.128	6.95	0.993
30	20	18	0.123	4.95	0.993
30	40	18	0.072	1.80	0.985

6.3.7.7 Comparison of specific parameters from the 4 mixtures.

To compare the response of every mixture to the chloride ingress, an analysis of the obtained parameters, was made at 2 different profile positions. Table 6-12 shows the summary of the diffusion parameters obtained at the splitting plane (0 mm) and at 40 mm away from it.

Table 6-12: Summary of obtained parameters for chloride ingress into concretes subjected to permanent 65% level of splitting stress and 3% sodium chloride exposure. Measures taken at the splitting plane and at 40 mm deviation.

	At the Splitting plane			**At 40 mm deviation**		
Mixture Denom.	Δx mm	Surf. Conc. at Δx (%)	D x 10^{-12} m^2/s	Δx mm	Surf. Conc. at Δx (%)	D x 10^{-12} m^2/s
S0	13.0	0.166	2.15	13.0	0.193	0.87
S50	10.0	0.290	3.46	10.0	0.266	0.89
HSR	18.0	0.128	6.95	18.0	0.072	1.80
S70	6.5	0.160	23.00	10.0	0.400	9.60

The purpose is to compare the chloride transport at the micro-cracked zone that occurs at the splitting plane and 40 mm away from it. In general, the zone with less mobility for chlorides is located away from the splitting zone (40 mm deviation) were diffusivities decrease. However, the influence of micro-cracks on the diffusion is felt up to

this location. This can be observed when examining the ratio that has the diffusivity of each mixture with respect to the lowest value obtained in mixture S0. The concretes arranged in decreasing order of performance are (S0, S50, HSR, S70) and their relative diffusion values are correspondingly (1.0, 1.6, 3.2, 10.7) at 0 mm deviation and (1.0, 1.0, 2.1, 11.0) at 40 mm deviation from the splitting plane. This suggests that the effect of the micro-cracks in the splitting plane, has a larger influence on the chloride transport that was sensed at 40 mm away from it.

6.3.7.8 Petrographic observations.

To gather more information that could explain the observed distribution of the chloride in the samples concrete slices were taken from all concrete specimens for thin section microscopy as shown in Figure 6-31 (a).

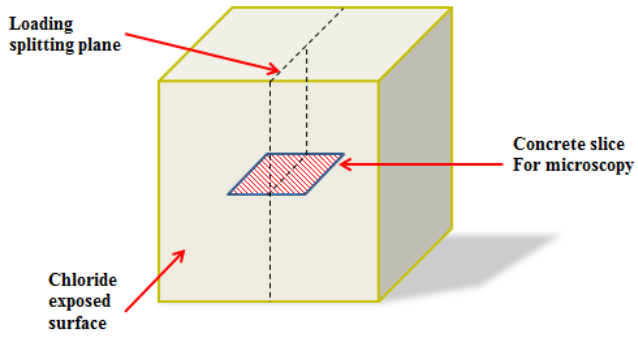

a)

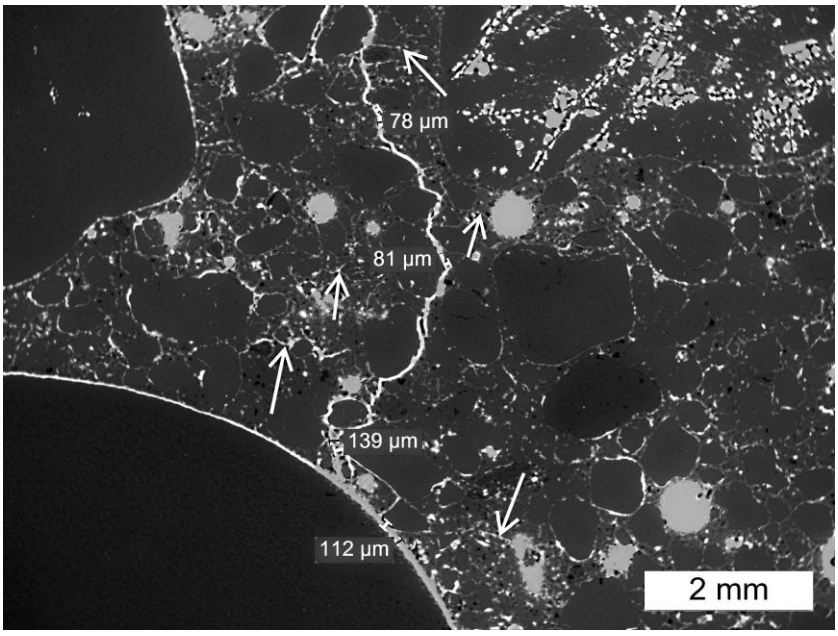

b)

Figure 6-31: Schematic view of concrete slice extraction for microscopy (a). Longitudinal micro-crack system following the splitting plane (139 – 78 µm). The Crack surrounds gravel surface and goes into the paste. A thinner micro-crack system is connected perpendicularly with the main crack system (1 – 5 µm). S70 sample after 30 weeks combined exposure. View under fluorescent light grey tones (b).

Microscopic observations showed that all the samples present a main crack system oriented parallel to the splitting plane. Figure 6-31 (bottom) shows a micro-crack located at the splitting plane of S70. The crack has a maximum opening of 139 µm but it gets thinner with concrete depth. The crack path follows a gravel surface, but also jumps from aggregate to aggregate surrounding them. A very fine network of micro-cracks (crack width between 1 – 4 µm) departs perpendicularly from the main crack system as also shown in Figure 6-32. A distinguished feature on this thin micro-crack system is that it presents an inter-granular development (it surrounds the sand grains) The micro-crack frequency is higher in S50 and S70 mixtures. In pure Portland cements S0 and HSR the finer micro-crack system is notably reduced. For these concretes, the highest crack width was about 20

µm while the thinner ones reach 5 and 3 µm. Furthermore, the cracks appear more clearly and well defined in the BFS mixtures than in S0 or HSR ones.

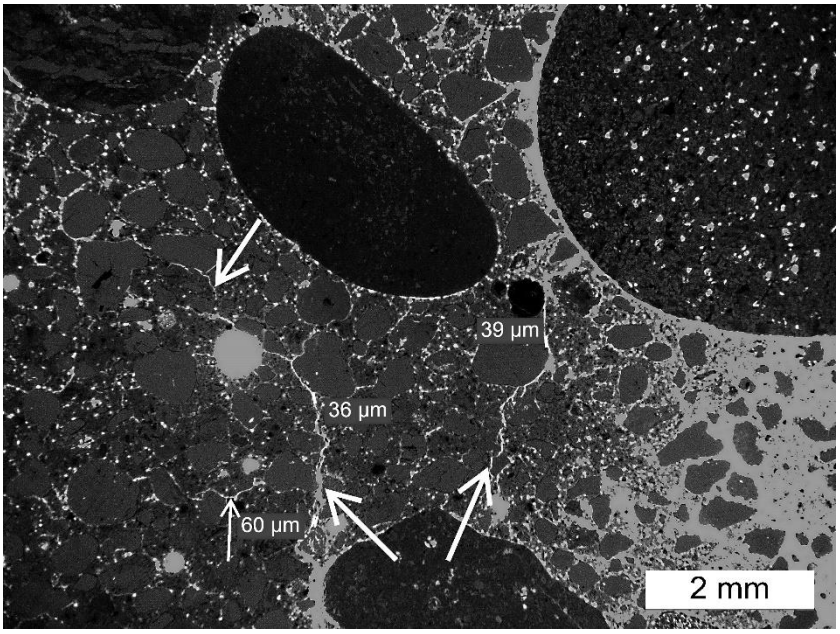

a)

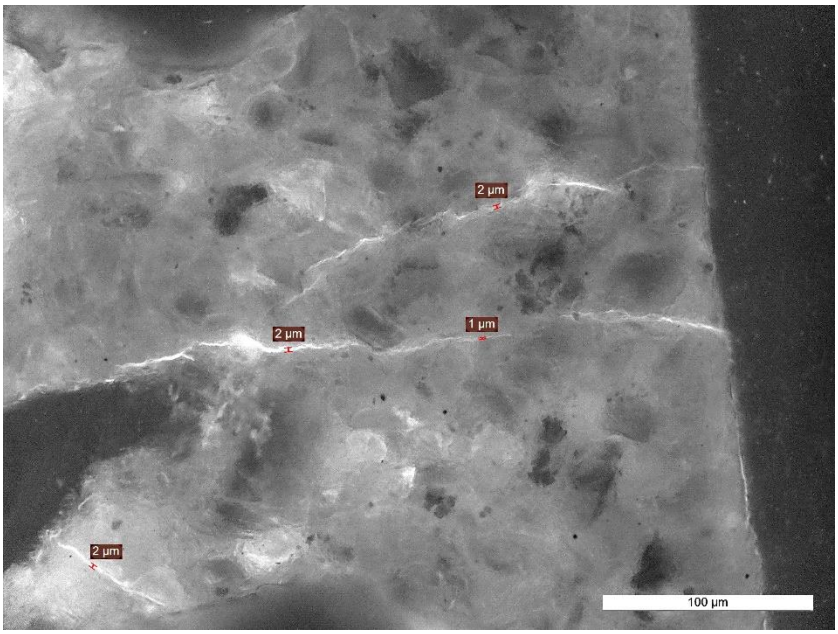

b)

Figure 6-32: Longitudinal cracks (60 – 36 µm) and thinner transverse micro-crack system which departs from it. in S50 at 30 weeks combined exposure, fluorescent light grey tones (a). Details of transverse micro-crack system (1 µm wide) which bridges between aggregates. Fluorescent light "grey tones" for S70, 30 weeks combined exposure (b).

The characteristic of the damage has similarities to the so called "Stress Corrosion Cracking" (SCC). A mechanism of deterioration found in metals, polymers and ceramics due to the partial dissolution of these materials in presence of the combined action of a corrosive agent under stressed conditions.

6.3.7.9 General interactive response of studied mixtures to chloride attack.

The cement paste in concrete is an active membrane whose physico-chemical characteristics are more or less known. On the other hand, the pore solution is an electrolyte. Therefore, we must recognize that

the diffusion of chloride ions and their counterparts into concrete must share an interactive exchange with this paste and the solution. Thus, chloride penetration into concrete should be more complex than mere diffusion through an inert porous material. According to Zhang T. et al [4], chloride diffusion into concrete may be affected by the following factors:

1) Reduction of chemical potential and diffusing driving force because of ionic interaction.

2) Retardation of the drift velocity of chlorides due to the lagging motion of the cations.

3) Effect on the chloride drift from the interaction between the electrical double layer on the solid surface and ionic clouds surrounding the diffusing chloride ions.

Considering that this research just took into consideration the action of one attacking salt (NaCl), it is believed that the interaction of this salt and the electrical double EDL layer plays the most important role in trying to explain the obtained results.

When a mineral surface is in contact with aqueous solution an electric double layer forms at the interface. The electrical double layer in contact with the pore solution is composed of a double ion layer: a first immobile layer of ions with opposite sign to the charged mineral surface, and a diffuse layer. The second layer is made of hydrated counter ions (opposite in sign to the first layer) that show a transition from high concentration at the fixed layer border toward a balanced concentration in the bulk solution. The shear plane is located close to the counter ion / diffuse layer boundary. The potential at the shear plane is called the zeta potential [22].

It has been observed that the existence of the EDL in gel pores (< 10 nm) promotes a higher interaction with chloride ions than the same salt in capillary pores [10]. Because these pores show great specific surface there is a big chance that chloride ions are adsorbed into their active sites through reaction shown in equation (6-2). Small pores

favor the overlapping of EDL. In such conditions the EDL cannot be further compressed even at high concentrations. Consequently, chloride diffusion is considerably reduced. Some materials like BFS in properly cured concrete tend to reduce the hydrated paste pore size [10]. That would explain the higher performance to stop chlorides found in S50 and S70 compared to those noticed in S0 and HSR for the non-loading conditions as seen in Figure 6-23.

However, a different behavior has been noticed in this research when the micro-structure is modified due to mechanical damage in presence of chlorides. In such conditions, micro-cracks are formed which let the aggressive solution penetrate further inside. In sound pastes the calcium in the pore solution Ca^{2+} is in equilibrium with the solid calcium composing the minerals. When aggressive solution from an external source contacts the mineral external boundary, the equilibrium is broken. Calcium is dissolved from the solid structure and diffuses towards the pore solution [28]. Moreover, the chloride solution that is used for the current experiment is devoid of calcium ions, and its initial measured pH is 8.0. Therefore, it can be considered an aggressive solution which penetrates the micro-crack system.

Generally, the process of calcium leaching in concrete is considered a slow process. However, there is evidence that many calcium bearing minerals experience higher solubility in the presence of chloride [29], this effect contributes to the attack. De Weerdt K. and Justnes H. [22] found CH depletion and CSH decalcification due to the leaching of the outermost layers from OPC pastes exposed to sea water. Consequently, if is there a CH depletion, there will also be a reduction of the pore solution pH in the attacked area.

Stress acting permanently on the concrete at a 65 % level, modifies the micro-pore network. The load creates strains and micro-cracks which damage the initially sound micro-pore network. At this point the larger voids and bulk solution become more important for the chloride transport.

Deeper ingress of chloride solution promotes calcium dissolution which initially is taken from available Portlandite. Calcium is gradually

leached out of the concrete due to a diffusion gradient towards the external attacking solution. If CH is depleted, calcium is taken from CSH gel and the damage increases. Yoon-Suk Choi "et al." [32], noticed an important deterioration of the mechanical properties of calcium leached concrete. In their research a better performance was observed for OPC concrete with w/c=0.5 than in mixtures with 30 % and 17 % replacement by BFS and FA respectively, for a w/b=0.5. The performance against chloride penetration was better for the OPC mixtures after calcium leaching.

The capacity that CSH has for chloride adsorption is also related to the availability of calcium in the pore solution [10, 22]. In our case, it would be expected that the mixtures with higher CH content can withstand better the leaching process and therefore the progressing damage. The amounts of available Portlandite in our mixtures are shown in Figure 6-33, after 1 year of curing (7 days 95 % RH and 60 % RH from there on).

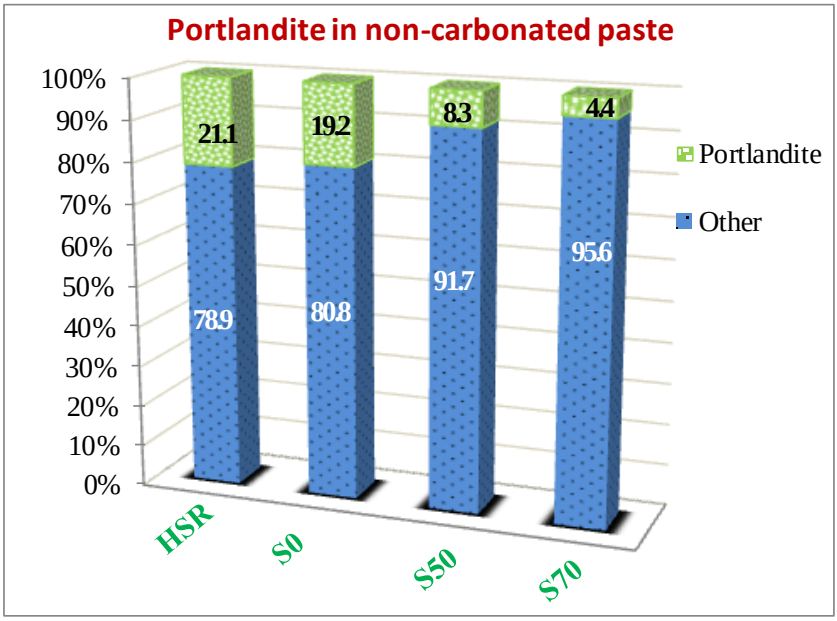

Figure 6-33: XRD Rietveld quantification of Portlandite for pastes extracted from the studied concretes at 1 year of age.

Along with calcium leaching there is also a decrease in the paste pH. This is expected considering the connection through cracks of the concrete internal solution with the bulk attacking solution whose pH is 8.0. According to the previous assertion, HSR which has a slightly higher CH content than S0 (Figure 6-33) would present a higher resistance to a pH decrease and therefore to leaching. However, besides the fact that OPC and HSR cements produce similar amount of Portlandite during hydration, many phases (solid phases in hydrated cement which have pH dependent dissolution characteristics) are also responsible to avoid a pH drop [40,41]. Reddy B. et al [40], observed a better performance in OPC to withstand pH drop compared to sulfate resistant cement.

In order to detect any pH drop in our tested samples, a semi-quantitative pH determination (the commercial product is called rainbow indicator) was administered to the ground powder. Thus, this colorimetric method was applied to each layer that was obtained from the profile located at the splitting plane at 30 weeks. The obtained results for S50 and S70 are shown in Figures 6-24 and 6-26 respectively. A pH reduction in the first 5 and 10 mm respectively, was noticed in both samples. On the other hand, Figures 6-28 and 6-30 show the pH reduction for samples S0 and HSR respectively, this zone is located at 3 and 4 mm correspondingly. The boundary considered for pH reduction is 11.0, below that value it is considered that most of the chemically bound chlorides are decomposed [40].

So far, we have analyzed that the combined action of chloride attack plus sustained splitting load provokes micro-cracking in the concrete. Subsequently, an aggressive solution gradually starts to interact with the paste minerals causing calcium leaching and pH reduction. The attack is more pronounced on the splitting plane where the binding capacity for chlorides is highly reduced. It is believed that the region presents some characteristics such as calcium depletion, low pH environment and microstructure alteration. These features favor free chloride mobility and low adsorption of this ion (equation 6-2) goes to the left).

The damage progresses from the main crack system towards sound areas creating a new finer micro-crack network oriented perpendicularly to the splitting plane. Thin section microscopic shows that the finer micro-crack system is more widespread in BFS mixtures than in OPC or HSR concretes.

6.3.7.10 Conclusions

Chloride penetration in concrete is very complicated process. There are many factors affecting concrete resistance against chloride ingress.

It was observed in this study that for non-loading conditions the ability to stop chloride penetration into concrete was improved by an increase in the BFS content of the mixes. Thus, a decreasing order of performance was found for samples S70, S50, S0 and HSR.

However, when the same mixes were subjected to combined attack of chloride solution plus a permanent splitting tensile load being 65 % of the failure load, a different order for the chloride penetration resistance was observed. Thus, the concrete types in the decreasing order of performance were S0, S50, HSR, and S70.

Petrographic observations showed a greater mechanical damage for the slag mixes S70 & S50 than for the pure Portland ones S0 & HSR.

It was observed that strained mixes at 50 and 70 % BFS replacement are more susceptible to chloride attack than the same samples under no-loading conditions. The attack provokes a reduction of the chloride level preferentially in zones where micro-cracking is present. Nevertheless, the attack is not confined only to the initially formed micro-crack area, but is propagated to more remote areas spreading the damage.

The reduction of the chloride level in the near surface vicinity has similarities to damages reported in concretes subjected to carbonation [10,16], concretes subjected to wet and dry cycles [17], or combination of wet & dry cycles plus cracks [18].

Sustained mechanical loading initiates micro-cracking which alters the physical-chemical equilibrium of sound paste. Calcium ions are progressively leached away from the concrete through the new cracked system. A pH reduction in the pore solution is also expected to occur due to the concentration gradient with the bulk attacking solution. This chemical unbalance provokes CH depletion and from there on CSH decalcification spreading the damage to wider zones. The propagation of the damage can be seen under the microscope as a secondary finer micro-crack system growing perpendicularly and away from the main cracks in the splitting zone.

The damaged zone has no capability to bind chloride (physically or chemically). Most of the chloride in this zone is believed to be in a free form.

It seems that mixtures that are capable to withstand a pH reduction in their pore solution have better performance to chloride penetration. The mineralogical composition of pure Portland cement and its high CH content help to better resist chloride ingress than the other studied mixtures.

References

[1] Goto S, Roy DM, Diffusion of ions through hardened cement pastes. Cem Con Res. 1981; 11:751-757

[2] Yu SW, Page CL, Diffusion in cementitious materials: 1. Comparative study of chloride and oxygen diffusion in hydrated cement pastes. Cem Con Res. 1991; 21:581-588

[3] Ngala VT, et al, Diffusion in cementitious materials: II. Further investigations of chloride and oxygen diffusion in well-cured OPC and OPC/ 30% PFA pastes. Cem Con Res. 1994; 25(4):819-826

[4] Zhang T, Gjorv OE, Diffusion behaviour of chloride ions in concrete. Cem Con Res. 1996; 26(6):907-917

[5] Zhang JZ, Buenfeld NR, Presence and possible implications of a membrane potential in concrete exposed to chloride solution. Cem Con Res. 1997; 27(6):853-859

[6] Buenfeld NR, Glass GK, et al, Chloride transport in concrete subjected to electric field. J Mater Civ Eng. 1998; 10(4):220-228.

[7] Zhang JZ, Buenfeld NR, Membrane potential and its influence in chloride transport in cementitious materials. In: Andrade C, Kropp J (eds) Testing and modelling the chloride ingress into concrete. 2nd International RILEM workshop. 2000; RILEM publication S.A.R.L., Cedex. p33.

[8] Castellote M, Alonso C, Andrade C et al, Oxygen and chloride diffusion in cement pastes as a validation of chloride diffusion coefficient obtained by steady-state migration test. Cem Con Res. 2001; 31:621-625

[9] Zhang JZ, Jian YL, Buenfeld NR, Measurement and modelling of membrane potentials across OPC mortar specimens between 0.5 M NaCl and simulated pore solutions. Cem Con Compos. 2002; 24:451-455

[10] Elakneswaran Y, Iwasa A., Nawa T, et al, Ion-cement hydrate interactions govern multi-ionic transport model for cementitious materials, Cem Con Res. 2010; 40: 1756-1765.

[11] Jiang F., Wittmann F.H., Zhao T., Influence of Sustained Compressive Load on Penetration of Chloride Ions into Neat and Water repellent Concrete, Proceeding of the first internal conference on performance-based and life-cycle structural engineering, Editors: J.G. Teng, J.G. Dai., S.S. Law, Y.Xia, and S.Y. Zhu, Hong Kong. 2012;992-997

[12] Yao Y. “et al.”, Test methods to determine durability of concrete under combined environmental actions and mechanical load: final report of RILEM TC 246-TDC, Materials and Structures. 2017; 50:123

[13] Choinska M. “et al.”, Effects and interactions of temperature and stress-level related damage on permeability of concrete. Cem Con Res. 2007; 37 (1): 79-88.

[14] Sugiyama T. “et al.”, Effect of Stress on Gas Permeability in Concrete. Materials Journal. 1996; 93 (5): 443-450

[15] Jones R. and Ricker R., Stress-Corrosion Cracking Materials Performance and Evaluation. Editor: Russel H. Jones, ASM International. 1992, 1-40.

[16] Malheiro R. et al, Effect of Carbonation on the Chloride Diffusion of Mortar Specimens Exposed to Cyclic Wetting and Drying, Proceedings XIII International Conference on Durability of Building Materials and Components, Sao Paulo-Brasil Sept. 2014, 482-489.

[17] Lee C.S., Yoon I.S., Prediction of deterioration process for concrete considering combined deterioration of carbonation and chlorides ions, Journal of the Korea concrete Institute, 2003; 15 (6): 902-912.

[18] Chunhua Lu et al, Experimental Analysis of Chloride Penetration into Concrete Subjected to Dying-Wetting Cycles. Journal Mater. Civ. Eng. 2015; 27 (12), 04015036-(1-10).

[19] Chunhua Lu et al, Effect of Transverse Crack on Chloride penetration into Concrete Subjected to Dying-Wetting Cycles. 4th International Conference on the Durability of Concrete Structures. Purdue University, West Lafayette, IN, USA. 2014; 169-175.

[20] Andrade C., et al, Mathematical Modelling of a Concrete Surface "Skin Effect" on Diffusion in Chloride Contaminated Media, Institute of Construction Sciences "Eduardo Torroja" of the CSIC. 1997: 39-44.

[21] Egüez H, De Belie N., De Schutter G., Proposed mechanism for the formation of oxychloride crystals during sodium chloride application as a deicer salt in carbonated concrete, Construction and Building materials, 2016; 109: 188-197.

[22] Elakneswaran Y, Nawa T, Kurumisawa K. Zeta potential study of paste blends with slag. Cement & Concrete Composites. 2009; 31: 72-76.

[23] Butler J., et al, Ionic equilibrium: Solubility and pH calculations, Wiley ed. 1998.

[24] Fuerstenau, M., et al, Adsorption mechanism in non-metallic activation systems. Transactions AIME 247; 1970: 11-14

[25] Basheer P.A.M., Nolan E., Near-surface moisture gradients and in situ permeation tests. Construction and Building Materials. 2001; 15: 105-114.

[26] Egüez H, Tsangouri E., De Belie N., De Schutter G., Chloride interaction with concretes subjected to a permanent splitting tensile stress of 65%, Construction and Building materials, 2016; 127: 527-538.

[27] Vollpracht A. “et al.”, The pore solution of blended cements: a review. Materials and structures. 2016; 49 (9): 3341-3367.

[28] Dawei Hu et al, Modelling of Lixiviation-Mechanical Coupling Behavior of Fiber Reinforced Concrete. Proceedings of COMSOL, Conference in Stuttgard, 2011.

[29] Harvie C, Moller N, Weare J. The prediction of mineral solubilities in natural waters: the Na-K-Mg-Ca-H-Cl-SO4-OH-HCO3-CO3-CO2-H2O system to high ionic strengths at 25 oC. Geochim. Cosmochim. Acta 48. 1984;723-751

[30] Hills J. “et al.”, The effect of sodium chloride dissolution of calcium silicate hydrate gels, Waste Management 26 (2006) 758-768.

[31] De Weerdt K. and Justnes H., The effect of sea water on the phase assemblage of hydrated cement paste. Cement & Concrete Composites. 2015; 55:215-222.

[32] Yoon Suk Choi et al, Effect of calcium leaching on the pore structure, strength, and chloride penetration resistance in concrete specimens. Nuclear Engineering and Design. 2013; 259:126-136.

[33] Schneider U., et al, Stress corrosion initiated cracking of concrete, Cem Con Res. 1986; 16: 535-544.

[34] Pignatelli I. “et al.”, A dissolution-precipitation mechanism is at the origin of concrete creep in moist environments, J Chem Phys, 2016; 145, 054701

[35] Wang H. “et al.”, Effect of external loads on chloride transport in concrete, J. Mater. Civ. Eng., 2011; 23: 1043-1049

[36] Wang H. “et al.”, Time-Dependent and Stress-Dependent chloride diffusivity of concrete subjected to sustained compressive loading, J. Mater. Civ. Eng., 2016; 04016059: 1-9

[37] Nguyen P., Amiri O., Study of electrical double layer effect on chloride transport in saturated concrete, Construction and Building Materials, 2014; 50:492-498

[38] Stuart S.J., Berne B.J., Effects of polarizability on the hydration of the chloride ion. The journal of physical chemistry. 1996; 100:11934-11943.

[39] Stuart S.J., Berne B.J., Surface curvature effects in the aqueous ionic solvation of the chloride ion. The journal of physical chemistry. 1999; A-103:10300-10307.

[40] Reddy B et al, On the corrosion risk presented by chloride bound in concrete. Cement & Concrete Composites. 2002; 24:1-5.

[41 Glass G.K. et al, Corrosion inhibition in concrete arising from its acid neutralization capacity. Corrosion Science. 2000; 42:1587-1598.

V CONCLUSIONS

CHAPTER 7. FINAL CONCLUSIONS AND FURTHER RESEARCH

This research was divided into 2 topics. The first deals with the Frost salt scaling in carbonated concrete, while the second with the chloride ingress in mechanically loaded concrete.

The thesis was divided into 5 parts and 7 chapters.

Part I with a single chapter 1, shows the general introduction with the following sub-sections: Literature review, Significance of the present research, Objectives and thesis outline.

Part II “Materials”, is comprised of chapter 2 which deals with the concrete mix composition. In this chapter the utilized materials are described and the concrete batching and curing conditions as well.

Part III analyzes the frost salt scaling in carbonated concrete. This part is split into chapters 3 and 4. The initial part of this section is presented in Chapter 3. The main purpose of this section was to characterize 4 types of concretes regarding their carbonation susceptibility. The greater susceptibility to carbonation of concrete made with BFS was verified. On the other hand, previous studies were confirmed which recognize the ability of Portland cement concrete to carbonate more slowly.

In Chapter 4, the frost salt scaling resistance of 4 previously carbonated concrete types were analyzed. A severe disruptive mechanism was observed, provoked by oxychloride salt crystallization pressure at low temperatures as the main cause of concrete scaling.

The concrete types with BFS utilized in this study, favor more the formation of oxychloride than OPC concretes.

Among the conditions that are thought to promote oxychloride salt crystallization are: a rapid cooling rate which assures a “supersaturated” region for chlorides which is thought to be present near the carbonation front at the highest chloride ’s peak beneath the concrete surface; simultaneously, carbonates dissolution as a source of calcium and hydroxyl ions needed for oxychloride crystal formation;

finally, oxychloride stability due to their low solubility product at low temperatures.

Any future work on this matter should consider the following question about chloride supersaturation: how low temperatures modify the chloride adsorption behavior at the CSH nano-pores network.

The inner high chloride concentration peak seems to play an important role as the point for oxychloride nucleation. Studies should be directed to understand its physico-chemical function. The characteristics of the electrical double layer and how it is affected by every SCM addition should be investigated.

Part IV analyzes the chloride ingress in mechanically loaded concrete. This part is divided into chapters 5 and 6.

In Chapter 5 an investigational technique to study the effect of mechanical load on chloride penetration into the pore space of concrete is proposed in detail. A Round-Robin test among 5 laboratories was made to test equivalent combined conditions of loading and chloride attack to OPC concrete. The obtained results show that the magnitude of stress should be taken into consideration to make durability and service life design more accurate.

The task for Chapter 6 was to analyse the chloride penetration under permanent compressive and splitting tensile stresses.

Both mechanisms of loading share some common characteristics. The concrete develops a progressively damaged layer, named in this thesis the skin layer or convection zone. This zone is characterized by a fast transport of chlorides and high diffusion coefficients. The chloride concentration within this near-surface layer is considerably lower compared to the observed chloride profile obtained in the reference non-loaded concrete. This suggests an alteration caused by the load towards the binding capacity (physical and chemical) of the cement paste.

For the splitting tensile tests, microscopic observations showed that all the samples present a main crack system oriented parallel to the splitting plane. Although, a very fine network of micro-cracks also

departs perpendicularly from the main crack system. A distinguished feature in this thin micro-crack system is that it presents an inter-granular development (it surrounds the sand grains). It is believed that a large chloride transport is present in this micro-cracked zone. The pH level was determined throughout the concrete profiles and a low pH zone was found progressing from the concrete's surface. This suggests a leaching zone caused by the cracking and the saline solution.

Petrographic observations showed a greater mechanical damage for the slag mixes S70 & S50 than for the pure Portland ones S0 & HSR.

An important observed characteristic of the chloride ingress into loaded concrete was the low chloride content located in the near-surface zone. Some theories like the calcium bearing minerals dissolution from the paste, or the double layer alteration by the mechanical load, were highlighted as a probable mechanism to explain the apparent lack of chloride binding capacity by the paste.

In that regard, further research is recommended to elucidate the effect of this behavior on the chloride ingress. On the other hand, if it is true that mechanical loading affects the binding capacity of hydrated cement paste, it should be investigated how the pore solution is affected in terms of chloride and other ions balance. And, it should be elucidated if this situation increases the corrosion risk of rebars in concrete.